TUDelft

Delft University of Technology

Safety Risk Assessment of Unmanned Aircraft System Operations for Urban Air Mobility

Jiang, C.

Important note
To cite this publication, please use the final published version (if applicable).
Please check the document version above.

Safety Risk Assessment of Unmanned Aircraft System Operations for Urban Air Mobility

Chengpeng Jiang

Safety Risk Assessment of Unmanned Aircraft System Operations for Urban Air Mobility

Dissertation

for the purpose of obtaining the degree of doctor
at Delft University of Technology
by the authority of the Rector Magnificus, Prof.dr.ir. T.H.J.J. van der Hagen
chair of the Board for Doctorates
to be defended publicly on
Tuesday 12th December 2023 at 12:30 o'clock

by

Chengpeng JIANG
Master of Science in Transportation Planning and Management,
Nanjing University of Aeronautics and Astronautics, China
born in Sichuan, China

This dissertation has been approved by the promotors:

Composition of the doctoral committee:

Rector Magnificus,   chairperson

Prof.dr.ir. H.A.P. Blom   Delft University of Technology, promotor

Dr. O.A. Sharpans'kykh   Delft University of Technology, copromotor

Independent members:

Prof.dr. J.H. Bolte   Ohio State University, United States of America

Prof.dr. X. Sun   Beihang University, China

Dr. L. Li   City University of Hong Kong, China

Prof.dr.ir. P.H.A.J.M. van Gelder   Delft University of Technology

Prof.dr.ir. R. Happee   Delft University of Technology

The only Zen you find on the tops of mountains is the Zen you bring up there.

Robert M. Pirsig

Acknowledgements

The past five years have been a journey to navigate through my doctoral studies, to experience the world and to explore myself. This journey would not have been as meaningful and enlightening without the significant individuals who have walked alongside me. I cherish the moments spent with each of you. These experiences and memories have been invaluable for me that I shall revisit in the years to come. Completing this doctoral thesis marks a milestone, and I am deeply thankful to everyone who has been an integral part of this journey.

First and foremost, my deepest appreciation goes to my promotor, Prof. Henk Blom. Thank you for your thorough guidance on my research over the past years, which has significantly shaped this thesis and my academic growth. I vividly recall our first meeting in Beijing back in 2018, attending your lectures, and exploring Forbidden City and the Summer Palace together. Reflecting on that week, I had already seen in you a scholar of profound knowledge, an approachable and humorous elder, and a companion who is optimistic and life-embracing. The invaluable lesson I learned from you is to hold onto own perspectives while keeping an open mind for communication and integration - a lesson that has helped me to turn my stubbornness into perseverance. Your pursuit of high-quality outcomes, the sustained commitment you have demonstrated over the years stand as a beacon for my own path, deeply influenced my future career aspiration and personal development.

To Dr. Alexei Sharpanskykh, I am truly grateful for your invaluable support and practical advice provided during my doctoral research. You showed me that being a doctoral candidate involves much more than just research; it's a broad and dynamic way of life. Early on, when I was just beginning to understand the scope of my doctoral pursuits, you encouraged me to find my own rhythm to do research and to engage with hobbies that kept me fascinated and balanced. These have made my doctoral journey much more vibrant and fulfilling. Thank you for giving the opportunities to participate various research projects that broaden my understanding of my research field. I always enjoy the meetings and conversations with you. Your ability to unlock new ways of thinking is impressive. You always bring me creative ideas and brighten my perspectives. I also thank you for giving me the encouragement and suggestions needed to continue moving forward when I was in tough times.

To Matthieu Vert, it is one of the best things to have you as my office mate from the beginning of my PhD. Without your presence, my doctoral life would have lacked much of its color. I love the parties you organized at your place, especially the comfortable coach. I'll always hold dear the memory of Christmas 2019, spending the holiday with your loving family stands out as one of the warmest memories of my doctoral years. I always enjoy the conversations with you that lead to interesting insights and mutual enhancement of perspectives. Your relaxed approach to life, passionate exploration, and free spirit have shown me alternative ways to experience and appreciate the possibilities life has to offer. I believe our friendship only grow deeper with time. Both Yina and I are looking forward to your visit to China. And I, too, can't wait for the day to join your castle party.

To Hao Ma, you were the first person I met when I started my PhD, bringing warmth and familiarity to my early days in Delft and at ATO. As my senior colleague, you offered valuable advice on various aspects of my doctoral research. Your easygoing nature always bring comfort, creating an atmosphere where everyone feels at ease. You always willingly share life's observations and amusing stories, adding much joy to the otherwise mundane

routine of doctoral life. I am also very grateful for your companionship over the years, for the basketball games, workouts, and countless meals and drinks together. Thank you for being a reliable 'big brother' throughout my doctoral journey.

To Borrdephong Rattanagraikanakorn, I am delighted to have you as a research mate during my doctoral studies. Your outstanding work in Multi Body System (MBS) modelling provided a solid foundation for my subsequent research. I am truly thankful for your thorough guidance and assistance in both MBS modelling and the drone experimental tests. Beyond our academic collaboration, you are also a friend in life. Those discussions and chats with you, through my highs and lows, have always been a source of comfort and cheer. I look forward to meeting you in Thailand and welcome you to China, along with Mai and your adorable son.

To Juseong, we started our PhDs around the same time, and I'm truly glad to have your accompany during this journey. Though our research topics rarely intersect, the discussions with you are always enlightening, offering me fresh perspectives. Your positive attitude and humor always light up the room with laughter, making the interactions with you comfortable and joyful. In research, your hard work and impressive accomplishments also inspire me to strive for excellence of my own. Thank you for the companion throughout these years. I look forward to the future gatherings with you in the Netherlands.

To my dear colleagues at ATO, thank you all for the companionship and support throughout my journey. Qichen, I've always enjoyed the workouts and basketball games with you, and it is good to have these reunite for chats and meals after your graduation. Rui, you are like an elder sister and thank you for your help and care in my early PhD. Stef, I am glad to be your office mate at the beginning of my PhD and thanks for the help and advice. Vis, the fun ATO activities you organized have always been the highlights in my memory. Alessandro, your recommended Italian pasta recipe is really good. Wenhua, the dinners at your house are always delightful. Malte, thank you for the birthday party invites and the delicious German bread source. Thomas, your unique humor never fails to liven up our gatherings. And to Elise, Macia, Marta, Mihaela, Hemmo, Ingeborg, Simon, Iordanis, Haonan, Mahdi, Marie, Ilias, Mike, Gulcin, the small talks in the office and during lunch and coffee breaks have made all the difference in my daily work life. I am also thankful to Bruno for administrative support during my PhD, and our secretaries, Nathalie and Vera, for their patient assistance with the daily affairs. Thanks to Paul for his technical support with network and server issues.

This thesis wouldn't reach its complete state without the collaborative efforts of brilliant minds. To Dr. Lishuai Li, I am truly thankful for facilitating my collaboration with Antwork and providing invaluable advice throughout the process. To Lei Zhang, Qinghai Chen, and Yansong Chen from Antwork, thank you for the drones provided for the experimental tests and the technical support offered. To Huan Wang from Zhejiang University, thank you for providing the drone testing equipment and the support during the tests. It was a pleasure to get to know Xingyu He in the final stages of my PhD, to collaborate on a paper, and to enjoy a delightful journey through Europe together.

I would also like to thank my friends Jingwei Dong, Yingfu Xu, Xiujie Shan, Bo Li, Pan Zhang, and Yiyuan Zou. Your presence has enriched my doctoral life beyond research, adding a spectrum of color and vitality to my journey. With each shared experience, whether it's a conversation, a gathering for meals, or collective adventures, you have played a role in shaping a period of my life filled with friendship and warm memories.

I owe a debt of gratitude to my beloved parents, whose boundless love and support sustained me throughout my doctoral journey. Though miles may have separated us, the emotional distance between us has only grown closer. Dad, your dedication to education as a teacher instilled in me the values of learning and an endless curiosity. Mom, your perseverance

in the face of adversity taught me to persist no matter the challenges. You have shaped my educational pursuits from the very beginning, leading me to this significant milestone. I am proud to carry forward the dreams you once held for yourselves, and I am touched by the pride you take in my achievements. Thank you for being the unseen backbone of my success. Your influence is evident on every page of this thesis.

Lastly but most importantly, Yina, I would like to express my heartfelt gratitude to you. Thank you for your unwavering companionship and support. Our long-distance relationship, with you in China and me in the Netherlands, has been challenging due to the geographical distance and time difference. I realize that these years have not been easy for you, having to face work and life's challenges on your own, while I couldn't always provide immediate comfort or even a warm hug. Especially during the times we couldn't meet because of the pandemic, which also delayed my graduation. I am deeply grateful for all that you have borne with me and the encouragement and support during my hard times. Thank you for supporting my dreams, allowing me this luxurious span of time to complete my PhD studies. Fortunately, we've tried hard to tackle obstacles together and present for each other's changes and growth through daily calls, chats and video exchange. The physical distance and time difference have not severed our connection but instead deepened it with love and trust. I look forward to a bright future where we face life's trials side by side and heart by heart. With you, I am home.

Chengpeng Jiang

16 November, 2023

Summary

Safety Risk Assessment of Unmanned Aircraft System Operations for Urban Air Mobility

Chengpeng Jiang

Technology developments has enabled Unmanned Aircraft System (UAS) to be adopted for various applications, including Urban Air Mobility (UAM) – an air transportation system for passengers and cargo in and around urban environments. The operations of UAS in urban environment inevitably raises concerns about the safety impact of UAS.

The operational characteristic of UAS is largely different from the conventional commercial aviation. which brings novel safety issues for which the safety learning process has just started. To address these novel safety issues of UAS operations, it is essential to systematically study them within a formal setting of safety risk assessment.

Safety risk assessment involves a process that comprises risk indicators, risk analysis and risk evaluation. In recent years, regulators and researcher have dedicated significant efforts to developing risk assessment for UAS operations. These approaches are largely adopted from safety risk assessment of commercial aviation. However, it is essential to recognize that UAS operations have large differences with commercial aviation. Therefore there remains shortcomings and improvements to be made to the risk assessment of UAS operations.

This thesis addresses the further development of risk assessment methods for UAS operations for Urban Air Mobility (UAM). The main risk posed by UAM is third party risk (TPR) posed to people on the ground. Therefore, the focus of this thesis is on improving risk assessment methods for ground TPR.

The first study focuses on the TPR indicators for UAS operations. Based on these TPR indicators of commercial aviation, novel TPR indicators and nine separate third party fatality terms are identified. Subsequently, current UAS regulations are evaluated regarding their coverage of these nine third party fatality terms. By doing so, the research provides a more comprehensive understanding of the overall third party risk posed by UAS operations.

The second study aims to develop a safety risk assessment method for the novel ground TPR indicators proposed in the first study. To achieve this, a Monte Carlo simulation based risk assessment approach is proposed and applied to a hypothetical UAS urban parcel delivery case. The results show that the proposed annual ground TPR model and indicators provide an accumulated understanding of the risk posed to people on the ground. The non-negligible level of uncertainty in the models adopted highlights the need for further development of more accurate sub models for UAS ground TPR assessment.

The third study aims to improve the accuracy of the common ground TPR model, where a key limitation lays in the assumption that the product of impact PoF and size of impact area are independent of each other. To address this, an improved characterization is developed and evaluated using dynamical simulation of MBS model of a UAS impacting a human body. The comparison of the novel approach to existing approaches shows significant advantages of the novel developed approach.

The fourth study applies the novel approach developed in the third study to an urban parcel delivery UAS, weighting 15kg, equipped with airbag and parachute. A key motivation is that existing models do not address the risk mitigating effects of equipping a UAS with a combination of airbag and parachute. For the UAS equipped with an airbag Multi Body System (MBS) and Finite Element (FE) models are developed. Subsequently, these models are used to assess ground TPR for different cases with and without airbag and parachute. This analysis show that the method developed in the third study is able to quantify the risk reducing effects of the combination parachute and airbag.

The four interrelated series of studies have developed novel insights and methods in Third Party Risk assessment of UAS operations. These novel insights and methods can provide enhanced safety feedback to a UAS design process, and can stimulate further development of UAS regulation.

Contents

Introduction

This chapter provides an introduction to UAS operations for Urban Air Mobility, safety issues and safety risk assessment of UAS operations. It describes the thesis focus, overall aim and objectives. Furthermore, the thesis overview will be clarified by means of short chapter descriptions which explain how each individual chapter is linked to the overall research.

1.1 UAS Operations for Urban Air Mobility

An Unmanned Aircraft (UA), also called Unmanned Aerial Vehicle (UAV) or drone is an aircraft flown without a pilot-in-command on-board. A UA is either remotely and fully controlled from another place (ground, another aircraft, space) or programmed and fully autonomous [ICAO, 2005]. When piloted remotely, an UA and its associated elements are referred to as an Unmanned Aircraft System (UAS) [ICAO, 2011]. The UAS with take-off weight less than 25 kg is referred to as Small Unmanned Aircraft System (sUAS) [FAA, 2023a].

New technologies such as the enhancement of battery technologies and electric propulsion as well as major investments made into start-ups have enabled the advancements in UAS technology and increased accessibility to UAS. The adoption of UAS has rapidly increased in recent year for a variety of applications, e.g. recreation, aerial photography, agriculture. For recreational use, UAS are becoming more accessible to hobbyist, allowing for individuals to capture unique photographs and videos. UAS equipped with high-resolution cameras and sensors have revolutionized the field of aerial photography. UAS can capture images and data from previously inaccessible or dangerous locations, providing valuable information to various industries. The technology has been widely used in fields such as real estate, environmental monitoring, inspection and journalism. For example, in agriculture, UAS have become increasingly useful in crop monitoring and pesticides spraying; this helps farmers to optimize crop yields, reduce costs, and minimize environmental impact [Merz et al., 2022]. A safety improvement application example is employment of UAS for surveillance in support of the analysis and mitigation of disaster risks for safety-critical industrial sites [Aiello et al., 2020].

The capability of UAS to transport payloads, has facilitated the development of new UAS for Urban Air Mobility (UAM) – defined as an air transportation system for passengers and cargo in and around urban environments [EASA, 2021]. In recent years, UAS have been employed for UAM applications such as medical services, parcel delivery and passenger transport. Companies like Zipline [Zipline, 2023], Antwork [Antwork, 2023], Matternet [Matternet, 2023] are exploring the use of UAS in delivering medical supplies and providing emergency medical services, improving response times and saving lives. UAS are also used for parcel deliveries to customers [JD, 2017; Amazon, 2023; Wing, 2023]. This technology promises to revolutionize the delivery industry, reducing delivery time and cost while increasing efficiency. Companies like Airbus [Airbus, 2023], Ehang [Ehang, 2023] and Volocopter [Volocop, 2023] have designed UAS for passenger transport. The potential benefits of UAS passenger transport include reducing traffic congestion, faster travel times, and improving accessibility to remote or hard-to-reach areas.

Depending on the design and application, UAS can range from a small unit to the size of a small aircraft, and can be employed in low altitude and urban environment, as well as in high altitude airspace integrated into conventional air transportation system. The estimated market size of UAM in Europe, including R&D, vehicle manufacturing, operations and infrastructure construction, will be approximately 4.2 billion EUR in 2030 [EASA, 2021]. FAA forecasted that by 2025, the yearly number of recreational and commercial UAS usage in the USA can reach 2-3 million flights per year [FAA,2021]. However, concerns have been raised about the impact of increasing UAS operations on society. Public and future UAM users' confidence and acceptance will be critical. Issues such as public safety, noise pollution, and privacy invasion have been identified as main factors in the societal acceptance of UAS operations. Among these issues, safety concerns come first. On the other hand, it is also shown that the public trust the conventional manned aviation safety levels and would be reassured if these levels were met by UAS operations [EASA, 2021].

Conventional manned aviation has reached a high level of safety [NTSB, 2021]. This is the result of decades of experience with, and lessons learned from safety events; these have strongly influenced several safety-critical processes, such as aircraft design, aircraft maintenance, air traffic management (ATM), and certification processes. The introduction of UAS into the system brings novel safety issues for which the safety learning process has just started. Novel safety issues will be posed by UAS operations with large volumes, of different aircraft types and sizes performing various tasks, and with close proximity to people. The performance envelopes of UAS also greatly differ from those for which today's air traffic procedures were designed [EUROCONTROL, 2018]. A significant challenge for regulatory authorities is the lack of well understanding of the novel safety issues posed by UAS operations. Therefore, to safely integrate UAS into our society, it is important to improve the understanding of novel safety issues posed by UAS operations.

1.2 Safety Issues of UAS Operations

Safety issues related to UAS operations can be caused by various factors, including UAS malfunctions, operator errors and environmental conditions. These factors can result in accidents such as UAS collisions with other aircraft or objects, as well as crashes of the UAS to the ground.

In considering the safety issues for UAS operation, it is important to take into account the different parties involved. In terms of societal acceptance, different parties have varying perceptions regarding their involvement with an operation, as well as the benefits and harms associated with it. This is especially important in determining the safety criteria or thresholds that should be adopted for specific operations. Understanding the perspectives of different parties and their respective safety concerns can help regulatory authorities to establish appropriate safety regulations and guidelines for UAS operations. The types of parties involved in UAS operations are [Clothier et al., 2018]:

- First parties, consisting of people and property directly associated with the operation;

- Second parties, consisting of people and property not associated with UAS operation, but directly derive benefit from the operation;

- Third parties, consisting of people and property not associated with, nor deriving direct benefit from the UAS operation.

First parties include the UAS operator and observer, as well as UAS itself. Unlike manned aviation that has crew members on-board, the first party individuals of UAS operation are not on-board and hardly exposed to the safety issues of UAS. Therefore the main consideration for the first party safety issues is the UAS itself.

Regarding second parties, UAS operations can be divided in two types: those with and without passengers on board. For UAS without passengers on board, the second party encompasses people and property being served by the UAS, such as infrastructure being inspected and people receiving delivery packages. In these cases, the safety concerns mainly revolve around property damage or injury to people in close proximity to the UAS. In contrast, for UAS with passengers on board, such as autonomous air taxi, the second party individuals on board are highly exposed to the UAS safety issues, which are at an equivalent level of conventional aviation. Safety issues for UAS operations with passengers on board include collision with other aircraft, malfunction of the UAS, and adverse weather conditions.

Regarding third parties, UAS can be divided in two types: those operating in segregated airspace and those integrated with manned aviation. For UAS operation in segregated airspace, the main safety issue is related to people and property on the ground. For UAS operation integrated with manned aviation, a significant additional safety issue is collision with other manned aircraft or with UAS carrying passengers on-board. Complementary to first, second and third party safety issues, UAS operations also create other societal issues, such as noise hindrance, as well as privacy and security issues [EASA, 2021].

In order to better understand and address these safety issues, it is essential to systematically study them within a formal setting of safety risk assessment.

1.3 Safety Risk Assessment

Safety risk assessment involves a process that comprises risk indicators, risk analysis and risk evaluation. The aim of the analysis part is to examine the safety risk of a safety-critical operation using domain-specific risk indicators. Subsequently, in risk evaluation, the outcomes of the risk analysis are compared against predefined risk criteria. If the level of risk exceeds the risk criteria, risk mitigation strategies can be developed and implemented to reduce the risk to an acceptable level.

Safety Risk Analysis

Safety risk analysis of a safety-critical operation typically addresses the following three questions [Rausand, 2011]:

    i.   What may happen? (Hazards)

    ii. What is the likelihood of happening? (Probability)

    iii. What are the consequences? (Severity)

Safety risk analysis is a process to answer the above questions, i.e. to identify hazards, to evaluate the probability and severity of the hazards of a safety-critical operation. Probability and severity of a safety-critical operation are commonly measured in terms of well-developed safety risk indicator.

The overall risk R of an operation satisfies a summation over all hazard types:

$$R = \sum_h P\{h\} \cdot R_h$$

where $P\{h\}$ is the probability of hazard type h, and R_h is the conditional risk given hazard type h.

This equation shows that there are two approaches in conducting a safety risk analysis:

    i.   To quantify $P\{h\}$ and R_h per hazard type, followed by a summation over all hazard types;

    ii. To develop a model of the operation that covers all hazard types, and to use this model to quantify the overall risk R of the operation.

Both approaches are in use for commercial aviation. The first approach is common practice in airworthiness certification, e.g. [FAA, 2011]. The second approach is common practice in mid-air collision risk quantification [ICAO, 2002].

Safety Risk Indicators

The definition of R follows from the specific choice of Safety Risk Indicator(s). A risk indicator is defined as a mathematical function of the probability of an event and the consequences of that event [Jonkman et al., 2003]. In commercial aviation, examples of safety risk indicators are "probability of accident per operation", "probability of fatal accident per operation" [Boeing, 2022; IATA, 2022; NTSB, 2021] and "probability of Mid Air Collision (MAC) per operation" [ICAO, 2002], with "operation" referring to "flight" or "flight hour"

Safety Risk Criteria

Outcomes of a safety risk analysis for relevant risk indicators are then compared with risk criteria established by regulatory authorities. Each safety risk criterion applies to a specific safety risk indicator. There are two approaches in defining safety risk criteria: i) for overall risk R, and ii) for the combination of $P\{h\}$ and R_h per hazard type.

The establishment of risk criteria forms a comprehensive process, requiring regulatory decisions that are based on research contributions and public feedback. An implicit part of this process is to select the right safety risk indicators and to develop method for their safety risk analysis.

1.4 Existing UAS Safety Risk Indicators, Criteria and Analysis

In this section, the existing UAS safety risk indicators, criteria, and analysis methods are reviewed. Also, a review is given how these are used in regulatory UAS safety risk assessment frameworks.

UAS Safety Risk Indicators

In UAS literature [e.g. Clothier et al., 2007; Melnyk et al., 2014; la Cour Harbo, 2019; la Cour Harbo and Schiøler, 2019; Kim, 2019] and regulations [JARUS, 2015, 2019; FAA, 2019], safety risk indicators for UAS operations have been identified for two types of safety risk: i) air risk, and ii) ground risk. Air risk is the safety risk posed by UAS to other flights (UAS, commercial aviation, or general aviation). Ground risk is the safety risk posed to third parties on the ground.

Regarding air risk, for overall risk of UAS operations, the developed safety risk indicators are:

- "Probability of losing detect and avoid functions per UAS flight hour" [JARUS, 2015];

- "Probability of Mid Air Collision (MAC) with other aircraft (manned or unmanned) per UAS flight hour" [JARUS, 2015];

- "Probability of MAC with manned aircraft per UAS flight hour" [JARUS, 2017; la Cour Harbo and Schiøler, 2019].

In support of a UAS airworthiness certification process, [FAA, 2019] has adopted safety risk indicators per hazard type, where the severity includes possible fatalities on the ground.

Regarding ground risk, only one common safety risk indicator has been adopted: the "Expected number of ground fatalities per UAS flight hour" [Clothier et al., 2007; Melnyk et al., 2014; Breunig et al., 2018; JARUS, 2019; Kim, 2019; la Cour Harbo, 2019].

UAS Safety Risk Criteria

For UAS operations, a widely used principle in deriving UAS safety risk criteria is Equivalent Level of Safety (ELOS). The ELOS principle is to use statistical accident data from commercial aviation to set risk criteria value for UAS operations. This means that for ELOS two steps have to be adopted: 1) to choose a suitable Risk Indicator; and 2) to identify requirements or accident statistics from commercial aviation that allow to assess the Risk Criteria for the safety Risk Indicator from step 1).

Regarding air risk, for the risk indicator "Probability of losing detect and avoid functions per UAS flight hour", the risk criterion is commensurate with that of a large transport aircraft, giving a probability of 10^{-7} per UAS flight hour [JARUS, 2015]. For the risk indicator "probability of Mid Air Collision (MAC) with other aircraft (manned or unmanned) per UAS flight hour". Risk criterion of 10^{-9} per UAS flight hour is used. [JARUS, 2015].

Regarding ground risk, for the risk indicator of "expected number of fatalities per UAS flight hour", risk criterion values have been assessed from historical involuntary ground fatalities in conventional commercial aviation [Grimsley, 2004; Clothier and Walker, 2006]. This leads to risk criterion values ranging from 10^{-6} to 7.6×10^{-8} fatalities per UAS flight hour; the lower value has been proposed by [JARUS, 2017].

UAS Safety Risk Analysis

Regarding air risk analysis, [la Cour Harbo and Schiøler, 2019] proposed a quantitative method to analyse the probability of MAC between UAS and General Aviation (GA) aircraft. The method assumes that flight directions and geographical positions of UAS and GA aircraft are uniformly distributed in the predefined area. The probability of MAC is determined based on product of four terms: the probability of horizontal collision, the probability of vertical collision, the probability of GA aircraft operating below altitude threshold and the effectiveness of mitigations.

Regarding ground risk analysis, one quantitative method has been developed [Clothier et al., 2007; Melnyk et al., 2014] and widely adopted [Ancel et al., 2017; Bertrand et al., 2017; la Cour-Harbo, 2019; Primatesta et al., 2020; Shao, 2020]. This method evaluates ground TPR using a product of five terms: UAS failure rate, population density of the overflown area, probability of ground person being sheltered, size of the impact area of the crashing UAS, and the Probability of Fatality (PoF) in case a human is hit in the impact area.
Analytical sub-models have been developed for each of these five terms. For the UAS failure rate, various models have been developed, such as Fault Tree Analysis (FTA) [Reimann et al., 2014], Failure Modes Effects Analysis (FMEA) [Freeman et al., 2014], Bayesian Belief Network (BBN) [Barr et al., 2017, Han et al., 2022], and Petri nets [Goncalves et al., 2017]. Accident reports [Schaefer, 2003] and expert knowledges [Murtha, 2009] are also used for the estimation of UAS failure rate. For the crash impact area, the models vary from a weight-based area model [Ale and Piers, 2000], to a planform area model [Weibel & Hansman, 2004], and a gliding area model [RCC, 2001]. For the PoF of impact, one model stems from the injury model derived from explosive [RCC, 2000, 2001]; another model stems from blunt force experimental data [Magister, 2010]. The models adopted for impact PoF and crash impact area produce a large variation of outcomes [Melnyk et al., 2014; Washington et al., 2017].

Regulatory UAS Safety Risk Assessment Frameworks

Regulators had to adopt UAS risk assessment frameworks while research is ongoing. Existing UAS regulatory frameworks distinguish low-risk, medium-risk, and high-risk UAS categories. In Europe, these are defined as Open, Specific and Certified categories

respectively [EASA, 2015]. In USA, these are defined as Recreational, Under Part 107 rule and Advanced categories respectively [FAA, 2023b]. The high-risk category includes UAS that pose a level of risk similar to manned aviation. The medium-risk category typically addresses UAS, often weighting less than 25kg, for which risk assessment is needed. For the low-risk category UAS, no risk assessment is required.

For the high-risk categories of UAS operation, risk indicators and analysis methods from airworthiness certification process of manned aircraft are adopted [NATO, 2007; JARUS, 2015; FAA, 2019]. [JARUS, 2015] adopts risk criteria from conventional commercial aircraft for equivalent classes of UAS. [FAA, 2019] and [NATO, 2007] adopt for airworthiness certification a matrix from commercial aviation, showing combinations of frequency and severity that define hazard types to be acceptable or not.

For medium-risk categories of UAS operation, [JARUS, 2019] developed the Specific Operations Risk Assessment (SORA) method. Both for air risk and ground risk, SORA adopts qualitative assessment approaches.

1.5 Discussion and Focus of The Thesis

Although significant research has been dedicated to developing risk indicators, risk criteria and risk analysis methods for UAS operations, need for further improvements remain. These needs are discussed below; first for safety risk indicators, then safety risk analysis, and finally for safety risk criteria.

Regarding safety risk indicators, there are two important shortcomings:

- Existing UAS ground risk indicators do not take into account that the risk posed to persons at a specific ground location, depends on the annual amount of UAS overflying this specific location.
- Existing UAS air risk indicators do not differentiate between UAS with or without on-board passengers.

Regarding safety risk analysis, different limitations apply to ground risk and air risk. The common model adopted for ground risk has important limitations:

- One notable drawback is the lack of validation of the developed sub-models for UAS impact.
- Furthermore, it is shown that there is a significant diversity in the parametric models for impact PoF and for crash impact area [Melnyk et al., 2014; Washington et al., 2017].
- In recent years, researchers have started to utilize dynamical modelling and simulation approach for impact risk analysis, employing Finite Element (FE) model [Koh et al., 2018; Arterburn et al., 2017, 2019; Weng et al., 2021] and Multi Body System (MBS) model [Rattanagraikanakorn et al., 2019, 2020a,b, 2022]. The dynamical simulation has demonstrated the ability to produce risk results that align with experimental tests. However, these dynamical simulation approaches remain to be integrated with risk analysis.

For air risk, safety risk analysis methods do not make proper distinction between second and third parties in the air. Similar as for ground risk, an additional shortcoming is that the annual number of UAS flights in an airspace area are not considered in the existing safety risk analysis methods. The importance of both shortcomings will increase with the future expected increase of passenger UAS flights.

Regarding <u>safety risk criteria</u>, the existing ones consider for UAS operation only the unit of UAS flight hour. Similarly, as has been identified for safety risk indicators and safety risk analysis, this poses important limitations regarding air risk and ground risk.

It can be concluded that existing UAS safety risk assessment approaches are largely adopted from airworthiness certification and ground fatality statistics per flight hour of a conventional commercial aircraft. However, it is essential to recognize that UAS operations have large differences with commercial aviation in terms of aircraft characteristics, operation environment, task types, and commercial incentives to operate in urban areas.

1.6 Overall Aim and Objectives of This Thesis

This thesis addresses the further development of risk assessment methods for UAS operations for Urban Air Mobility (UAM). Future UAM is expected to involve high operational volumes in urban areas. The main risk posed by UAM is third party risk (TPR) posed to people on the ground. Therefore, the focus of this thesis is on improving risk assessment methods for ground TPR. During the thesis work, it was found that relevant experimental data was available for small UAS; for this reason, the application examples typically are for small UAS.

From a research perspective, it is important to gain an in-depth understanding of existing literature on safety risk of UAS operations, and to further improve this understanding for UAS operations in urban environments. This improved understanding of safety risk of UAS operations will provide regulators and other parties with enriched information in further improving the regulatory framework. Therefore the overall aim of this thesis is:

To improve the understanding and analysis of safety risk posed by UAS operations for UAM

To achieve this overall aim, a series of objectives are addressed in the subsequent chapters:

Objective 1: To identify TPR indicators for UAS operations

In literatures TPR indicators for UAS operations are not yet well established. In commercial aviation such TPR indicators has been well developed in the form of individual risk and collective risk. As UAS is a new type of operation integrated into the conventional airspace, it is logical to extend the TPR indicators from commercial aviation to UAS operation.

Objective 1 is addressed in Chapter 2. Firstly, reviews are made of existing TPR indicators in use for annual commercial flights around an airport. Based on these TPR indicators of commercial aviation, novel TPR indicators and nine separate third party fatality terms are identified. Subsequently, current UAS regulations are evaluated regarding their coverage of these nine third party fatality terms. The conclusion is that for most current regulations the nine third party fatality terms are partially covered, and none of them consider the accumulation of risk by multiple UAS flights.

Objective 2: To develop a safety risk assessment approach for the novel ground TPR indicators identified in chapter 2

Literature on safety risk analysis primarily focuses on ground TPR posed by a single UAS flight. However, as shown in chapter 2, there is also need for indicators of ground TPR that are posed by multiple UAS flights over a specific area during a given time period, such as a year. Objective 2 is to develop a safety risk assessment method for these novel ground TPR indicators, and to illustrate its application to a UAS based parcel delivery operation.

Objective 2 is addressed in Chapter 3. A Monte Carlo simulation based risk assessment approach is developed for the indicators of ground TPR that are posed by the annual UAS flights over a given area. This simulation-based assessment method is applied to a hypothetical UAS urban parcel delivery case, and compared to ground TPR of a single UAS flight. The results show that from a societal perspective, the proposed annual ground TPR model and indicators provide an accumulated understanding of the unsafety posed to people on the ground, rather than the established UAS flight hour oriented ground TPR indicator.

Objective 3: To enhance the commonly adopted ground TPR model and its assessment through dynamical simulation of a Multi Body System (MBS) model

A key limitation of the common ground TPR model is the assumption that the product of impact PoF and size of impact area are independent of each other. This assumption is not valid, as the laboratory controlled impact experiments have shown that the impact PoF is highly dependent of the impact geometries between UAS and human [Arterburn et al, 2017; Campolettano et al., 2017; Koh et al., 2018; Arterburn et al., 2019]. To address this limitation, there is a need for an improved mathematical model for UAS TPR.

Objective 3 is addressed in Chapter 4. An improved characterization is proposed, that replaces the product of crash impact area and impact PoF with an integration over risk values for different locations of a human relative to the UAS crash centre, and taking into consideration of various impact geometries (UAS attitude, human face direction, etc.). The proposed model is evaluated using dynamical simulation of MBS model of a UAS impacting on human body. The comparison of proposed model to common model results shows that the common model overestimates the risk up to two orders in magnitude.

Objective 4: **To evaluate the effect of risk mitigation measures implementing the enhanced TPR model with dynamical simulation approach**

UAS operations are considered not (yet) safe enough to be allowed to operate in urban areas with high population density. To abridge this safety gap, further UAS developments have been proposed, such as designing more reliable UAS, risk aware path planning, and use of risk mitigation measures of parachute and airbag. Among the developments, the effect parachute combined with airbag haven't been explored. Such exploration becomes possible with the enhanced TPR model and dynamical simulation risk analysis methodology developed in Chapter 4.

Objective 4 is addressed in Chapter 5 where a 15kg urban parcel delivery UAS with airbag and parachute systems is considered. The ground TPR of the UAS is evaluated adopting the enhanced TPR model with dynamical simulation. Risk is assessed for different cases with or without airbag and parachute. The obtained results shows that a combination of parachute and airbag may provide effective risk mitigation for use of a 15 kg delivery UAS.

1.7 Recommended Reading of This Thesis

Figure 1.1 shows the recommended reading paths for this thesis. Each chapter can be read on its own and each are published articles with fully written story line. There are two research line within this thesis. Chapter 3 is based on the novel ground TPR indicators proposed in Chapter 2. Chapter 5 adopts the improved ground TPR model from Chapter 4. Chapter 6 draws conclusions.
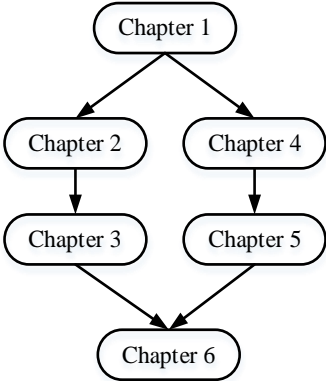
Figure 1.1 The recommended reading paths for this thesis

In reading chapters 2 through 5, one should be aware that these are copied from published papers. Hence, in these chapters no reference is made to preceding chapters in this thesis, instead reference is made to the published papers:

Chapter 2: "Third party risk indicators and their use in safety regulations for UAS operations"

Paper with the same title has been published in the Proceedings of 2020 AIAA Conference [Jiang et al., 2020].

Chapter 3: "Third party risk modelling of unmanned aircraft system operations with application to parcel delivery service"

Paper with the same title has been published in the journal Reliability Engineering and System Safety [Blom et al., 2021]

Chapter 4: "Improved characterization of third party risk posed by UAS flights to ground population"

Paper with the same title has been submitted to the journal Risk Analysis in January 2023. [Jiang et al., 2023]

Chapter 5: "Effect of Parachute and Airbag in Reducing Safety Risk Posed by Small UAS to People on the Ground"

Paper with the same title has been submitted to the journal Transportation Research Interdisciplinary Perspectives in August 2023 [Jiang et al., 2023]

References

Aiello, G., Hopps, F., Santisi, D., & Venticinque, M., 2020. The employment of unmanned aerial vehicles for analyzing and mitigating disaster risks in industrial sites. IEEE transactions on engineering management, 67(3), 519-530.

Airbus, 2023, Urban Air Mobility, URL: https://www.airbus.com/en/innovation/low-carbon-aviation/urban-air-mobility [retrieved 20th, July, 2023]

Ale, B. J. M., & Piers, M. (2000). The assessment and management of third party risk around a major airport. Journal of hazardous materials, 71(1-3), 1-16.

Amazon, 2023, Amazon Prime Air prepares for drone deliveries, URL: https://www.aboutamazon.com/news/transportation/amazon-prime-air-prepares-for-drone-deliveries [retrieved 20th, July, 2023]

Antwork, 2023, Antwork Introduction, URL: https://www.antwork.link/introduction.html [retrieved 20th, July, 2023]

Arterburn, D., M. Ewing, R. Prabhu, F. Zhu, D. Francis, 2017. UAS Ground Collision Severity Evaluation, ASSURE Task A4 Final Report. FAA UAS Center of Excellence. , URL: https://www.assureuas.org/projects/completed/a4/ASSURE_A4

Arterburn, D., G. Olivares, J. Bolte, R. Prabhu and S. Duma, 2019. UAS Ground Collision Severity Evaluation 2017-2019, ASSURE Task A14 Final Report. FAA, Atlamtic City, NJ, URL: https://www.assureuas.org/projects/completed/a14/ASSURE_A14

Barr, L. C., Newman, R., Ancel, E., Belcastro, C. M., Foster, J. V., Evans, J., & Klyde, D. H., 2017. Preliminary risk assessment for small unmanned aircraft systems. In 17th AIAA Aviation Technology, Integration, and Operations Conference (p. 3272).

Bertrand, S., Raballand, N., Viguier, F., & Muller, F., 2017. Ground risk assessment for long-range inspection missions of railways by UAVs. In 2017 International Conference on Unmanned Aircraft Systems (ICUAS) (pp. 1343-1351). IEEE.

Blom H A P, Jiang C, Grimme W B A, Mitici M, & Cheung Y S, 2021. Third party risk modelling of Unmanned Aircraft System operations, with application to parcel delivery service. Reliability Engineering & System Safety, 2021: 107788. Volume 214

Boeing, 2022, Statistical summary of commercial jet airplane accidents, August, 2022.

Breunig, J., Forman, J., Sayed, S., Audenaerd, L., Branch, A., & Hadjimichael, M., 2018, Modeling risk-based approach for small unmanned aircraft systems. MITRE CORP MCLEAN VA.

Clothier, R., & Walker, R., 2006, Determination and evaluation of UAV safety objectives. In Proceedings of the 21st international conference on unmanned air vehicle systems (pp. 18-1). University of Bristol.

Clothier, R., Walker, R., Fulton, N., & Campbell, D., 2007. A casualty risk analysis for unmanned aerial system (UAS) operations over inhabited areas. In Proceedings of AIAC12: 2nd Australasian Unmanned Air Vehicles Conference (pp. 1-16). Bristol UAV Conference.

Clothier, R. A., Williams, B. P., & Hayhurst, K. J., 2018. Modelling the risks remotely piloted aircraft pose to people on the ground. Safety science, 101, 33-47.

EASA, 2015, Concept of Operations for Drones: A risk based approach to regulation of unmanned aircraft, European Union Aviation Safety Agency

EASA, 2021, Study on the societal acceptance of Urban Air Mobility in Europe, European Union Aviation Safety Agency, 19th, May, 2021

Ehang, 2023, Passenger transportation an logistics, URL: https://www.ehang.com/uam/ [retrieved 20th, July, 2023]

EUROCONTROL, 2018, UAS ATM Integration Operational Concept. European Organisation for the Safety of Air Navigation. Edition: 1.0. 27th, Nov, 2018.

FAA, 2011, AC 23.1309-1E: System Safety Analysis and Assessment for Part 23 Airplanes, Federal Aviation Administration.

FAA, 2019. *FAA Safety Management System Manual*. Federal Aviation Administration Air Traffic Organization. April, 2019.

FAA, 2021, Aerospace Forecast Fiscal Years 2021–2041. Federal Aviation Administration

FAA, 2023a, Part 107 of CFR 14 - Small Unmanned Aircraft System. Federal Aviation Administration, URL: https://www.ecfr.gov/current/title-14/chapter-I/subchapter-F/part-107 [retrieved 7th, July, 2023].

FAA, 2023b, "Drones". Federal Aviation Administration, URL: https://www.faa.gov/uas [retrieved 20th, July, 2023]

Freeman, P., & Balas, G. J., 2014. Actuation failure modes and effects analysis for a small UAV. Proceedings of 2014 IEEE American Control conference, pp. 1292-1297.

Grimsley, F., 2004, Equivalent safety analysis using casualty expectation approach. In AIAA 3rd" Unmanned Unlimited" Technical Conference, Workshop and Exhibit (p. 6428).

Han, P., Yang, X., Zhao, Y., Guan, X., & Wang, S., 2022. Quantitative ground risk assessment for urban logistical unmanned aerial vehicle (UAV) based on Bayesian network. Sustainability, 14(9), 5733.

IATA, 2023, IATA releases 2022 airline safety performance, International Air Transport Association, 7th March 2023.

ICAO, 2002, Manual on airspace planning methodology for the determination of separation minima. Doc. 9689-AN/953, amended version, August 2002, Montreal Canada, International Civil Aviation Organization, tech. rep., 2002

ICAO, 2005, Global Air Traffic Management Operational Concept. Doc 9584. International Civil Aviation Organization.

ICAO, 2011, Unmanned Aircraft Systems (UAS). Circular 328-AN/190. International Civil Aviation Organization.

JARUS, 2015, "AMC RPAS.1309: Safety Assessment of Remotely Piloted Aircraft Systems," Joint Authorities for Rulemaking of Unmanned Systems, Issue: 2, Nov, 2015.

JARUS, 2017, JARUS guidances on Specific Operations Risk Assessment (SORA), Edition: 1.0.

JARUS, 2019, JARUS guidances on Specific Operations Risk Assessment (SORA), Edition: 2.0.

JD, 2017, Drone delivery program, JD.com, Inc. May, 2017

Jiang C., Blom H.A.P., Sharpanskykh A., 2020. Third Party Risk Indicators and their use in safety regulations for UAS operations. Proceedings AIAA Aviation Forum 2020, 10.2514/6.2020-2901.

Jiang C, Blom H.A.P., Rattanagraikanakorn, B., 2023. Improved characterization of Third Party Risk posed by UAS flights to ground population, Submitted to Risk Analysis, January 2023.

Jiang C, Blom H. A. P., Rattanagraikanakorn, B., 2023. Effect of parachute and airbag in reducing safety risk posed by small UAS to people on the ground. Submitted to Transportation Research Interdisciplinary Perspectives, August 2023.

Jonkman SN, Van Gelder PHAJM, Vrijling JK. An overview of quantitative risk measures for loss of life and economic damage. J Hazard Mater 2003;A99:1–30.

Kim, S. H., 2019, Third-party risk of mid-air collision between small unmanned aircraft systems. In AIAA Aviation 2019 Forum (p. 3052).

Koh, C. H., Low, K. H., Li, L., Zhao, Y., Deng, C., Tan, S. K., Chen, Y., Yeap, B. C., & Li, X., 2018. Weight threshold estimation of falling UAVs (Unmanned Aerial Vehicles) based on impact energy. Transportation Research Part C: Emerging Technologies, 93, 228-255. doi:https://doi.org/10.1016/j.trc.2018.04.021

la Cour-Harbo, A., 2019, Quantifying Risk of Ground Impact Fatalities for Small Unmanned Aircraft. Journal of Intelligent & Robotic Systems, 93(1), 367-384. doi:10.1007/s10846-018-0853-1

la Cour-Harbo, A., & Schiøler, H., 2019, Probability of Low-Altitude Midair Collision Between General Aviation and Unmanned Aircraft. Risk Analysis, 39(11), 2499-2513.

Magister, T., 2010, The small unmanned aircraft blunt criterion based injury potential estimation. Safety science, 48(10), 1313-1320.

Matternet, 2023, On-demand delivery platform, URL: https://mttr.net/product [retrieved 20th, July, 2023]

Melnyk, R., Schrage, D., Volovoi, V., & Jimenez, H. (2014). A third-party casualty risk model for unmanned aircraft system operations. Reliability Engineering & System Safety, 124, 105-116

Merz, M., Pedro, D., Skliros, V., Bergenhem, C., Himanka, M., Houge, T., Martos-Carvalho, J. P., Lundkvist, H., Curuklu, B., Hamren, R., Ameri, A. E., Ahlberg, C.,. & Johansen, G., 2022. Autonomous UAS-based agriculture applications: general overview and relevant European case studies. Drones, 6(5), 128.

Murtha, J. F., 2009. An evidence theoretic approach to design of reliable low-cost UAVs (Doctoral dissertation, Virginia Tech).

NATO, 2007, UAV Systems Airworthiness Requirements (USAR), STANAG 4671, North Atlantic Treaty Organization.

NTSB, 2021, Aviation accident statics 2002-2021, National Transportation Safety Board.

Rattanagraikanakorn, B., Schuurman, M., Gransden, D.I., Happee, R., De Wagter, C., Sharpanskykh, A., & Blom, H.A.P., 2019. Modelling Head Injury due to Unmanned Aircraft Systems Collision: Crash Dummy vs Human Body, Proc. 19th AIAA Aviation Technology, Integration, and Operations Conference (ATIO2019), June 2019, Dallas, TX, 10.2514/6.2019-2835.

Rattanagraikanakorn, B., Gransden, D. I., Schuurman, M., De Wagter, C., Happee, R., Sharpanskykh, A., & Blom, H.A.P., 2020a. Multibody system modelling of unmanned aircraft system collisions with the human head. International Journal of Crashworthiness, 25(6), 689-707.

Rattanagraikanakorn, B., Blom, H.A.P., Sharpanskykh, A., De Wagter, C., Jiang, C., Schuurman, M. J., Gransden, D. I., & Happee, R., 2020b. Modeling and Simulating Human Fatality due to Quadrotor UAS Impact. Proceedings of AIAA AVIATION 2020 FORUM. June 2020, 10.2514/6.2020-2902.

Rattanagraikanakorn, B., 2022, Modelling Collision Consequences of Unmanned Aircraft Systems on Human, PhD thesis.

Rausand, M., 2011, Risk Assessment–Theory, Methods, and Applications. John Wilwy & Sons. Inc., Hoboken, New Jersey. Volocopter, 2023

RCC, 2000, Common risk criteria for National test ranges; Inert debris, Supplement to Standard 321-00. Range Commanders Council.

RCC, 2001, Range Safety criteria for Unmanned Air Vehicles, Rationale and methodology supplement. Supplement to Document 323-99, Range Commanders Coucil, April 2001.

Reimann, S., Amos, J., Bergquist, E., Cole, J., Phillips, J., & Shuster, S., 2013. UAV for Reliability. Aerospace Vehicle Design. AEM, 4331.

Schaefer, R., 2003. Unmanned aerial vehicle reliability study. Office of the Secretary of Defense, Washington, DC, 4-5.

Shao, P. C., 2020. Risk assessment for UAS logistic delivery under UAS traffic management environment. Aerospace, 7(10), 140.

Washington, A, Clothier, R.A., Silva, J., 2017, A review of unmanned aircraft system ground risk models, Progress in Aerospace Sciences, Vol. 95, pp. 24-44.

Weibel, R., & Hansman, R. J., 2004, Safety considerations for operation of different classes of UAVs in the NAS. Unmanned Unlimited, Technical Conf., Workshop and Exhibit, 20-23 Sept. 2004, Chicago, IL, AIAA-2004-6421, pp. 1-11.

Weng, Y. B. Bian, K. Gunasekaran, J. Gholipour, C. Vidal and H. Mao, 2021. Modelling Small Remotely Piloted Aircraft System to Head Impact for Investigating Craniocerebral Response, J. of Biomechanics, doi:https://doi.org/10.1016/j.jbiomech.2021.110748

Wing, 2023, Drone delivery, URL: https://wing.com/ [retrieved 20th, July, 2023]

Zipline, 2023, Instant delivery & logistics, URL: https://www.flyzipline.com/ [retrieved 20th, July, 2023]

2

Third Party Risk Indicators and Their Use in Safety Regulations for UAS Operations

Use of Unmanned Aircraft Systems (UAS) is growing rapidly around the world. Very different types of UAS are used for applications such as aerial photography, inspection, emergency and Urban Air Mobility (UAM), operating in low altitude and urban environment, as well as in high altitude airspace integrated with the conventional air transportation system. As a new airspace user, UAS brings novel safety challenges to the current aviation system. For current aviation the main safety issues concern first and second parties, i.e. lives and property of crew and passengers. In contrast, the main safety concern of UAS operations is third party risk (TPR), i.e. the risk posed to people and properties that have no responsibility for the UAS operation and neither benefit in some way from the UAS operation. In order to ensure the safe operation of UAS, there is a need for an evaluation of safety regulation developments for UAS operations against relevant TPR indicators. The aim of this paper is to identify relevant TPR indicators for UAS operations and to evaluate safety regulations against these TPR indicators. The main finding is that current UAS safety regulations do not consider the accumulation of TPR contributions from many UAS flights per annum over rural or urban populations.

Nomenclature

ARC   = Air Risk Class
ATC   = Air Traffic Control
ATO   = Air Traffic Organizations
CAT   = Commercial Air Transport
ConOps = Concept of Operations
GA   = General Aviation
GRC   = Ground Risk Class
OSO   = Operational Safety Objectives
RPAS   = Remotely Piloted Aircraft System
SAIL   = Specific Assurance and Integrity Levels
SORA   = Specific Operations Risk Assessment
SRM   = Safety Risk Management
TPR   = Third Party Risk
UA   = Unmanned Aircraft
UAM   = Urban Air Mobility
UAS   = Unmanned Aircraft System

2.1 Introduction

Unmanned Aircraft System (UAS) - including Remotely Piloted Aircraft System (RPAS) and automated air vehicles - are increasingly becoming a part of our day-to-day lives. The major driver of this development is that UAS can be employed for novel operations – e.g. recreation, aerial photography, emergency, inspection, urban air transport, long distance cargo transport – both in low altitude and urban environment, as well as in high altitude airspace integrated with the current air transportation system. Depending on the design, UAS can range from a small unit to the size of a small aircraft. Having UAS as part of daily operations is getting closer to reality as the immense effort has been put into developing UAS Concept of Operations (ConOps), rules, regulations and supporting infrastructures that are crucial to a safe operation [1].

The current aviation system has become so safe due to the contributions of many factors such as initial airworthiness (design, manufacturing quality), continuing airworthiness (maintenance) and operational approvals, Air Traffic Management (ATM), airborne safety nets, cockpit automation, etc. Moreover, an overarching factor is that all this has been reached thanks to decades of evolutionary developments that benefitted from feedback from experience and the diligent application of lessons learned from safety events. The introduction of UAS brings uncertainties into the system, with a large number of flights, of different types and sizes for various tasks, and with performance envelopes greatly different from those for which today's air traffic procedures were designed [1].

For current aviation the main safety issues concern first and second parties, i.e. lives and property of crew and passengers. In contrast, the main safety concern of UAS operations is third party risk (TPR), i.e. the risk posed to people and properties that have no responsibility for a UAS flight and neither benefit in some way from a UAS flight. In order to ensure the safe operation of UAS, there is a need to identify relevant TPR indicators for UAS operations and to evaluate safety regulation for UAS operations against these TPR indicators. An early study of this type has been conducted by [2], however significant UAS regulations updates have been developed since then [3]. The aim of this paper is to develop relevant TPR indicators for UAS

operations and to compare EASA/JARUS and FAA safety regulations against these TPR indicators.

The paper is organized as follows. Section 2.2 reviews existing TPR indicators, and use this to identify relevant TPR indicators and TPR fatality terms for UAS operations. Section 2.3 reviews the safety regulations from EASA/JARUS and FAA. Section 2.4 evaluates these regulations against the relevant TPR indicators and third party fatality terms identified in section 2.2. Section 2.5 draws conclusions.

2.2 Relevant TPR Indicators and TPR Fatality Terms

This section starts with a review of relevant TPR indicators in use for commercial aviation. Subsequently these indicators are used as a basis for the definition of relevant TPR indicators for UAS operations, as well as the relevant TPR fatality terms. This approach differs from a straightforward application of TPR indicators in commercial aviation to UAS operation, e.g. [2].

2.2.1 TPR indicators in commercial aviation

In commercial aviation [4] first party is the aviation personnel (who provide the air transportation service); second party are the passengers (for whom the air transportation is provided); third party are the people exposed for reasons unrelated to the flight, for instance people living in the airport vicinity. Common indicators for TPR in commercial aviation are Individual Risk, Collective Risk and the so-called FN curve for societal risk, e.g. [5,6].

Individual risk $R_I(s)$ of commercial air transport is defined as: *"The probability that an average unprotected person, who resides permanently at ground location s, would get killed due to the direct consequences of aircraft accidents during a given annum."* It should be noted that the Individual risk indicator is population-independent, i.e. it does not make any difference if a ground location *s* is in a wasteland or in the center of a large city. Individual risk defines iso-risk contours that can be used for zonal policies regarding any current or future use of an (urban) area that is exposed to non-negligible Individual risk levels. For example, in The Netherlands the maximum acceptable level of $R_I(s)$ is 10^{-6} per annum for populated areas around hazardous installations, transport routes and airports [7].

Collective risk R_C is the expected number of third party fatalities $R_C = E\{n_F\}$ in a given area *X* due to the direct consequences of aircraft flight accidents during a given annum [8]. If there are *N* flights to happen in a given annum then we know [9]:

$$R_C = E\{n_F\} = \sum_{i=1}^{N} E\{n_F^i\} = \sum_{i=1}^{N} R_C^i \tag{1}$$

with $R_C^i = E\{n_F^i\}$ the expected number of third party fatalities due to a potential accident of the *i*-th flight.

In commercial aviation, another well-established societal risk indicator is the FN curve $R_{FN}(n)$:

$$R_{FN}(n) \triangleq P\{n_F \geq n\}, \text{ for } n \geq 1 \tag{2}$$

which reads in words, e.g. [9]: *"The probability that a group of n or more third party persons will be fatally injured due to the direct consequences of aircraft accidents during a given annum."*

Some literature sources, e.g. [5] refer to *"more than n"* in this definition, which defines $R_{FN}^{>}(n)$ as follows:

$$R_{FN}(n) \triangleq P\{n_F \geq n\} = R_{FN}(n+1), \text{ for } n \geq 0 \tag{3}$$

The relation between the FN curve $R_{FN}(n)$ and collective risk $R_C = E\{n_F\}$ has been well established, e.g. [9]:

$$R_C = E\{n_F\} = \sum_{n=1}^{\infty} R_{FN}(n) = \sum_{n=0}^{\infty} R_{FN}^{>}(n) \tag{4}$$

[5] explains that the FN curve $R_{FN}(n)$ is used in various countries to express and limit third party risks, predominantly of hazardous installations. Regulation in these countries typically adopts an $R_{FN}(n)$ limiting criterion of the following form:

$$R_{FN}(n) < C/n^{\alpha} \tag{5}$$

where α is the steepness of the limit line and C a constant that determines the position of the limit line. A steepness $\alpha = 1$ is called risk neutral (e.g. in UK); a steepness $\alpha = 2$ is called risk averse (e.g. in the Netherlands). In the latter case larger accidents are weighted more heavily and are thus only accepted with a relatively lower probability. The different views regarding risk aversion parameter α make $R_{FN}(n)$ less useful as a common risk indicator than Collective risk $R_C = E\{n_F\}$ [10].

2.2.2 TPR indicators for UAS

For UAS operations, risks involved with first, second and third parties are defined as follows [11]. First party risk applies to people and property directly associated with the UAS operation (e.g. pilot, Unmanned Aircraft itself). Second party risk applies to people and property not associated with the UAS operation, but directly derive benefit from the UAS operation (e.g. passenger on-board, infrastructure being inspected, parcel being delivered). Third party risk applies to people and property not associated with, nor deriving direct benefit from the UAS operation.

By comparing this definition of first, second and third parties with those in commercial aviation, some differences can be observed. Although these differences may look futile at first impression, they do have significant consequences. To make this explicit let's compare first, second and third party fatalities for the following two mid-air collisions: i) mid-air between two commercial aircraft; vs. ii) mid-air of a UAS to a commercial aircraft. In case i), first party fatalities may be among the crew of the two aircraft, second party fatalities may be among the passengers on-board the two aircraft, and third party fatalities may be among persons on the ground if one or both aircraft crash to the ground. In case ii) there typically are no first or second party fatalities for the UAS operation; instead all on-board fatalities among crew and passengers of the commercial flight are third party fatalities, which add to fatalities on the ground if the UAS and/or the commercial aircraft crash to the ground. These significant differences in third party fatalities for these two cases, illustrate the need to explicitly define TPR indicators for UAS operations.

For a commercial UAS operation involving many flights we define the following three TPR indicators: Collective risk, Collective ground risk, and Individual risk as follows:

Collective risk R_C of UAS operations is defined as: *"The expected number of third party fatalities in a given area X due to the direct consequences of UA flight accidents during a given annum."*

Collective ground risk $R_{Cground}$ of UAS operations is defined as: *"The expected number of third party fatalities on the ground in a given area X due to the direct consequences of UA flight accidents during a given annum."*

Individual risk $R_I(s)$ of UAS operations is defined as: *"The probability that an average unprotected person, who resides permanently at ground location s, would get killed or fatally injured due to the direct consequences of UA flight accidents during a given annum."*

For each of these TPR indicators we denote the contribution by the i-th UA flight as R_C^i, $R_{Cground}^i$, and $R_I^i(s)$ respectively. Hence for an UAS operation that conducts N UA flights per annum, we have:

$$R_C = \sum_{i=1}^{N} R_C^i \tag{6}$$

$$R_{Cground} = \sum_{i=1}^{N} R_{Cground}^i \tag{7}$$

If there are many UAS flights per annum, then the probability of a person at location s missed by all UAS flights per annum equals the product over the miss probabilities of all UAS flights. Hence, the probability $R_I(s)$ that an Unprotected average person, who resides permanently at location s, is per annum killed or fatally injured due to the direct consequences of one of the N UA flights satisfies:

$$R_I(s) = 1 - \prod_{i=1}^{N}[1 - R_I^i(s)] \tag{8}$$

To characterize the relation between Collective risk R_C and Collective ground risk $R_{Cground}$, one should notice that the following five types of UAS accidents have the potential of third party fatalities:

- Type 1: i-th UA flight collides with a commercial air transport (CAT) flight;

- Type 2: i-th UA flight collides with a general aviation (GA) flight;

- Type 3: i-th UA flight collides with an urban air mobility (UAM) UA carrying on-board passenger(s);

- Type 4: i-th UA flight collides to the ground as a consequence of a mid-air collision of types 1-3 or with another UA flight.

- Type 5: i-th UA flight collides to the ground without preceding mid-air collision.

Hence the Collective risk of the i-th UAS flight, R_C^i, satisfies the following sum of five terms:

$$R_C^i = E\{n_F^i\} = E\{n_{F_{CAT}}^i\} + E\{n_{F_{GA}}^i\} + E\{n_{F_{UAM}}^i\} + E\{n_{F_{UASair}}^i\} + E\{n_{F_{UASground}}^i\} \tag{9}$$

where $E\{n_{F_{CAT}}^i\}$ denotes the expected number of on-board and ground fatalities at the side of a CAT flight due to a collision of type 1, $E\{n_{F_{GA}}^i\}$ denotes the expected number of on-board and ground fatalities at the side of a GA flight due to a collision of type 2, $E\{n_{F_{UAM}}^i\}$ denotes the expected number of on-board and ground fatalities at the side of a UAM flight due to a collision of type 3, $E\{n_{F_{UASair}}^i\}$ denotes the expected number of fatalities on the ground due to a collision of type 4, and $E\{n_{F_{UASground}}^i\}$ denotes the expected number of fatalities on the ground due a collision of type 5.

For Collective risk R_C of a UAS operation involving N UAS flights per annum the above means:

$$R_C = E\{n_F\} = \sum_{i=1}^{N}\left[E\{n_{F_{CAT}}^i\} + E\{n_{F_{GA}}^i\} + E\{n_{F_{UAM}}^i\} + E\{n_{F_{UASair}}^i\} + E\left\{n_{F_{UASground}}^i\right\}\right] \tag{10}$$

Furthermore, each of the expected number of third party fatalities at the side of CAT, GA and UAM due to a collision with the i-th UA flight can be written as a sum of onboard fatalities and fatalities on the ground, i.e.

$$E\{n_{F_{CAT}}^i\} = E\{n_{F_{CATonboard}}^i\} + E\{n_{F_{CATground}}^i\}$$

$$E\{n_{F_{GA}}^i\} = E\{n_{F_{GAnboard}}^i\} + E\{n_{F_{GAground}}^i\}$$

$$E\{n_{F_{UAM}}^i\} = E\{n_{F_{UAMonboard}}^i\} + E\{n_{F_{UAMground}}^i\}$$

For Collective ground risk of the i-th UA flight, $R_{Cground}^i$, this means:

$$R_{Cground}^i = E\left\{n_{F_{CATground}}^i\right\} + E\left\{n_{F_{GAground}}^i\right\} + E\left\{n_{F_{UAMground}}^i\right\} + E\{n_{F_{UASair}}^i\} + E\left\{n_{F_{UASground}}^i\right\} \qquad (11)$$

Similarly, Collective ground risk $R_{Cground}$ of a UAS operation involving N UAS flights per annum satisfies:

$$R_{Cground} = \sum_{i=1}^{N}\left[E\left\{n_{F_{CATground}}^i\right\} + E\left\{n_{F_{GAground}}^i\right\} + E\left\{n_{F_{UAMground}}^i\right\} + E\{n_{F_{UASair}}^i\} + E\left\{n_{F_{UASground}}^i\right\}\right]$$

$$(12)$$

2.3 UAS Safety Management Frameworks

This section evaluates the UAS safety management frameworks from EASA/JARUS and from FAA.

2.3.1 EASA/JARUS UAS safety management frameworks

EASA and JARUS developed a regulatory concept introducing three risk categories for UAS, which are Open, Specific, and Certified [12,13].

- Open category represents very low risk UAS operations requiring no involvement of aviation authorities;
- Specific category UAS presents a limited risk to people and property requiring risk mitigation, depending on the type of operation and nature of the risk, airworthiness requirement may be included;
- Certified category UAS is regulated following the traditional approach to conventional aircraft, including type certification and compliance to airworthiness requirement.

Different regulation limitations and requirements between Open, Specific and Certified UAS operations [14,15] are shown in Table 1. The Open category is divided into three subcategories A1, A2 and A3 with different operational limitations and technical requirements. Specific UAS operations are required to obtain an operational authorisation where the above requirements for Open category are not met, and the operator shall perform a risk assessment and submit to a competent authority. Certified category operations are conducted with relatively high risk (e.g. flying over assemblies of people, carrying people or dangerous goods, etc.) or when the competent authority, based on the risk assessment by the operator, considers the risk cannot be adequately mitigated.

Table 1. Characteristics of Open, Specific and Certified UAS Operations [14,15]

Category	Open			Specific		Certified
Sub-category	A1	A2	A3	N/A		N/A
Class	C0 / C1	C2	C2 / C3 / C4	N/A		N/A
MTOW	<900g	<4kg	<25kg	N/A		N/A
Flying altitude	<=120m	<=120m	<=120m	<=120m		N/A
Range	VLOS	VLOS	VLOS	VLOS/BVLOS		VLOS/BVLOS
Autonomous level	Manually			Manually/Autonomous		Manually/Autonomous
Over assemblies of people	Not allowed	Not allowed	Not allowed	Not allowed		Allowed
Over uninvolved person	C0 (<250g, <19m/s)	30m away or 5m away in low speed mode(<3m/s)	150m from residential, commercial, industrial, recreational area	Allowed	Not allowed	Allowed
Risk assessment requirement	Not required			Risk assessment conducted by operator/ Hold of LUC (Light UAS operator certificate)		Required, RPAS.1309 [13] applies
Authorisation/ certification requirement	Online examination of the operator	Certificate of remote pilot competency	Certificate of remote pilot competency	Application for operational authorisation		Certificate of design, production and maintenance
Size	<3m (C3 UAS operation)			<=1m	<=3m	No requirement
Airspace	Uncontrolled			Uncontrolled/ Controlled (coordination required)		Uncontrolled/controlled
Transportation	No transportation of people or dangerous goods					Allowed for transportation of people/dangerous goods

SORA Method for Specific category

For Specific category UAS operations, JARUS developed the SORA (Specific Operations Risk Assessment) method [16,17] to support the application for authorization. [17] explains the risk assessment aim of SORA through the three quantitative equations that are shown in Figure 1. The 1st and 3rd equations capture fatality and economic risks respectively posed to third parties on the ground. The 2nd equation captures fatality risk to third parties on-board manned aircraft. [17] also explains that it would not be realistic to conduct a quantitative risk assessment for a UAS operation in the Specific category. Therefore the SORA method [16] has been developed as an expert-based decision process to determine qualitative levels of risk posed by a UAS operation to third parties on the ground and to third parties in the air.

The SORA method is a decision process to assign requirements to the UAS operation that bring it under proper control with a sufficient level of confidence. The main steps of the SORA method are:

- Determination of the Ground Risk Class (GRC). Intrinsic GRC is determined using Table 5. Subsequently Table 6 show how mitigation measures reduce Intrinsic GRC to Final GRC.
- Determination of the Air Risk Class (ARC). Initial ARC is determined using the process in Figure 3. Strategic mitigations are identified to reduce the Initial ARC level to Residual ARC level. Subsequently Table 7 translates Residual ARC to Tactical Mitigation Performance Requirements (TMPR).
- Assignment of requirements. Table 8 translates Final GRC and Residual ARC into Specific Assurance and Integrity Level (SAIL); Table 9 translates SAIL into Operational Safety Objectives (OSO).

Neither [16] nor [17] provide an explanation how these main SORA steps make use of the quantitative equations in Figure 1.
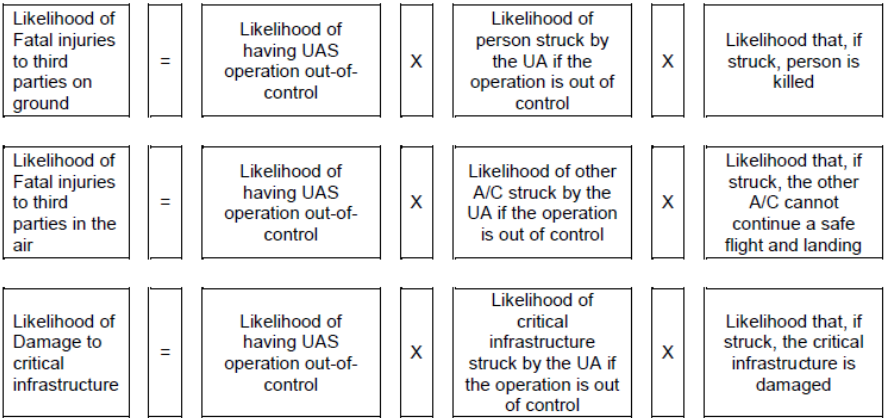
Figure 1. Third party risk equations forming the basis of SORA (source: Figure 5 in [17])

AMC RPAS.1309 for Certified Category

For Certified category UAS operations, an airworthiness certification process (AMC RPAS.1309 [13]) is adopted for UAS. Note that the use of this process is also applicable to other UAS categories (Open / Specific) if high airworthiness standard is needed (e.g. flight over crowds of people). Different types of UAS ranging from light UAS to conventional aircraft equivalent UAS are considered:

- LUAS (Light Unmanned Aeroplane System) [18];
- LURS (Light Unmanned Rotorcraft System) [19];
- RPAS-23 (Small unmanned airplane) [20];
- RPAS-25 (Large unmanned airplane) [21];
- RPAS-27 (Unmanned rotorcraft with MGTOW <= 6000 pounds) [22];
- RPAS-29 (Unmanned rotorcraft with MGTOW > 6000 pounds) [23].

The risk requirements for these types of UAS are given in Table 10.

The definitions for the severity classes are shown in Table 11. Note that for the manned aircraft equivalent UAS (RPAS-23 Class IV, RPAS-25 and RPAS-29), existing mean of compliance for conventional aircraft ([20], [21] and [23]) are applied, however the severity definitions are different from that of UAS. The main difference lays in the hazardous and catastrophic classes. UAS severity definitions consider consequence of one or multiple fatalities as catastrophic, while conventional aircraft standards consider fatal injury to one occupant as hazardous and multiple fatalities as catastrophic.

2.3.2 FAA UAS safety management frameworks

FAA regulatory framework [24] for UAS operations distinguishes the following three categories, the characteristics for each of these are shown in Table 2.

- Recreational UAS operation,
- Work/Business UAS operation,
- Advanced UAS operation.

For the recreational UAS category no safety risk assessment is required [25, 26]. For Work/Business UAS operation small unmanned aircraft rules apply [27] under certain constraints such as less than 55 lbs, VLOS only, not over persons (see Table 2). For the risk assessment of a work/business UAS operation, Advisory Circular 107-2 [28] applies, in which

a qualitative overall safety risk assessment is encouraged though not obliged. All other UAS operations are considered to fall in the Advanced category; for such UAS operation a Safety Risk Management (SRM) is mandatory. Figure 2 shows that the applicable SRM process depends on the UAS operating airspace. The two main risk management processes for Advanced UAS operations are:

- SRM [29] for UAS operation in uncontrolled airspace applying Order 8040.4B [30],
- SRM for UAS operation in controlled airspace applying ATO SMS Manual [31].

Order 8040.4B / UAS SRM Policy for Advanced Category

Order 8040.4B [30] is established for SRM for manned aviation. As a supplement to Order 8040.4B, UAS SRM policy [29] is established for conducting SRM for UAS requesting to operate in uncontrolled airspace (e.g. below 400ft in Class G airspace). UAS SRM Policy adopts the risk criteria for general aviation from Order 8040.4B. The risk matrix, likelihood and severity definitions are shown in Table 12 to Table 14.

Table 2. Characteristics of UAS Operations in FAA Safety Regulations [26,27,32-34]

Category	Recreational	Work/Business	Advanced
MTOW	N/A	<=25kg	N/A
Flying altitude	<= 400ft (Class G airspace) / Within UASFM altitude	<= 400ft	N/A
Range	VLOS	VLOS	VLOS / BVLOS
Collaboration level	Single-UAS	Single-UAS	Single / Multi-UAS
Autonomous level	Manually	Manually	Manually/Autonomous
Flight ground speed	N/A	<=100 mph	N/A
Flight time	N/A	Daylight	Daylight / Night
Over uninvolved person	Not allowed	Not allowed	Allowed
Risk assessment requirement	Not required	Encouraged	Required
Authorisation/ certification requirement	Aeronautical Knowledge and Safety Test, Registered aircraft	Remote pilot certificate, Registered aircraft	Remote pilot certificate, Application for waiver / exemption / certification
Airspace	Uncontrolled / Controlled (FAA authorized fixed sites)	Uncontrolled / Controlled (ATC permission)	Uncontrolled / Controlled
Transportation	N/A	No carriage of hazardous materials	N/A
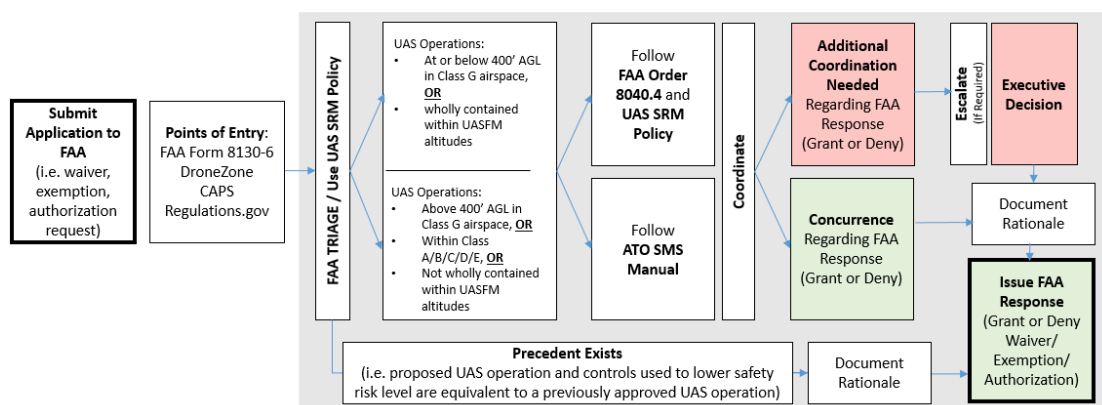
Figure 2. SRM for an Advanced UAS Operation [29]

ATO SMS Manual for Advance Category

ATO SMS Manual [31] provides principles and guidelines for ATO (Air Traffic Organizations) to ensure safety operation, in which SRM is part of it. SRM in ATO SMS Manual is adopted for UAS operations in controlled airspace (e.g. above 400ft in Class G airspace or out of Class G airspace). The risk matrix and severity definitions are given in Table 15 and Table 16. The quantitative criteria for likelihood are given in Table 17 in terms of expected occurrence rate per operation/flight hour/operational hour. Which of these three occurrence rate units applies depends on the type of NAS change in ConOps [31]:

- per operation is applicable for a Terminal Radar Approach Control (TRACON) center, Air Route Traffic Control Center (ARTCC) with small, busy sectors, or an airport traffic control tower;
- per flight hour is applicable for the oceanic domain or for an ARTCC with a larger sector;
- per operational hour is applicable for a system acquisition or modification.

2.4 Evaluation of UAS TPR Indicator and TPR Fatailty Terms

This section first evaluates which of the eight third-party fatality terms defined in section III are covered by each of the EASA and FAA regulations. The details of this evaluation is shown in Table 3. Subsequently Eq. (9)-(12) are used to translate this in terms of the UAS TPR indicators; these results are shown in Table 4. Subsequently the findings in Table 3 and Table 4 are discussed.

Table 3. Third-party fatality terms that are addressed by EASA and FAA regulations

Third-party fatality terms of *i*-th UAS flight	Regulations & Operation category					
	EASA/JARUS SORA	EASA/JARUS AMC RPAS.1309		FAA Advisory Circular 107-2	FAA UAS SRM policy /order 8040.4B	FAA ATO SMS Manual
	Open /Specific /Certified	Certified (for ground risk)	Certified (for air risk)	Work /business	Advanced (in uncontrolled airspace)	Advanced (in controlled airspace)
1.$E\left\{n_{F_{UASground}}^{i}\right\}$	Yes*)	Yes	-	Yes*)	Yes	Yes
2.$E\{n_{F_{UASair}}^{i}\}$	-	-	-	-	-	Yes
3.$E\{n_{F_{CATonboard}}^{i}\}$	Yes*)	-	Yes	-	-	Yes
4.$E\{n_{F_{CATground}}^{i}\}$	-	-	-	-	-	Yes
5.$E\{n_{F_{GAnboard}}^{i}\}$	Yes*)	-	Yes	-	-	Yes
6.$E\{n_{F_{GAground}}^{i}\}$	-	-	-	-	-	Yes
7.$E\{n_{F_{UAMonboard}}^{i}\}$	Yes*)	-	Yes	-	-	Yes
8.$E\{n_{F_{UAMground}}^{i}\}$	-	-	-	-	-	Yes

*) No quantification

Table 4. Applicable UAS TPR Indicators

Regulation/Policy	Operation Category	Applicable TPR Indicator
EASA/JARUS SORA	Open/Specific/Certified	-
EASA/JARUS AMC RPAS.1309	Certified (for ground risk)	$R^i_{Cground}$*) per hazard and per flight hour
EASA/JARUS AMC RPAS.1309	Certified (for mid-air collision risk)	R^i_C on-board per hazard and per flight hour
FAA Advisory Circular 107-2	Work/business	-
FAA Order 8040.4B	Advanced (in uncontrolled airspace)	$R^i_{Cground}$*) per hazard and per year UAS operation
FAA ATO SMS Manual	Advanced (in controlled airspace)	R^i_C per hazard and per flight hour

*) excluding ground fatalities due to a preceding mid-air collision

EASA/JARUS SORA

From the explanation provided in section 2.3.1, it is clear that the SORA method aims to cover both third party fatalities on the ground and on-board of manned aircraft. However none of these assessments is aimed to be quantitative. Moreover the SORA method does not aim to address any of the even terms in Table 3, i.e. follow-up consequences of a preceding mid-air collision of a UAS with a manned aircraft or with another UAS. The qualitative nature of SORA means that there is no contribution in Table 4.

EASA/JARUS AMC RPAS.1309

AMC RPAS.1309 is adopted for EASA/JARUS Certified category. Risk is evaluated per hazard and per UAS flight hour. In [35], catastrophic failure condition refers to "one or more fatalities that can occur either in the air (mid-air collision) or on the ground". Subsequently risk posed to third parties on the ground and in the air risk are addressed separately.

- For third parties on the ground, [2,35] assumes that risk is a function of accident rate, population density, impact dynamics, and area of impact. It is further explained that accident rate is here meant to include accidents due to system failures instead of mid-air collision. For Table 3 this means that the first term $E\left\{n^i_{F_{UASground}}\right\}$ is covered, but not the second term $E\{n^i_{F_{UASair}}\}$. For Table 4 this means that $R^i_{Cground}$ is partly covered.
- For third parties in the air, a mid-air collision with a manned aircraft is considered as having catastrophic consequences [35]. For Table 3 this means that the on-board third-party fatality terms ($E\{n^i_{F_{CATonboard}}\}$, $E\{n^i_{F_{GAnboard}}\}$ and $E\{n^i_{F_{UAMonboard}}\}$) are covered. However the ground fatality terms that represent ground fatalities after a mid-air collision are not covered. Mid-air collisions between UAS is not covered; hence the second term $E\{n^i_{F_{UASair}}\}$ is not covered. For Table 4 the above means that the on-board parts of R^i_C are covered.

FAA Advisory Circular 107-2

Advisory Circular 107-2 [28] provides an example of risk assessment for UAS operation, in which third-party fatality for ground collision of an UAS is considered. For Table 3 this means that the first term $E\left\{n^i_{F_{UASground}}\right\}$ is covered. However there is no quantification as the evaluation of likelihood is qualitative. For Table 4 this means there is no contribution.

FAA Order 8040.4B / UAS SRM Policy

Order 8040.4B [30] and UAS SRM Policy [29] is adopted for FAA Advanced category with UAS operation in uncontrolled airspace. Risk is evaluated per hazard and per year of the UAS operation. Third party risk for persons on the ground is addressed; hence the first term $E\left\{n_{F_{UASground}}^i\right\}$ is covered. Because in uncontrolled airspace there is no collision of a UAS with a manned aircraft the terms 3 through 8 are not covered. Possible collisions between two UAS are neither considered; hence the second term $E\left\{n_{F_{UASair}}^i\right\}$ in Table 3 is not covered. For Table 4 this means that $R_{Cground}^i$ is partly covered.

FAA ATO SMS Manual

FAA ATO SMS Manual is adopted for FAA Advanced category with UAS operation in controlled airspace. Risk is evaluated per hazard and per UAS flight hour. In Table 16, the phrase "fatality or fatal injury to persons other than the unmanned aircraft system crew" refers to all types of third-party fatalities. This means that both third parties on board and on the ground due to an accident involving a UAS are covered; hence all eight terms in Table 3 are covered. For Table 4 this means that R_C^i is fully covered.

Discussion of results in Tables 3-4

The results in Table 3 and Table 4 show that for medium risk UAS operations the safety management frameworks of EASA/JARUS and FAA do not address TPR indicators. Table 3 and Table 4 also show that the situation is better for high risk UAS operations. For UAS operations in controlled airspace the FAA safety risk management framework covers all eight third party terms. For UAS operations in uncontrolled airspace the FAA safety risk management framework only considers the first term, i.e. ground fatalities due to a UAS crash to the ground, if this UAS has not been subject of a preceding mid-air collision with another UAS. The Certified risk management framework of EASA/JARUS even excludes all ground fatality consequences from a preceding mid-air collision, i.e. both between two UAS and between a UAS and a manned aircraft. The results also show that none of the risk management frameworks evaluated address the accumulation of contributions from multiple UAS flights to the TPR indicators R_C, $R_{Cground}$ and $R_I(s)$.

2.5 Conclusion

This paper has studied TPR indicators and TPR fatality terms for UAS operations and their use in EASA/JARUS and FAA safety regulations. In commercial aviation the TPR indicators are Individual risk, Collective risk and Societal risk; each of these three addresses fatality risk posed to persons on the ground only. In addition to posing risk to persons on the ground, UAS operations may also pose third party risks to crew and passengers on board manned aircraft. In section 2.2 this is captured through the definition of three TPR indicators for UAS operations: i) Collective risk R_C for expected number of fatalities due to UAS operations; ii) Collective ground risk $R_{Cground}$ for expected number of fatalities on the ground due to UAS operations; and iii) Individual risk $R_I(s)$ for the probability that an unprotected person at ground location *s* will be killed due to UAS operations. The latter two (ii and iii) consider ground fatalities only, which is similar to Collective risk and Individual risk of commercial aviation. The newly proposed TPR indicator (i) also considers fatalities on-board manned aircraft due to a collision with a UAS. To make the definitions of R_C, $R_{Cground}$ and $R_I(s)$ explicit, the contributions R_C^i, $R_{Cground}^i$ and $R_I^i(s)$ by the *i*-th UAS flight have been characterized in detail.

In Section 2.3 the UAS safety regulations from EASA/JARUS and FAA for different types of UAS operations are identified and subsequently analysed regarding the applicable risk assessment methods. Both EASA/JARUS and FAA distinguish three categories of UAS operations: i) Low risk category (Open in EASA/JARUS, Recreation in FAA); ii) Medium risk category (Specific in EASA/JARUS, Work/Business in FAA); and iii) High risk category (Certified in EASA/JARUS, Advanced in FAA). For the low risk category safety risk assessment is not required. For the medium risk category, both EASA/JARUS and FAA propose qualitative assessment methods (SORA and Advisory Circular 107-2 respectively). For high risk category, both EASA/JARUS and FAA prescribe quantitative safety risk assessment methods. For each of these safety risk assessment methods the basic steps have been reviewed.

In section 2.4 the safety assessment frameworks of EASA/JARUS and FAA have been evaluated against the TPR indicators and TPR fatality terms for UAS operations which have been developed in section 2.2. This evaluation shows that the EASA/JARUS and FAA methods for the medium risk category UAS operations (SORA and Advisory Circular 107-2) do not address any of the TPR indicators. For the high risk category of UAS operations the safety frameworks of EASA/JARUS and FAA address relevant contributions to R_C^i and $R_{Cground}^i$. For controlled airspace the FAA methods cover all possible contributions. For uncontrolled airspace the FAA methods cover ground fatalities due to a UAS crash to the ground that was not been preceded by a mid-air collision. The EASA/JARUS risk assessment methods addresses either on-board fatalities due to a mid-air collision or ground fatalities due to a UAS crash to the ground that was not preceded by a mid-air collision. None of the safety methods from EASA/JARUS and FAA cover the accumulation to TPR indicators R_C and $R_{Cground}$ and $R_I(s)$ by many UAS flights per annum over a given area.

The main conclusions that can be drawn from this study are twofold. Firstly, for medium risk UAS operations none of the current regulations require assessment of any contribution to relevant TPR indicators. Secondly, the identified focus of EASA/JARUS and FAA on methods that assess the TPR contributions per individual UAS operation, means that these methods fall short in capturing the accumulation of contributions by many UAS flights per annum to TPR indicators R_C and $R_{Cground}$ and $R_I(s)$ for rural or urban areas.

To grasp the criticality of these main conclusions, imagine a commercial UAS operation involving a very large number of UAS flights per annum over a rural or urban area that falls outside controlled airspace. For each individual UAS flight at most a quantitative assessment of (a part of) $R_{Cground}^i$ is required. However, what is not required is to assess if the accumulation of the $R_{Cground}^i$ contributions to $R_{Cground}$ and $R_I(s)$ remain acceptably safe if the annual number of UAS flights in an urban area keeps on growing. This example shows that in order to safely manage future increase of UAS flights over rural and urban areas, there is a need for the development of a quantitative safety management framework which addresses the accumulation of individual UAS flight contributions to Collective ground risk $R_{Cground}$ and to Individual risk $R_I(s)$.

Appendix

2A. SORA Method

Table 5. SORA's Intrinsic GRC Determination [16]

Intrinsic UAS Ground Risk Class				
Max UAS characteristics dimension	1 m / approx. 3ft	3 m / approx. 10ft	8 m / approx. 25ft	>8 m / approx. 25ft
Typical kinetic energy expected	*< 700 J (approx. 529 Ft Lb)*	*< 34 KJ (approx. 25000 Ft Lb)*	*< 1084 KJ (approx. 800000 Ft Lb)*	*> 1084 KJ (approx. 800000 Ft Lb)*
Operational scenarios				
VLOS/BVLOS over controlled ground area	1	2	3	4
VLOS in sparsely populated environment	2	3	4	5
BVLOS in sparsely populated environment	3	4	5	6
VLOS in populated environment	4	5	6	8
BVLOS in populated environment	5	6	8	10
VLOS over gathering of people	7			
BVLOS over gathering of people	8			

Table 6. SORA's Mitigations for Final GRC determination [16]

Mitigation Sequence	Mitigations for ground risk	Robustness		
		Low/None	Medium	High
1	M1 - Strategic mitigations for ground risk[e]	0: None -1: Low	-2	-4
2	M2 - Effects of ground impact are reduced[f]	0	-1	-2
3	M3 - An Emergency Response Plan (ERP) is in place, operator validated and effective	1	0	-1
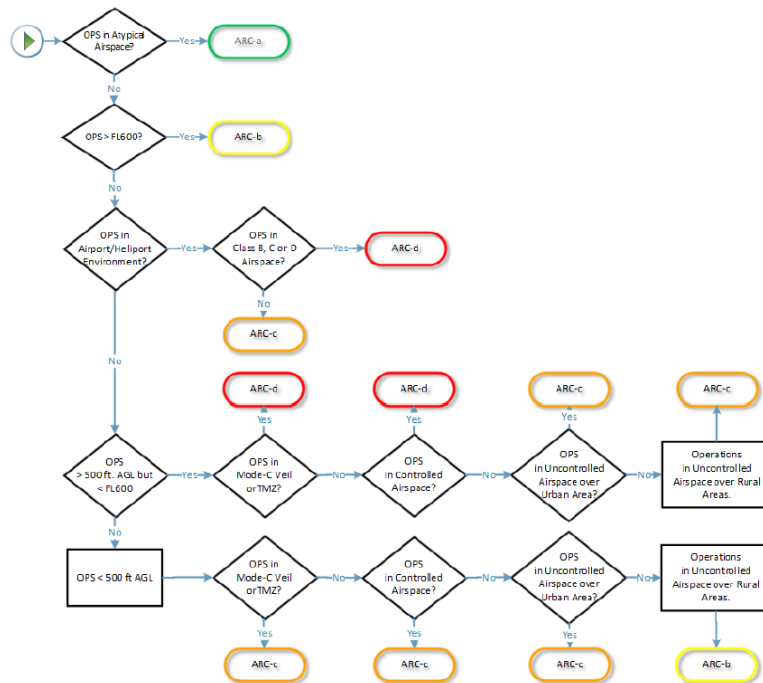
Figure 3. SORA ARC assignment process [16]

Table 7. SORA's TMPR and TMPR level of Robustness Assignment [16]

Residual ARC	Tactical Mitigation Performance Requirements (TMPR)	TMPR Level of Robustness
ARC-d	High	High
ARC-c	Medium	Medium
ARC-b	Low	Low
ARC-a	No requirement	No requirement

Table 8. SORA SAIL determination [16]

SAIL Determination				
	Residual ARC			
Final GRC	a	b	c	d
≤2	I	II	IV	VI
3	II	II	IV	VI
4	III	III	IV	VI
5	IV	IV	IV	VI
6	V	V	V	VI
7	VI	VI	VI	VI
>7	Category C operation			

Table 9. SORA's Recommended OSO [16]

OSO Number (in line with Annex E)		SAIL					
		I	II	III	IV	V	VI
	Technical issue with the UAS						
OSO#01	Ensure the operator is competent and/or proven	O	L	M	H	H	H
OSO#02	UAS manufactured by competent and/or proven entity	O	O	L	M	H	H

2B. JARUS safety risk criteria

Table 10. AMC RPAS.1309 Safety Risk Requirement [13]

Classes of RPAS	Complexity Level	Classification of failure Conditions				
		No safety effect	Minor	Major	Hazardous	Catastrophic
		Allowable Qualitative Probability				
		No Probability Requirement	Probable	Remote	Extremely Remote	Extremely Improbable
		Allowable Quantitative Probabilities (per flight hour)				
CS-LUAS / CS-LURS	I	No Probability Requirement	$<10^{-3}$	$<10^{-4}$	$<10^{-5}$	$<10^{-6}$
	II	No Probability Requirement	$<10^{-3}$	$<10^{-5}$	$<10^{-6}$	$<10^{-7}$
RPAS-23 Class I	I	No Probability Requirement	$<10^{-3}$	$<10^{-4}$	$<10^{-5}$	$<10^{-6}$
	II	No Probability Requirement	$<10^{-3}$	$<10^{-5}$	$<10^{-6}$	$<10^{-7}$
RPAS-23 Class II	I	No Probability Requirement	$<10^{-3}$	$<10^{-5}$	$<10^{-6}$	$<10^{-7}$
	II	No Probability Requirement	$<10^{-3}$	$<10^{-5}$	$<10^{-7}$	$<10^{-8}$
RPAS-23 Class III	I	No Probability Requirement	$<10^{-3}$	$<10^{-5}$	$<10^{-7}$	$<10^{-8}$
	II	No Probability Requirement	$<10^{-3}$	$<10^{-5}$	$<10^{-7}$	$<10^{-9}$
RPAS-27	I	No Probability Requirement	$<10^{-3}$	$<10^{-4}$	$<10^{-5}$	$<10^{-6}$
	II	No Probability Requirement	$<10^{-3}$	$<10^{-5}$	$<10^{-6}$	$<10^{-7}$
RPAS-23 Class IV [1]	N/A[4]	No Probability Requirement	$<10^{-3}$	$<10^{-5}$	$<10^{-7}$	$<10^{-9}$
RPAS-25 [2]	N/A[4]	No Probability Requirement	$<10^{-3}$	$<10^{-5}$	$<10^{-7}$	$<10^{-9}$
RPAS-29 [3]	N/A[4]	No Probability Requirement	$<10^{-3}$	$<10^{-5}$	$<10^{-7}$	$<10^{-9}$

1. The probability requirement is from AC 23.1307-1E [20].
2. The probability requirement is from AMC 25.1309 [21].
3. The probability requirement is from AC 29-2C [23].
4. Large RPAS systems are deemed to be complex (i.e. Equivalent to CL II)

Table 11. AMC RPAS.1309 Safety Risk Severity Definitions [13]

No safety effect	Minor	Major	Hazardous	Catastrophic
Failure conditions that would have no effect on safety. For example, failure conditions that would not affect the operational capability of the RPAS or increase the remote crew workload.	Failure conditions that would not significantly reduce RPAS safety and that involve remote crew actions that are within their capabilities. Minor failure conditions may include a slight reduction in safety margins or functional capabilities, a slight increase in remote crew workload, such as flight plan changes.	Failure conditions that would reduce the capability of the RPAS or the ability of the remote crew to cope with adverse operating conditions to the extent that there would be a significant reduction in safety margins, functional capabilities or separation assurance. In addition, the failure condition has a significant increase in remote crew workload or impairs remote crew efficiency.	Failure conditions that would reduce the capability of the RPAS or the ability of the remote crew to cope with adverse operating conditions to the extent that there would be the following: (i) Loss of the RPA where it can be reasonably expected that a fatality will not occur, (ii) A large reduction in safety margins or functional capabilities, (iii) High workload such that the remote crew cannot be relied upon to perform their tasks accurately or completely.	Failure conditions that could result in one or more fatalities.

2C. FAA Order 8040.4B / UAS SRM Policy Safety Risk Criteria

Table 12. Risk Matrix of UAS SRM Policy and Order 8040.4B [30]

Severity \ Likelihood	Minimal 5	Minor 4	Major 3	Hazardous 2	Catastrophic 1
Frequent A	[Green]	[Yellow]	[Red]	[Red]	[Red]
Probable B	[Green]	[Yellow]	[Yellow]	[Red]	[Red]
Remote C	[Green]	[Green]	[Yellow]	[Yellow]	[Red]
Extremely Remote D	[Green]	[Green]	[Green]	[Yellow]	[Red] * / [Yellow]
Extremely Improbable E	[Green]	[Green]	[Green]	[Green]	[Yellow]

High Risk [Red]
Medium Risk [Yellow]
Low Risk [Green]

* High Risk with Single Point and/or Common Cause Failures

Table 13. Severity Definitions of UAS SRM Policy and Order 8040.4B [30]

Minimal 5	Minor 4	Major 3	Hazardous 2	Catastrophic 1
Negligible safety effect	Physical discomfort to persons Slight damage to aircraft/vehicle	Physical distress or injuries to persons Substantial damage to aircraft/vehicle	Multiple serious injuries; fatal injury to a relatively small number of persons (one or two); or a hull loss without fatalities	Multiple fatalities (or fatality to all on board) usually with the loss of aircraft/ vehicle

Table 14. Likelihood Definitions of UAS SRM Policy and Order 8040.4B [30]

	Qualitative	Quantitative
Frequent A	Expected to occur routinely	Expected to occur more than 100 times per year (or more than approximately 10 times a month)
Probable B	Expected to occur often	Expected to occur between 10 and 100 times per year (or approximately 1-10 times a month)
Remote C	Expected to occur infrequently	Expected to occur one time every 1 month to 1 year
Extremely Remote D	Expected to occur rarely	Expected to occur one time every 1 to 10 years
Extremely Improbable E	Unlikely to occur, but not impossible	Expected to occur less than one time every 10 years

2D. ATO SMS Safety Risk Criteria

Table 15. ATO SMS Manual Risk Matrix [31]

Severity / Likelihood	Minimal 5	Minor 4	Major 3	Hazardous 2	Catastrophic 1
Frequent A	Low	Medium	High	High	High
Probable B	Low	Medium	High	High	High
Remote C	Low	Medium	Medium	High	High
Extremely Remote D	Low	Low	Medium	Medium	High
Extremely Improbable E	Low	Low	Low	Medium	Medium / High*

Table 16. ATO SMS Manual Severity Definitions [31]

Minimal 5	Minor 4	Major 3	Hazardous 2	Catastrophic 1
Discomfort to those on the ground. Loss of separation leading to a measure of compliance greater than or equal to 66 percent.	Low Risk Analysis Event severity, two or fewer indicators fail*. Non-serious injury to three or fewer people on the ground	Medium Risk Analysis Event severity, three indicators fail. Non-serious injury to more than three people on the ground. A reduced ability of the crew to cope with adverse operating conditions to the extent that there would be a significant reduction in safety margins. Manned aircraft making an evasive maneuver, but proximity from unmanned aircraft remains greater than 500 feet.	High Risk Analysis Event severity, four indicators fail. Incapacitation to unmanned aircraft system crew. Proximity of less than 500 feet to a manned aircraft. Serious injury to persons other than the unmanned aircraft System crew.	A collision with a manned aircraft. Fatality or fatal injury to persons other than the unmanned aircraft system crew.

*Risk Analysis Event severity indicators are as follows:

a. Proximity. Failure transition point of 50 percent of required separation or less.

b. Rate of Closure. Failure transition point greater than 205 knots or 2,000 feet per minute (consider both aspects and utilize the higher of the two if only one lies above the transition point).

c. ATC Mitigation. ATC able to implement separation actions in a timely manner.

d. Pilot Mitigation. Pilot executed ATC mitigation in a timely manner.

Table 17. ATO SMS Manual Likelihood Definition [31]

Likelihood	Operations: Expected Occurrence Rate (per operation / flight hour / operational hour)
Frequent A	(Probability) ≥ 1 per 1000
Probable B	1 per 1000 > (Probability) ≥ 1 per 100,000
Remote C	1 per 100,000 > (Probability) ≥ 1 per 10,000,000
Extremely Remote D	1 per 10,000,000 > (Probability) ≥ 1 per 1,000,000,000
Extremely Improbable E	1 per 1,000,000,000 > (Probability) ≥ 1 per 10^{14}

Reference

[1]   EUROCONTROL, "UAS ATM Integration Operational Concept," European Organisation for the Safety of Air Navigation, Edition: 1.0, 27th, Nov, 2018.

[2]   Lin, X., Fulton, N. L., and Horn, M. E. T. 'Quantification of High Level Safety Criteria for Civil Unmanned Aircraft Systems,' IEEE Aerospace Conference, Big Sky, MT, 19th, June, 2014. doi: 10.1109/AERO.2014.6836463

[3]   Stöcker, E. C., Bennett, R., Nex, F., Gerke, M., and Zevenbergen, J. A. "Review of the current state of UAV regulations," Remote sensing Vol. 9, No. 5, 2017, p. 459. doi: 10.3390/rs9050459

[4]   EUROCONTROL, "Feasibility study on the integration of third party risk near airports into IMPACT," Deliverable D2, 15th, June, 2015.

[5]   Jonkman, S., Van Gelder, P., and Vrijling, J. "An overview of quantitative risk measures for loss of life and economic damage," Journal of hazardous materials Vol. 99, No. 1, 2003, pp. 1-30. doi: 10.1016/S0304-3894(02)00283-2

[6]   Bohnenblust, H. "Risk-based decision making in the transportation sector," Quantified societal risk and policy making. Springer, 1998, pp. 132-153.

[7]   Bottelberghs, P. H. "Risk analysis and safety policy developments in the Netherlands," Journal of Hazardous Materials Vol. 71, No. 2000, 2000, pp. 59-84. doi: 10.1016/S0304-3894(99)00072-2

[8]   Smets, H. "Frequency distribution of the consequences of accidents involving hazardous substances in OECD countries," Etudes et Dossiers, 1996.

[9]   Laheij, G. M., Post, J. G., and Ale, B. J. "Standard methods for land-use planning to determine the effects on societal risk," Journal of Hazardous Materials Vol. 71, 2000, pp. 269-282. doi: 10.1016/s0304-3894(99)00083-7

[10]   Evans, A. W., and Verlander, N. Q. "What is wrong with criterion FN‑lines for judging the tolerability of risk?," Risk analysis Vol. 17, No. 2, 1997, pp. 157-168. doi: 10.1111/j.1539-6924.1997.tb00855.x

[11]   Clothier, R. A., Williams, B. P., and Hayhurst, K. J. "Modelling the risks remotely piloted aircraft pose to people on the ground," Safety science Vol. 101, 2018, pp. 33-47. doi: 10.1016/j.ssci.2017.08.008

[12]   EASA, "Concept of Operations for Drones: A risk based approach to regulation of unmanned aircraft," European Union Aviation Safety Agency, 1st, May, 2015.

[13]   JARUS, "AMC RPAS.1309: Safety Assessment of Remotely Piloted Aircraft Systems," Joint Authorities for Rulemaking of Unmanned Systems, Issue: 2, Nov, 2015.

[14]   EU, "Commision Delegated Reulation," European Union, 12th, Mar, 2019.

[15]   EU, "Commision Implementing Regulation," 24th, May, 2019.

[16]   JARUS, "JARUS guidances on Specific Operations Risk Assessment (SORA)," Edition: 2.0, 30th, Jan, 2019.

[17]   JARUS, "JARUS guidelines on Specific Operations Risk Assessment (SORA)," Edition: 1.0, 26th, June, 2017.

[18]   JARUS, "Recommendations for Certification Specification for Light Unmanned Aeroplane Systems," Edition: 0.3, 9th, Nov, 2016.

[19]   JARUS, "Certification Specification for Light Unmanned Rotorcraft Systems," CS-LURS, Edition: 1.0, 30th, Oct, 2013.

[20]   FAA, "Advisory Circular: System Safety Analysis and Assessment for Part 23 Airplanes," Federal Aviation Administration, 17th, Nov, 2011.

[21]   EASA, "Certification Specifications and Acceptable Means of Compliance for Large Aeroplanes," European Aviation Safety Agency, Amendment 23, 15th, July, 2019.

[22]   FAA, "Advisory Circular: Certification of Normal Category Rotorcraft (27-1B)," 29th, June, 2018

[23]   FAA, "Advisory Circular: Certification of Normal Category Rotorcraft (29-2C)," 2nd, July, 2018.

[24]   FAA. "Unmanned Aircraft Systems (UAS)". URL: https://www.faa.gov/uas/ [retrieved 30th, April, 2020]

[25]   FAA. "49 USC 44809: Exception for limited recreational operations of unmanned aircraft". URL: https://uscode.house.gov/view.xhtml?req=granuleid:USC-prelim-title49-section44809&num=0&edition=prelim [retrieved 14th, May, 2020]

[26]   FAA, "Exception for Limited Recreational Operations of Unmanned Aircraft " AC 91-57B, 31st, May, 2019.

[27]   FAA, "Summary of Small Unmanned Aircraft Rule (Part 107)," 21st, Jun, 2016.

[28]   FAA, "Advisory Circular: Small Unmanned Aircraft Systems (sUAS)," AC 107-2, 21st, June, 2016.

[29]   FAA, "Unmanned Aircraft Systems Safety Risk Management Policy," ORDER 8040.6, 4th, Oct. 2019.

[30]   FAA, "Safety Riks Mangement Policy," ORDER 8040.4B, 2nd, May, 2017.

[31]   FAA, "FAA Safety Management System Manual," April, 2019.

[32]   FAA. "Certification". URL: https://www.faa.gov/uas/advanced_operations/certification/ [retrieved 19th, November, 2018]

[33]   FAA. "Part 107 Waivers". URL: https://www.faa.gov/uas/commercial_operators/part_107_waivers/ [retrieved 1st. August. 2019]

[34]   FAA. "Special Authority for Certain Unmanned Aircraft Systems (Section 44807)". URL: https://www.faa.gov/uas/advanced_operations/section_333/ [retrieved 12th, May, 2020]

[35]   JARUS, "Scoping Paper to AMC RPAS.1309: Safety Assessment of Remotely Piloted Aircraft Systems," Issue: 2, Nov, 2015.

<div align="right">

3

</div>

Third Party Risk Modelling of Unmanned Aircraft System Operations, with Application to Parcel Delivery Service

Commercial aviation distinguishes three indicators for third party risk (TPR): i) Expected number of ground fatalities per aircraft flight hour; ii) Individual risk; and iii) Societal risk. The latter two indicators stem from TPR posed to population by operation of hazardous installations. Literature on TPR of Unmanned Aircraft System (UAS) operations have focused on the development of the first TPR indicator. However the expected increase of commercial UAS operations requires an improved understanding of third party risk (TPR). To support such improvement, this paper extends the existing TPR model for UAS operations with societal and individual risk indicators. The extension is developed both at modelling level and at assessment level. Subsequently the extended approach is applied to a hypothetical UAS based parcel delivery service in the city of Delft. The results obtained for the novel UAS TPR indicators show that this aligns commercial UAS operations with land use policies and standing TPR regulation for airports and hazardous facilities.

3.1 Introduction

An Unmanned Aircraft (UA) is an aircraft which is intended to operate with no pilot on board. A UA is either piloted from the ground or is autonomous. When piloted from the ground the UA and associated ground elements are referred to as an Unmanned Aircraft System (UAS) [1]. UAS have the ability to virtually replace manned aircraft and aerial platforms in many applications due to the considerable cost savings for not having to fly a helicopter or airplane with associated crew and fuel costs or transportation of a heavy aerial platform. The future possibilities are endless: imagine flying taxis, parcel delivery, medical aid; the list goes on and on. Because the safety risks of these UAS based operations are not well understood, under current regulations such commercial UAS operations over rural areas are not allowed [2,3]. To manage the future risk of commercial UAS operations over an urban area there is a need for models of third party risk (TPR) posed to persons on the ground by a large number of UA flights per annum.

For conventional aviation, third party risk (TPR) models have been well developed [4,5,6]. These models allow to assess changes in risk posed to persons on the ground due to changes in the amount of flights, new departure/arrival routes, the impact of a new airport, the risk of constructing a residential building in a certain area, etc. TPR models of conventional aviation are typically quantified using statistical analysis of large scale collected incident and accident data. Because sufficient statistical incident/accident data is not available for UA flights, TPR analysis of UA flights is largely based on prospective models. Modelling ground TPR of a UAS operation involves an off-nominal UAS behaviour model, an off-nominal UA flight descent model, and a ground crash impact consequence model. The latter model captures population density, crash impact area, shelter and injury effects. Weibel and Hansman [7] show that the large range of UA types affects each of these model elements. Clothier and Walker [8] identifies and evaluates safety objectives of UAS operations. Dalamagkidis et al. [9] provides an in-depth overview of the spectrum of research issues in integrating UAS in the National Airspace System. Lum and Waggoner [10] show that a key bottleneck for safe integration of UAS operations in the National Airspace System is the risk posed to persons on the ground in a metropolitan area (e.g. Seattle area). Melnyk et al. [11] provides literature reviews for each of the five terms in the product of this ground TPR model. Subsequently, [11] uses this accumulated knowledge for the assessment of prospectively calculated TPR per flight hour for flying various UA types over various population densities. Finally these prospectively calculated TPR per flight hour are compared against statistically calculated TPR per flight hour for manned aviation and each difference is translated into a requirement on UAS system failure rate, i.e. the rate of events that cause an inability to maintain coordinated flight. For UAS operations in an urban area the derived requirement on UAS system failure rates range from 3.42×10^{-4} per flight hour for a mini UA (≤ 2 kg), to 2.01×10^{-8} per flight hour for a heavy UA (> 4550 kg).

The potential of commercial use of small UAS for various applications has directed further development of TPR modelling and simulation. For small fixed-wing UAS, Rudnick-Cohen et al. [12,13], Bertrand et al. [14] and La Cour-Harbo [15,16] develop MC simulation approaches to evaluate the crash location density and its effect on ground TPR. [16] also extends this to small helicopter UA flights. Monte Carlo simulation of crash location density of a multi-rotor UA flight poses complementary challenges. Foster and Hartman [17] conduct large scale simulations of a high fidelity model of multi-rotor UA behaviour under different propulsion failures. Under abrupt power failure, the resulting tumbling mode descend yields a near-ballistic trajectory. Under a cascading power failure the multi-rotor UA enters into erratic transition dynamics and an out-of-control descent. In order to make UA behaviour under failure

conditions better predictable, Cunningham et al. [18] develops a model of controlled termination of an anomaly UA flight. This creates a near-vertical descent by putting the UA in a sustained condition of high angle of attack and high drag using pro-spin controls. Ancel et al. [19] adopts the latter model for ground TPR assessment of a small multi-rotor UA flight. La Cour-Harbo [20] models ballistic descent of small UAs. Primatesta et al. [21] uses these TPR models for real-time navigation of a small UA flight such that it approximately minimizes TPR in flying over an urban area.

The above mentioned studies consider TPR from a UA flight perspective. However, there also is a need to assess TPR from a population perspective, i.e. to assess the accumulated TPR that is posed to a population by a UAS based operation that conducts a large number of flights per annum. For commercial aviation this population perspective on TPR has been well developed in the form of individual and societal risk [4,5,6]. The objective of this paper is to extend the existing TPR model for UAS flights with individual and societal risk models that can be assessed through conducting MC simulations. The existing and novel TPR approaches are subsequently compared for a hypothetical UAS-based parcel delivery service.

This paper is organized as follows. Section 3.2 reviews existing TPR models for commercial aviation and for UAS operations. Section 3.3 extends these TPR models to UAS operations involving a large number of flights per annum over an urban area. Section 3.4 develops a Monte Carlo simulation method for the assessment of the extended TPR models. Section 3.5 develops a model for UAS based parcel delivery service in the city of Delft. Section 3.6 evaluates the TPR risks for this parcel delivery service using the model and simulation approach from sections 3.3 and 3.4. Section 3.7 draws conclusions and identifies follow-on research.

3.2 TPR Models in Aviation Research Literature

3.2.1 TPR models for commercial aviation

In commercial aviation almost all fatalities concern persons onboard aircraft. This explains why in commercial aviation the TPR indicator of the expected number of ground fatalities per flight hour plays a marginal role. Instead, commonly used indicators for TPR in commercial aviation are defined from a ground population perspective; these are individual risk and for societal risk the FN curve and collective risk [4,5,6].

Individual risk $R_I(y)$ of commercial air transport is defined as: *"The probability that an average unprotected person, who resides permanently at ground location y, would get killed or fatally injured due to the direct consequences of an aircraft accident during a given annum."* Notice that by its definition, the individual risk indicator $R_I(y)$ does not make any difference if a ground location y is in a rural area or in the center of a city. Individual risk defines risk contours on a location map that are used for zonal policies regarding any current or future use of a given area that is exposed to non-negligible Individual risk levels.

The mathematical characterization of Individual risk of $R_I(y)$ satisfies [5]:

$$R_I(y) = \sum_d [N_d P(C|d) p_s(y|d) \, |A(d)| \, P(F|y \in A(d))] \tag{2.1}$$

where N_d is the annual number of flights of type d, $P(C|d)$ is the accident probability model, $p_s(.|d)$ is the crash location model, $|A(d)|$ is the crash area size, and $P(F|y \in A(d))$ is the fatality model. Formal definitions of these five terms are given in the box below.

To capture societal risk the FN curve $R_{FN}(n)$ is defined as [22]: "*The probability that a group of n or more third party persons will be killed or fatally injured due to the direct consequences of an aircraft accident during a given annum.*", i.e. for $n \geq 1$:

$$R_{FN}(n) = 1 - \prod_d [1 - P\{n_F^d \geq n\}]^{N_d} \cong \sum_d [N_d P\{n_F^d \geq n\}] \tag{2.2}$$

with n_F^d the number of third party fatalities due to an accident of a type d flight. Some literature sources, e.g. [6] refer to "more than n", which defines $R_{FN}^>(n)$ as $R_{FN}^>(n) = R_{FN}(n+1)$, for $n \geq 0$.

Safety regulation of hazardous installations in various countries typically adopts an $R_{FN}(n)$ limiting criterion of the following form, e.g. [6]:

$$R_{FN}(n) < C/n^\alpha \tag{2.3}$$

where α is the steepness of the limit line and C a constant that determines the position of the limit line. A steepness $\alpha = 1$ is called risk neutral (e.g. in UK); a steepness $\alpha = 2$ is called risk averse (e.g. in the Netherlands). In the latter case larger accidents are weighted more heavily and are thus only accepted with a relatively lower probability. Within Europe there is an effort to develop a common approach in setting values for C and α [23].

Another societal risk indicator is Collective risk R_C, which is defined as

$$R_C = E\{n_F\} \tag{2.4}$$

where n_F is the number of persons on the ground in a given area Y that are killed or fatally injured due to the direct consequences of aircraft flight accidents during a given annum [24]. Collective risk R_C is known to be equal to a summation over the FN-curve, e.g. [22]:

$$R_C = \sum_{n=1}^{\infty} R_{FN}(n) = \sum_{n=0}^{\infty} R_{FN}^>(n). \tag{2.5}$$

To express the relation between Collective risk and Individual risk common practice is to assume that people on the ground are unprotected to a crash of a commercial aircraft. Under this assumption [22] shows:

$$R_C = \int_Y R_I(y)\rho(y)dy \tag{2.6}$$

where $\rho(y)$ is the population density as a function of crash center location y, and Y is the area that may be affected by aircraft accidents.

3.2.2 TPR models for UAS operations

Literature on TPR models for UAS operations has focused on $R_{Cground}^i = E\{n_{F,i}^{UAS}\}$, where $n_{F,i}^{UAS}$ is the number of persons on the ground that are killed or fatality injured due to the i-th UA flight colliding to the ground, This has resulted in the following characterization [14,19]:

$$R_{Cground}^i = E\{n_{F,i}^{UAS}\} = \int_Y R_I^i(y)[1 - P(S|y,i)]\rho(y)dy \tag{2.7}$$

where $R_I^i(y)$ is the individual risk for an unprotected person at location y posed by the i-th flight, $P(S|y,i)$ is the shelter protection model and $\rho(y)$ is the population density in the area Y considered.

The characterization of $R_I^i(y)$ in UAS literature satisfies [14, 16, 21]:

$$R_I^i(y) = \sum_{e \in E}[P(e|i)p_s(y|i,e)\,|A(d_i,e)|\,P(F|y \in A(d_i,e))] \tag{2.8}$$

where E is the set of possible crash event types, $P(e|i)$ is ground crash probability, $p_s(.|i,e)$ is the crash location model, $|A(d_i,e)|$ is the size of the crash impact area, $P(F|y \in A(d_i,e))$ is the unprotected fatality model.

Formal definitions of the terms in eqs. (2.7-2.8) are given in the box below.

Formal definitions of the terms in equations (2.7-2.8)

$R_I^i(y)$ = probability that an unprotected average person at ground location *y* is killed or fatally injured due to ground crash by *i*-th flight.

$P(S|y,i)$ = probability that a person at location *y* is sheltered against a crash of the *i*-th UA flight.

$\rho(y)$ = population density as a function of location *y*.

$P(e|i)$ = probability of event type *e* ground crash by *i*-th UA flight.

$p_s(.|i,e)$ = pdf of crash location of *i*-th UA flight due to event type *e*.

$|A(d_i,e)|$ = size of event type e crash impact area of UA type d_i.

$P(F|y \in A(d_i,e)) = P(F|y \in A(d_i,e), d_i, e)$ = probability that a crash of a UA flight of

---

3.2.3 Submodels developed in literature

The difference between eq. (2.7) and eq. (2.6) is that (2.7) includes shelter protection and (2.6) not. The main difference between eq. (2.8) and eq. (2.1) is that eq. (2.1) accumulates over all annual flights, and (2.8) not. Another difference is that eq. (2.8) differentiates regarding types of flight and crash event, while (2.1) differentiates regarding type of flight only. In spite of the similarities there are significant differences in the approaches used for the numerical evaluation of the product terms in these equations. For commercial aviation the numerical evaluation of (2.1-2.2) is largely based on statistical modelling of accident data from the past [5]. Because for future UAS operations such accident data is not available, use has to be made of dedicated submodels.

An event $e \in E$ types consists of two indicators: e_H for the hazard causing the UA crash and e_θ the mode of the descend path to the ground. La Cour-Harbo [16] distinguishes four e_θ modes: ballistic descend, uncontrolled glide, parachute descend, and fly-away. For a quadcopter [17] distinguishes several complementary e_θ modes. The e_H types include all UAS system

failures, i.e. events that would cause an inability to maintain coordinated flight [11]. UAS system failure causes may vary from human error, unexpected adverse weather, or collision with a bird, a building or with another UA. Weibel and Hansman [7], Lum et al. [25], Dalamagkidis et al. [9], Melnyk et al. [11] consider effects of system failures of UA flights over areas with homogeneous population density. The homogeneous population density assumption simplifies the assessment of equations (2.7-2.8) in the sense that there is no need to take the shape of crash location density $p_s(.\,|i,e)$ into account.

Melnyk et al. [11] provides a very good review of the various submodels needed to evaluate equations (2.7-2.8). More recent studies have further extended the submodels for location density $p_s(.\,|i,e)$ and event types $P(e|i)$. For the latter, Barr et al. [26] developed a Bayesian Belief Net, Bertrand et al. [14] developed a Fault Tree model, while Kim [27, 28] and La Cour-Harbo and Schioler [29] developed collision probability models between UAs and between a UA and low-flying General Aviation. For the evaluation of the location density $p_s(.\,|i,e)$ in equation (2.8), probabilistic models and MC simulation methods have also been developed for fixed wing UA [12-15], for helicopter [30,16], and for multi-rotor UA [17,18,20].

3.3 Novel TPR Indicators for UAS Operation

For a commercial UAS operation involving many flights per annum, there is need for novel TPR indicators from a population perspective. Based on the TPR indicators in subsection 3.2.1, this section elaborates for UA crash to the ground: Individual risk $R_I^{UAS}(y)$ and societal indicators FN-curve R_{FN}^{UAS} and Collective ground risk $R_{Cground}^{UAS}$ in subsections 3.3.1 and 3.3.2 respectively. In subsection 3.3.3 impact velocity is incorporated.

3.3.1 Individual risk of UAS operations

Individual risk $R_I^{UAS}(y)$ due to possible crashes to the ground by a UAS operation involving multiple flights per annum is defined as: "The probability that an average unprotected person, who resides permanently at ground location *y*, would get killed or fatally injured due to the direct consequences of a ground crash by a UA flight during a given annum."

Aalmoes et al. [31] proposed a version of equation (2.1) as the basic model for Individual risk $R_I^{UAS}(y)$. To take advantage of the TPR model development in literature, it has an advantage to connect the above Individual risk definition to equations in subsection 2.2 and the developed sub-models in subsection 2.3. To make the connection N UA flights per annum over the area *Y* are assumed. Then the probability of a person at location *y* being missed by all *N* UA flights per annum equals the product over the miss probabilities $\left[1 - R_I^i(y)\right]$ for the $i = 1,.., N$ UA flights. Hence, Individual risk $R_I^{UAS}(y)$ satisfies:

$$R_I^{UAS}(y) = 1 - \prod_{i=1}^{N}\left[1 - R_I^i(y)\right] \tag{3.1}$$

with $R_I^i(y)$ satisfying equation (2.8). Often $R_I^{UAS}(y) \ll 0.1$, then eq. (3.1) can be approximated by $R_I^{UAS}(y) \cong \sum_{i=1}^{N} R_I^i(y)$.

3.3.2 FN-curve and Collective ground risk of UAS operations

For a UAS operation involving multiple flights per annum over an area *Y* the FN curve $R_{FN}^{UAS}(n)$ is defined as the "*The probability that in an area Y a group of n or more third party persons will be killed or fatally injured due to the direct consequences of ground crashes by UA flights during a given annum*", i.e. for $n \geq 1$:

$$R_{FN}^{UAS}(n) = 1 - \prod_{i=1}^{N}\left[1 - P\{n_F^i \geq n\}\right] \cong \sum_{i=1}^{N}\left[P\{n_F^i \geq n\}\right] \qquad (3.2)$$

where n_F^i is the number of persons on the ground that are killed or fatally injured due to a ground crash of the i-th UA flight. In contrast to commercial aviation ground crashes, for almost all UAS ground crashes $n_F^i \leq 1$. This implies that the FN-curve $R_{FN}^{UAS}(n)$ for UAS will decrease more steeply with increasing n than the FN-curve $R_{FN}(n)$ does for commercial aviation.

Collective ground risk $R_{Cground}^{UAS}$ of a UAS operation involving multiple flights per annum over an area Y is defined as: "*The expected number of persons on the ground in a given area Y that are killed or fatally injured due to the direct consequences of ground crashes by flights of the UAS operation during a given annum*". Hence for a UAS operation conducting N flights per annum:

$$R_{Cground}^{UAS} = \sum_{i=1}^{N} R_{Cground}^i \qquad (3.3)$$

where $R_{Cground}^i$ satisfies (2.7). Also for a UAS operation, collective ground risk equals the summation over the FN-curve, i.e.

$$R_{Cground}^{UAS} = \sum_{n=1}^{\infty} R_{FN}^{UAS}(n) \qquad (3.4)$$

Adopting FN requirement (2.3) also on $R_{FN}^{UAS}(n)$ and substituting this into (3.4) yields the following bound on collective ground risk

$$R_{Cground}^{UAS} < C \sum_{n=1}^{\infty} \frac{1}{n^\alpha} = C\,\zeta(\alpha) \qquad (3.5)$$

with $\zeta(.)$ the Riemann zeta function [32, p.807]. For $\alpha = 2$ this yields $\zeta(2) = \pi^2/6$. For $\alpha = 1$ this yields $\zeta(1) = \infty$, which means that the FN-curve requirement does not imply a bound on UAS collective ground risk $R_{Cground}^{UAS}$. Because the FN-curve for UAS operations will be steep in eq. (3.5) α should always be larger than 1, hence $\zeta(\alpha)$ is bounded.

3.3.3 Incorporating impact velocity

The last term in eq. (2.8), i.e. $P(F|y \in A(i,e))$, depends on the kinetic energy $\frac{1}{2}mv^2$ of the i-th UA flight at the moment of impact of crash type e. In evaluating this term, common practice is to adopt a certain impact velocity, e.g. [14,16,21]. Because the impact velocity may assume values from a set V, a better approach is to incorporate the impact velocity v in $P(F|y \in A(i,e))$. To do so we make use of the law of total probability:

$$P(F|y \in A(i,e)) = \int_V P(F,v|y \in A(i,e))dv \qquad (3.6)$$

Application of conditional probability to $P(F,v|y \in A(i,e))$ yields:

$$P(F|y \in A(i,e)) = \int_V P(F|v,y \in A(i,e))p(v|y \in A(i,e))dv \qquad (3.7)$$

where $p(v|y \in A(i,e))$ is the conditional density of impact velocity v given $y \in A(i,e)$ and $P(F|v,y \in A(i,e))$ is "*The conditional probability that an average person at a location in the crash impact area $A(i,e)$ of the i-th UA flight under event e, will be killed or fataly injured, given the velocity v of the UA at the moment of crash.*" Rudnick-Cohen et al. [13] and Haartsen et al. [30] propose MC simulation to evaluate $p(v|y \in A(i,e))$.

3.4 Novel TPR Indicators for UAS Operation

This section specifies the steps to numerically evaluate the novel TPR models for Individual risk and Collective risk. Subsection 3.4.1 explains the Monte Carlo simulation steps.

Subsection 3.4.2 explains the steps for the evaluation of Individual risk. Subsection 3.4.3 explains the follow-on steps for the evaluation of Collective ground risk, both for each individual flight and for the population in the area considered.

3.4.1 Monte Carlo simulation approach

We consider a UAS based operation conducting N flights per annum over an area Y, using different types of UAs. We assume the volume of airspace used by these N flights is separated from airspace in use by Commercial Air Transport, General Aviation and Urban Air Mobility operations. The objective is to estimate Individual risk $R_I^{UAS}(y)$ for each position $y \in Y$.

A straightforward way to accomplish this is to first conduct a Monte Carlo simulation for the generation of N nominal flight plans, and subsequently to conduct a Monte Carlo simulation of K flights for each of these N nominal flight plans. This approach would lead to a MC simulation consisting of simulating NK flights. However, for ground TPR assessment it suffices to only simulate the fraction of those flights that are subject to a failure event leading to a ground crash. Elaboration of this approach for MC based assessment of Individual risk yields the following series of Steps.

Step 0: Determine N delivery locations and UA types

Draw N independent delivery destination locations in the area Y according to the population density $\rho(y)$. Subsequently draw for each of these N destinations a delivery payload according to a known probability density of these payloads. Based on the i-th payload sample, select for the i-th flight a suitable UA type d_i from those in use by the parcel delivery service.

Step 1: Determine nominal flight plans for each of the N delivery flights

Determine for each of the N parcel delivery flights (outbound and inbound), a series of 3-dimensional waypoints, the nominal states $x_t^{i,nom}$, $t \in [0, T_i^{nom}]$, of a 4-dimensional nominal flight path through these waypoints, of nominal duration T_i^{nom}, $i = 1,..,$ N. The components of the nominal state $x_t^{i,nom}$ are 3D position $s_t^{i,nom}$, 3D velocity $v_t^{i,nom}$ and mode $\theta_t^{i,nom}$.

Step 2: Evaluate ground crash probability. Calculate for each of the N flights and each $e \in E$ the probability of crash:

$$P(e|i) = 1 - \exp\left\{-\int_0^{T_i^{nom}} \lambda_{i,e}(t)dt\right\} \tag{4.1}$$

with $\lambda_{i,e}(t)$ the rate of event e to happen at moment t during the i-th flight. A relevant event type for which $\lambda_{i,e}(t)$ is not constant in time is mid-air collision rate of the i-th UA flight with any of the other UA flights [28].

Step 3: Simulation of UA flights that crash.

Conduct for each of the N flights and each $e \in E$ a Monte Carlo simulation consisting of K_i runs that crash to the ground, i.e. for $k = 1,..,K_i$. The typical value for $K_i = [T_i^{nom}]$. For each (i, e) this is done in substeps 3.1-3.3:

Substep 3.1: Draw K_i independent event time samples $t_e^{i,k}$ from the density $\lambda_{i,e}(t)$ on the time interval $[0, T_i^{nom}]$.

Substep 3.2: Simulate for the i,k-th flight, for each $e \in E$ the UA state at moment of failure event $t_e^{i,k}$. The UA state components to be generated are 3D position $s_{te}^{i,k}$, 3D velocity $v_{te}^{i,k}$ and attitude $\theta_{te}^{i,k}$:

$$s_{te}^{i,k} = s_{te}^{i,nom} + \varepsilon_{te}^{s} \tag{4.2a}$$

$$v_{te}^{i,k} = v_{te}^{i,nom} + \varepsilon_{te}^{v} \tag{4.2b}$$

$$\Theta_{te}^{i,k} = e_{\theta} \tag{4.2c}$$

where e_{θ} is the applicable non-nominal descend mode component of e, ε_{te}^{s} is a Gaussian navigation error in horizontal and vertical position with standard deviations (σ_H^s, σ_V^s), and ε_{te}^{v} is an independent Gaussian deviation from nominal velocity with standard deviations (σ_H^v, σ_V^v).

Substep 3.3: For each e_{θ} that applies to the i,k-th flight, simulate the non-nominal descend on the time interval $[t_e^{i,k}, t_{c,e}^{i,k}]$, i.e. from $t_e^{i,k}$ until moment of ground crash $t_{c,e}^{i,k}$. This yields the UA state $x_{c,e}^{i,k}$, at moment $t_{c,e}^{i,k}$. The applicable differential equations to be used depend of the event type e and the desired model fidelity. As an example we provide the differential equations from [20] for a ballistic descent model of a quadcopter:

$$\dot{s}_t = v_t \tag{4.3a}$$

$$\dot{v}_t = Col\{0,0,g\} - C_D A_s \varrho_t \|v_t - w_t\|(v_t - w_t)/2m \tag{4.3b}$$

where g is the gravitational constant, C_D is the drag coefficient, A_s the surface area, m is the mass of UA with payload, ϱ_t and w_t are air density and wind velocity vector at moment t, respectively. The latter two are considered to be functions of 3-dimensional position s_t. Rather than adding the wind effect in the differential equation for the position as is done in [18], w_t is incorporated in the drag component of the acceleration [33].

3.4.2 Evaluation of Individual risk

The results from the Monte Carlo simulation approach of subsection 4.1 are now used to estimate Individual risk in a number of steps.

Step 4: Evaluation of the crash location model.

Calculate for each $e \in E$ and each $i = 1,..,N$ the estimate $\hat{p}_s(y_j|i,e)$ of the local hit density $p_s(y_j|i,e)$ for an arbitrary location y_j in grid cell G_j in area Y:

$$\hat{p}_s(y_j|i,e) = \hat{P}(j|i,e)/|G_j| \tag{4.4a}$$

where $|G_j|$ is the area size of the j-th grid cell and $\hat{P}(j|i,e)$ the estimated probability that the simulated crash locations $\boldsymbol{s}_{c,e}^{i,k}$, $k = 1,..,K_i$, is in grid cell G_j, i.e.

$$\hat{P}(j|i,e) = \sum_{k=1}^{K_i} \left[1\left[s_{c,e}^{i,k} \in G_j\right]\right]/K_i \tag{4.4b}$$

where $\boldsymbol{s}_{c,e}^{i,k}$ is the simulated UA position at crash moment $t_{c,e}^{i,k}$, and 1 is an indicator function, i.e. $1[true] = 1$, $1[false] = 0$.

Step 5: Evaluation of unprotected fatality model.

To estimate $\hat{P}(F|j,i,e)$ of $P(F|y \in A(i,e))$ in eq. (3.7) we evaluate for each j, i, e for which $\hat{P}(j|i,e) > 0$:

$$\hat{P}(F|j,i,e) = \hat{P}(F,j|i,e)/\hat{P}(j|i,e) \tag{4.5a}$$

with nominator

$$\hat{P}(F,j|i,e) = \sum_{k=1}^{K_i}\left[1\left[s_{c,e}^{i,k} \in G_j\right]P\left(F\middle|v_{c,e}^{i,k}, s_{c,e}^{i,k} \in A(i,e)\right)\right]/K_i \tag{4.5b}$$

Step 6: Evaluation of Individual risk per UA flight.

To estimate $\hat{R}_I^i(y)$ of $R_I^i(y)$ in eq. (2.8) we evaluate for an arbitrary location y_j in grid cell G_j, for each i-th flight:

$$\hat{R}_I^i(y) = \sum_{e \in E}[P(e|i)\,\hat{p}_s(y_j|i,e)\,|A(i,e)|\,\hat{P}(F|j,i,e)] \tag{4.6}$$

Step 7: Evaluation of Individual risk. Calculate the estimated individual risk for an arbitrary location y_j in grid cell G_j following eq. (3.1):

$$\hat{R}_I^{UAS}(y_j) = 1 - \prod_{i=1}^{N}[1 - \hat{R}_I^i(y)] \tag{4.7}$$

Step 8: Compare, for each j, $\hat{R}_I^{UAS}(y_j)$ versus applicable threshold values of acceptable level of Individual risk for commercial aviation around an airport. The applicable threshold in UK and The Netherlands for Individual risk is 10^{-6} per annum [34,35]. If $\hat{R}_I^{UAS}(y_j)$ is higher, then evaluate what this means to the UAS operation considered.

3.4.3 Evaluation of Collective ground risk by Monte Carlo simulation

For the evaluation of Collective ground risk, population density has to be taken into account as well as shelter protection using equations (2.7) and (3.3). This yields the following series of additional steps.

Step 9: Assess the population map $\hat{\rho}_j = \rho(y_j)|G_j|$ for each grid cell G_j.

Step 10: Assess for each grid cell G_j the probability of shelter protection against a ground crash of the i-th UA flight. This yields estimated shelter probability $\hat{P}(S|j,i)$ for each j,i.

Step 11: Estimate Collective ground risk per flight. Calculate $\hat{R}_{Cground}^i$, i.e. the estimated Collective ground risk per UA flight in area Y using eq. (2.7):

$$\hat{R}_{Cground}^i = \sum_j[\hat{R}_I^i(y)\,[1 - \hat{P}(S|j,i)]\,\hat{\rho}_j] \tag{4.8}$$

Step 12: Estimate Collective ground risk per flight hour for each flight. Calculate, for each i, the collective ground risk per UA flight hour $\hat{R}_{Cground}^i/T_i^{nom}$, and present the results for N flights in a histogram.

Step 13: Verify if a part of this empirical density passes an applicable threshold level. For example, [3] proposed a threshold of 10^{-6} fatal injuries on the ground per UA flight hour. For the part above the threshold it has to be evaluated what this means for the UAS operation considered.

Step 14: Calculate the estimated Collective ground risk using eq. (3.3):

$$\hat{R}_{Cground}^{UAS} = \sum_{i=1}^{N}\hat{R}_{Cground}^i \tag{4.9}$$

Step 15: Compare the estimated Collective ground risk versus an applicable threshold level of Collective ground risk. In eq. (3.5) such a threshold has been based on requirements posed on an FN-curve [34,35]. If the risk is higher, then evaluate what this means to the UAS operation considered.

3.5 Parcel Delivery Service by UAS

In this section we specify a hypothetical scenario of a UAS based parcel delivery service in the city of Delft. In section 3.5.1 the hub location is shown together with the population and

service radius while in section 3.5.2 the number of UA flights, parcel weight and parcel delivery locations are determined. In section 3.5.3 the wind distribution used for the scenario simulation is addressed. The UAS specifications are discussed in section 3.5.4, and the flight profile of a parcel delivery UA is shown in section 3.5.5.

3.5.1 Hub location, population and service area

For the UAS delivery area Y the city Delft is chosen. The hub is at an industrial area within the city, and the service radius is 2.5 km. An overview of the hub location, service radius and population distribution can be seen in Figure 1. The number of people living within the service area is estimated to be 120,838 using census data of Delft [36].

3.5.2 Number of UA flights, parcel weight and delivery locations

To estimate the number of UA flights per annum, we firstly estimate the number of parcel deliveries per person per year. The latter has been done by [37] for UAS based deliveries in Paris, France. The estimated number of deliveries per person per year is assumed to be 70% of the 2018 number of parcels delivered in Paris. With 12.3 million people and an estimated 161 million eligible parcels for the year 2018, that results in about 13.1 parcels per person per year. Based on the census data for the Delft area, this yields N=1,582,985 UAS based deliveries per year within the service radius in Figure 1.

The density of the parcel delivery locations is assumed to be the same as the population density within the delivery circle in Figure 1. The weight of the parcels is assumed to be uniformly distributed between 0.1 and 2.2 kg.
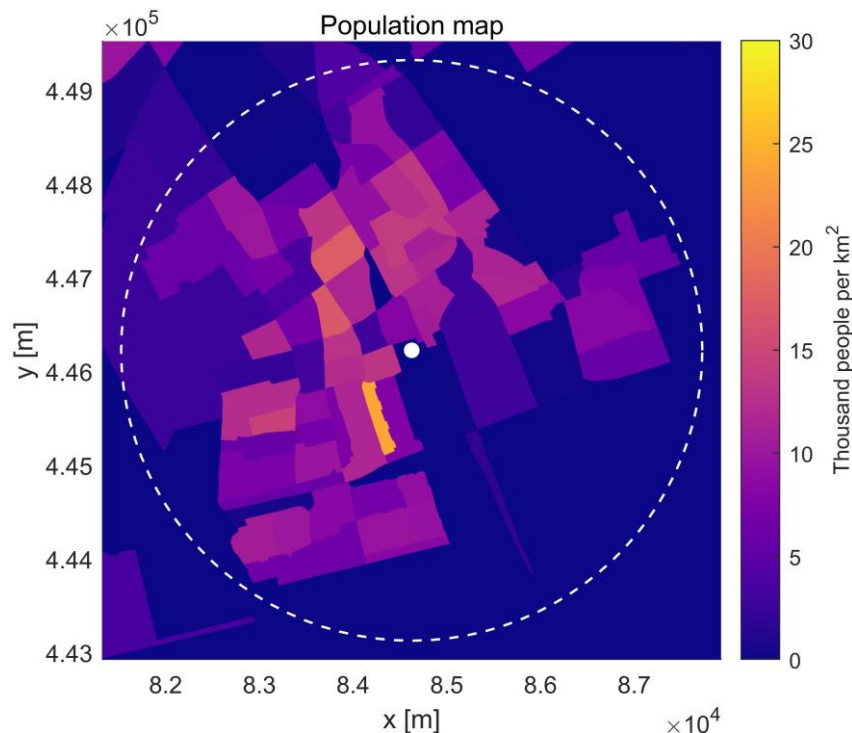
Figure 1: Hub location, service radius and population density [35]

3.5.3 Wind distribution

For the scenario vertical wind is assumed to be zero, and horizontal wind is based on actual wind measurements. Hourly wind data over the years 2013-2018 is used from the wind measurement post of Rotterdam [38]. The empirical wind vector w^e is measured over an open area at an altitude of 10m. In order to compensate for the altitude and air stability measurement

conditions, [33] has conversed this to the applicable height under an air stability exponent for an average urban area. The resulting empirical distribution of w^s at 120 m altitude is shown by the wind velocity distribution in Figure 2 and the wind rose in Figure 3. It is furthermore assumed that UA parcel delivery flights do not start when the expected wind velocity at cruise level is higher than $\|w_{max}\| = 10$ m s^{-1}.
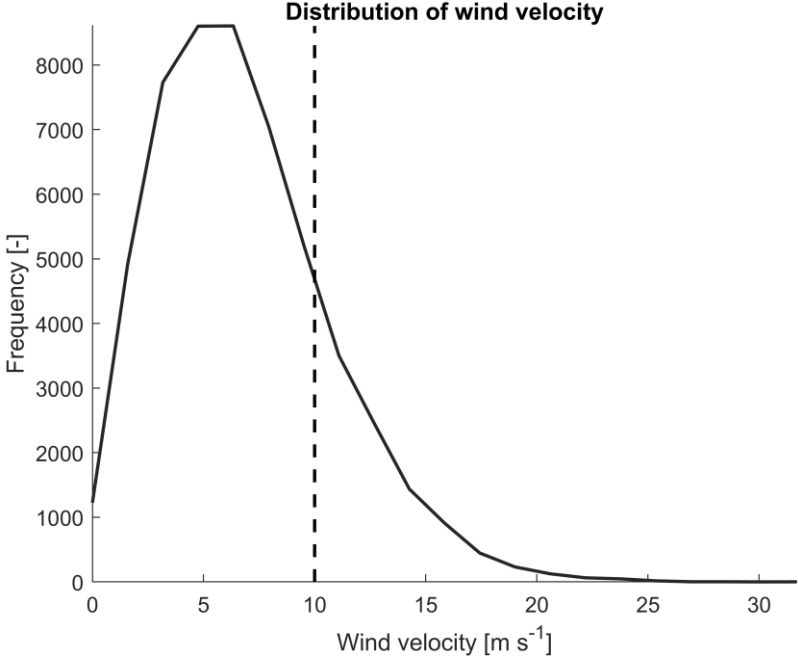
Figure 2: w^s velocity distribution at 120 m based on converted wind data; parcel delivery is stopped if w^s is above 10 m/s.
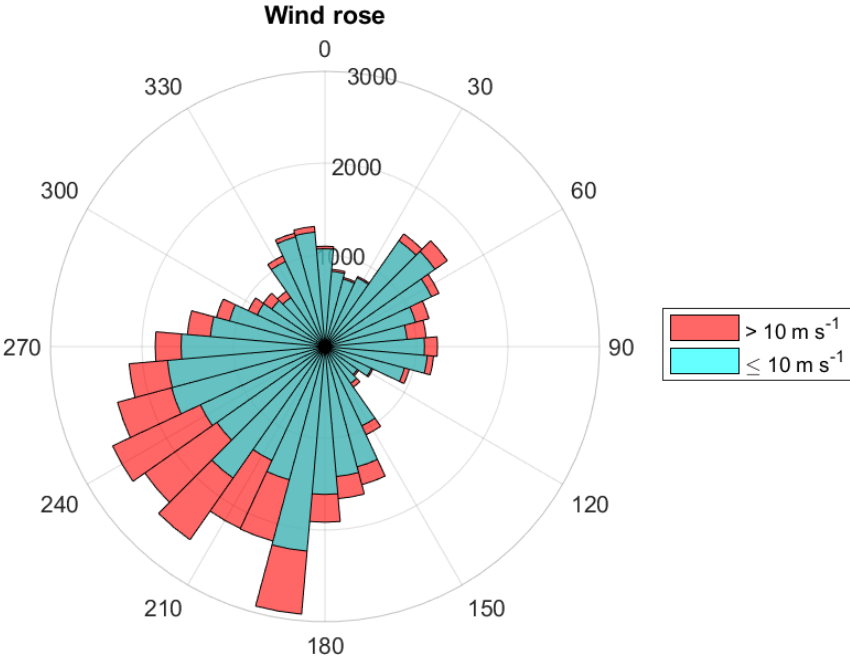
Figure 3: Wind rose of w^s velocity based on converted wind data.

3.5.4 Hypothetical UA specifications and UA selection

Two types of UAs are used for the parcel deliveries: a smaller UA with a payload of up to 1 kg and a larger UA with a payload of up to 3 kg. For every parcel that must be delivered,

the smallest UA that can deliver the parcel in terms of both payload and range is selected. A full list of parameter values for both UAs are given in Table 1.

Table 1: Adopted UAS parameter values

	UA$_{Small}$	UA$_{Large}$	Units
m_{drone}	2.7	6.0	Kg
$m_{payload}$	1	3	Kg
Range	15	25	Km
v_{cruise}	12	20	m s^{-1}
v_{ascent}	7.5	10	m s^{-1}
$v_{descent}$	6	8	m s^{-1}
C_D	N(0.7,0.2)	N(0.7,0.2)	
A_s	0.1	0.4	m^2
Planform area	1.1	3.9	m^2
σ_H^s	3.68	3.68	m
σ_V^s	7.65	7.65	m
σ_H^v	2.0	2.0	m/s
σ_V^v	2.0	2.0	m/s

The hypothetical larger UA in the parcel delivery scenario is based on the "MicroUAS MD4-3000 quadcopter UA" [39] which was used as an example for a delivery in the METROPOLIS report [40]. The hypothetical smaller UA is based on the MD4-1000 quadcopter from the same company for the sake of consistency [41]. The descent velocity is set to 80% of the ascent velocity to prevent vortex ring state of the rotors [42]. It is assumed that the drag coefficient C_D satisfies the probabilistic model adopted by [20] for ballistic descent of DJI Phantom 4. The latter has a symmetrical aerodynamic configuration that is similar to MD4-3000 and MD4-1000. The front area A_s is measured based on front images of MD4-3000 and of MD4-1000. Typically UA navigation is based on Global Positioning System, for which (σ_H^s, σ_V^s) values have been standardized under good satelluite coverage [43]. For (σ_H^v, σ_V^v) values from [20] are adopted.

3.5.5 Flight profile of a parcel delivery UA

One delivery flight consists of outbound and inbound paths. Hence for each parcel delivery a nominal flight profile from the hub to the delivery location and back is determined. A one-way profile is depicted in Figure 4. A UA with mass $m_{UA} + m_{payload}$ starts at the delivery hub, where it flies straight up (hover-ascent) with velocity v_{ascent} until it reaches altitude $h_{hover} = 50m$, where it transitions to a cruise-ascent, with horizontal velocity v_{cruise} an vertical velocity v_{ascent}. The UA continues this flight path until it reaches h_{cruise}=120m, where the UA transitions to a level cruise flight with velocity v_{cruise}. At some distance from the target, the UA transitions to a cruise-descent, with horizontal velocity v_{cruise} and vertical velocity $-v_{descent}$, until it reaches h_{hover} again. At that point, the UA transitions into a straight down path (hover-descent) with velocity $-v_{descent}$. During the return path the mass is m_{UA} and the flight profile is obtained in a similar way. Because $v_{ascent} \neq v_{descent}$ the return profile differs from the return profile, it rather is a mirror image. To avoid conflicts with outbound flights, return flights climb to a slightly higher level.
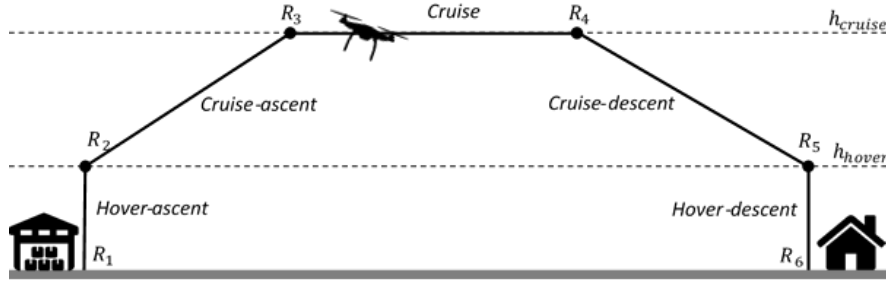
Figure 4: One-way flight profile for a parcel delivery UA.

3.6 Monte Carlo Simulation Results

The aim of this section is to assess and compare for the hypothetical parcel delivery service of section 3.5 the existing TPR indicator of Collective ground risk per flight (subsection 3.2.2) and the two novel TPR indicators: Individual risk per annum (subsection 3.3.1) and Collective ground risk per annum (subsection 3.3.2). For this assessment the MC simulation method of Section 3.4 is used. First subsection 3.6.1 describes the adopted TPR submodels. Then subsection 3.6.2 presents the results for the existing TPR indicator. Subsequently subsection 3.6.3 and 3.6.4 present the results for the two novel TPR indicators. Subsection 3.6.5 compares the results obtained for the three TPR indicators, and addresses effects of model assumptions.

3.6.1 TPR submodels adopted in the MC simulation

The TPR submodels that remain to be selected concerns equations (2.6-2.7). For operations by a mini UA over an urban area [11] derives a UAS system failure rate requirement of 0.342 per 1000 flight hour; the latter value we adopt, i.e. $\lambda_{i,H} = 3.42 \times 10^{-4}$ per hour, where the subscript H refers to all e_H that would cause a crash to the ground (due to inability to maintain coordinated flight). Regarding the mode e_θ of a quadcopter descend path to the ground we adopt the conservative assumption that the ballistic descent model of [20,33] applies (see substep 3.3).

For the probability of fatality, use is made of the Range Commanders Council [44] adopted Feinstein model:

$$P(F|y \in A(i,H),v) = Z(\frac{\ln E_{imp} - \ln a}{b}) \tag{6.1}$$

where Z is the cumulative standard normal distribution [9, p. 102]. $E_{imp} = m|v|^2/2$ is the kinetic energy of UA at moment of impact, with impact velocity vector v and with impact mass $m = m_{UA} + m_{payload}$ during outbound, or $m = m_{UA}$ during inbound. Hence Z defines an S-shaped curve that starts at probability zero for $E_{imp} = 0$, reaches probability ½ for $E_{imp} = a$ and asymptotically goes to probability 1 for large E_{imp}. Feinstein et al. [45] have used impact data to assess the mid-point value $a = 101.6$ Joule and standard deviation $b = 0.538$ of the effect of $\ln E_{imp}$.

The size of the crash impact area $|A(i,H)|$ is assumed to be equal to the size of the planform rectangle area of the i-th flight. The rationale for selecting this relative small crash impact area is that a ballistic UA descent leads to hitting a human mainly on the head, and that the UA weight has less effect if the head is hit off-center, e.g. by one of the rotor engines.

Regarding the shelter model, a fixed probability value of shelter protection is assumed. For the USA, [11] provides statistical value for the time spent outdoors of 7.8 % and for the time spent in vehicle of 5.5%. To take into account that in The Netherlands cycles and mobility scooters are frequently used instead of cars, for Delft we adopt a value of 10% that persons are unprotected outdoors, i.e. $\hat{P}(S|i, H) = 0.9$.

For the MC simulation, the adopted size of grid cells $|G_j| = 25 \; m^2$. The MC simulation took 6.1 hours on an ASUS RS700A-E9-RS4 with an AMD Epyc 7551 processor having 32 cores and 64 threads and 256 GB of RAM.

3.6.2 Estimated Collective ground risk per UA flight hour

In Step 12, for each of the N flights the collective ground risk per UA flight hour $\hat{R}^i_{Cground}/T^{nom}_i$ is calculated. The results are presented in the form of a histogram in Figure 5; this shows two increasing patterns with peaks at 3.2×10^{-7} and 1.2×10^{-6} stemming from flights by the small and large UA types respectively. The maximum value is 1.93×10^{-6} per flight hour; the mean value is 6.73×10^{-7} per flight hour.

For Step 13, the histogram in Figure 5 to compare $\hat{R}^i_{Cground}/T^{nom}_i$ against the applicable threshold value of 10^{-6} per UA flight hour. Although the mean value of $\hat{R}^i_{Cground}/T^{nom}_i$ is clearly smaller than the threshold value of 10^{-6}, $\hat{R}^i_{Cground}/T^{nom}_i > 10^{-6}$ for 497,401 of the 1,582,985 UA flights, i.e. 31.4%. The good news is that of these 31.4% of the UA flights the passing over the 10^{-6} threshold is rather limited, i.e. almost all less than a factor 1.5. In Figure 6, these flight paths of the UA flights with $\hat{R}^i_{Cground}/T^{nom}_i > 10^{-6}$ are projected on the population map. These paths fly across an area with relative high population density.
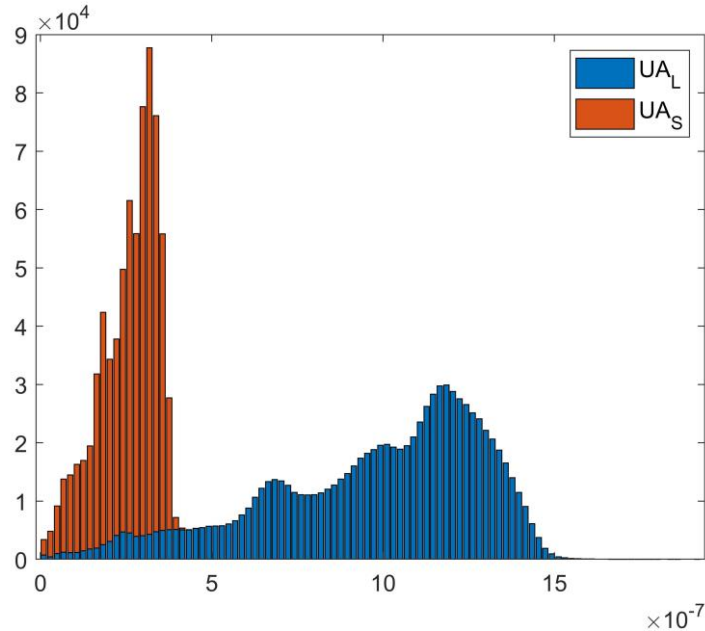
Figure 5: Histogram of $\hat{R}^i_{Cground}/T^{nom}_i$; blue = large UA, red = small UA
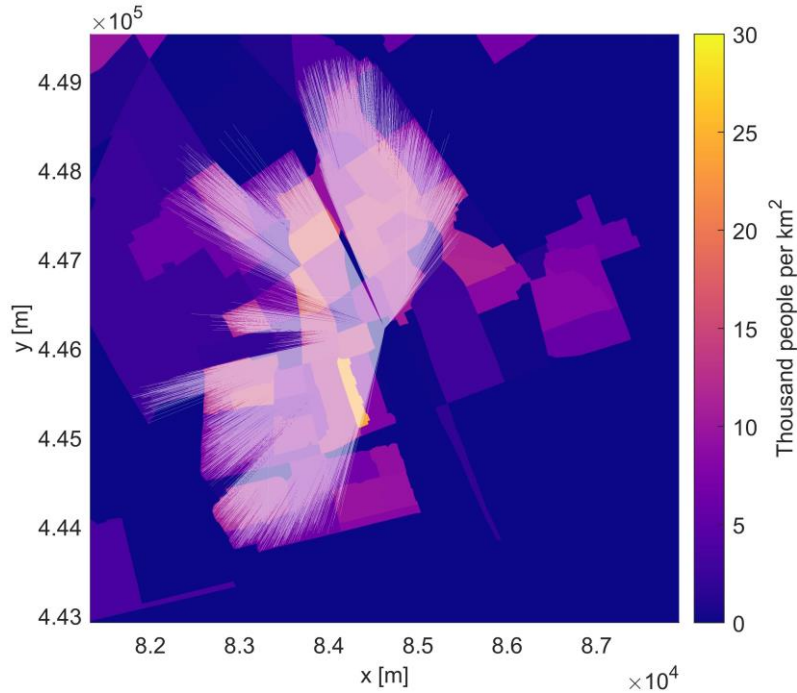
Figure 6: UA Flight Paths with $\hat{R}^i_{Cground}/T^{nom}_i > 10^{-6}$

3.6.3 Estimated Collective ground risk per annum

In Step 14, the estimated collective ground risk $\hat{R}^{UAS}_{Cground} = 0.063$ fatalities per annum for the UAS-based parcel delivery service in the city of Delft. For Step 15, we adopt eq. (3.5) as threshold. Standing regulation in The Netherlands for airports and hazardous installations [34,35] sets $C = 10^{-3}$ and $\alpha = 2$. This yields a threshold of 0.00165 fatalities per annum, which is 38x lower than the assessed $\hat{R}^{UAS}_{Cground} = 0.063$ fatalities per annum.

3.6.4 Estimated Individual Risk

For Step 7, estimated Individual risk $\hat{R}^{UAS}_I(j)$ for the considered area is shown in Figure 7. Because each delivery flight makes a steep climb and a steep descent near the hub, a relative large percentage of UA flight time is near the hub, which leads to the highest value of $\hat{R}^{UAS}_I(j) = 0.023$ per annum at the hub location. This reflects that the ascend/descent frequency is orders in magnitude higher near the delivery centre than it is at other areas, including the area with the highest population density.
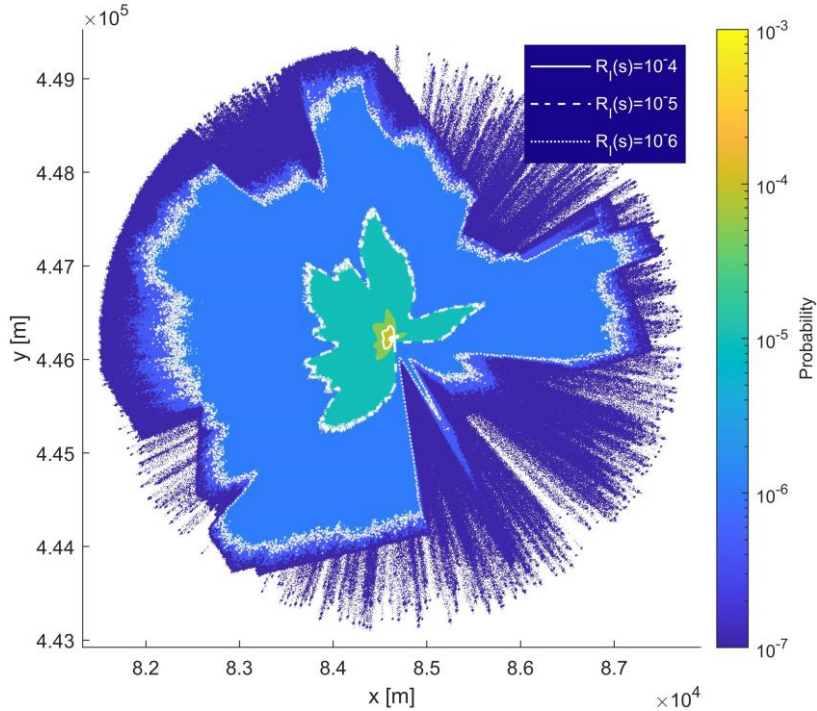
Figure 7: Individual risk $\hat{R}_I^{UAS}(j)$ within service area, with contours for $\hat{R}_I^{UAS}(j)$ =10⁻⁶, 10⁻⁵ and 10⁻⁴.

For Step 8 in comparing individual risk $\hat{R}_I^{UAS}(j)$ to applicable threshold, Figure 7 projects the 10^{-6}, 10^{-5} and 10^{-4} contours on the surface plot of $\hat{R}_I^{UAS}(j)$. This shows that for most of the area the threshold value of 10⁻⁶ per annum is passed. In Figure 8, individual risk contours of 10^{-6}, 10^{-5} and 10^{-4} are projected on the population map. This shows that the area within the 10^{-5} contour includes a significant part of the population. Calculated percentages in size and population of the areas within the three contours in Figure 8 are given in Table 2. This shows that the 10^{-6} individual risk contour includes 81.5% of the population within the delivery area considered. The 10^{-5} individual risk contour includes 13.9% of the population. The 10^{-4} individual risk contour includes 0.004% of the population only (5 persons).
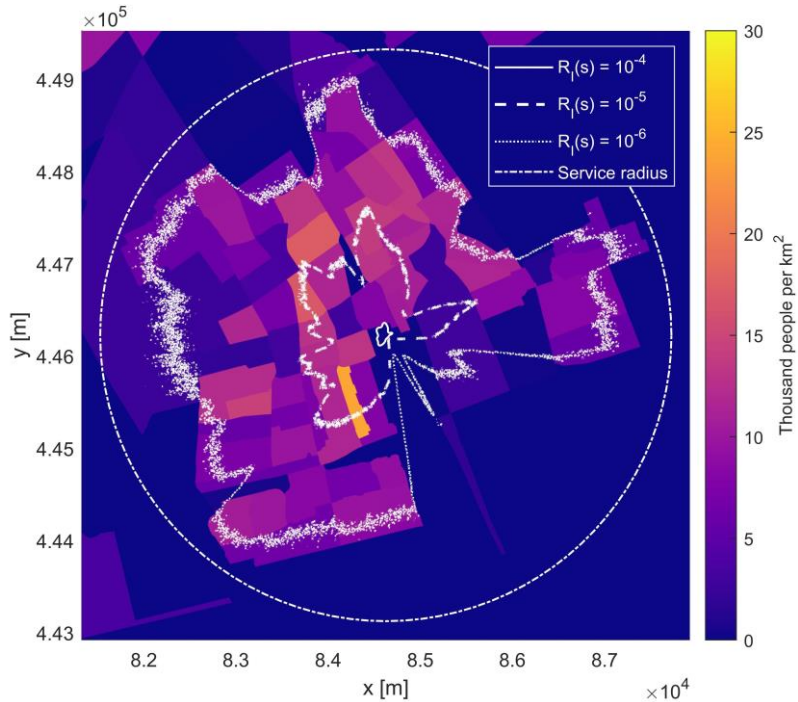
Figure 8: Individual Risk Contours of $\hat{R}_I^{UAS}(j) = 10^{-6}$, 10^{-5} and 10^{-4} projected on population map in Figure 1.

51

Table 2: Area and population within individual risk contours in Figure 9.

Individual Risk contour	% of area	% of population
$\hat{R}_I^{UAS}(j) > 10^{-6}$	64.5%	81.5%
$\hat{R}_I^{UAS}(j) > 10^{-5}$	9.0%	13.9%
$\hat{R}_I^{UAS}(j) > 10^{-4}$	0.1%	0.004%

3.6.5 Discussion of simulation results

For a hypothetical UAS-based parcel delivery service to the population in Delft, three TPR models for UAS operations have been assessed, i.e. Collective ground risk per UA flight hour, Collective ground risk per annum, and Individual risk. In literature on TPR of UAS operations only the Collective ground risk per UA flight hour is assessed. Therefore we first discuss the simulation results obtained for this commonly used model, and subsequently address the results obtained for the two novel TPR models.

If the assessed Collective ground risk per UA flight hour is averaged over all N = 1,582,985 UA delivery flights per annum, then it is about a factor 1.5 lower than the applicable threshold of 10^{-6} per flight hour proposed for Europe [3]. However for 31.4% of the individual UA flights the applicable threshold is passed, by at most a factor 1.9. The passing of this threshold does not apply to parcel deliveries by the small UA; it only applies to about 50% of the parcels delivered by the larger UA.

In contrast to the existing Collective ground risk per UA flight hour, the two novel TPR models pose more serious safety obstacles. For the novel TPR indicator Collective ground risk per annum the simulation results show a level that is a factor 38 higher than the standing regulation for airports and hazardous installations [34, 35].

The simulation results for the Individual risk show for most locations, except those near the outer range, assessed $\hat{R}_I^{UAS}(j)$ values that go beyond the applicable threshold of 10^{-6} probability of fatality per annum due to UA hit of an unprotected person [34,35]. The percentages where this threshold is not satisfied accounts for 64.5% of the area and 81.5% of the population within the considered area. In view of standing regulation in The Netherlands, if this threshold value of 10^{-6} is not satisfied for commercial air traffic around Schiphol, then the following zonal policies have been implemented around the airport. All housing within the 10^{-5} contour have been demolished, all housing development inside the 10^{-6} contour has been banned, and a waiver has been given for the houses in between these two contours. Introducing a similar zonal policy to the hypothetical UAS-based parcel delivery service in Delft would mean that 13.9% of the population in the area has to leave their housing, and that 81.5% - 13.9% = 67.6% of the population a waiver is needed to remain living in their current housing.

A factor 10 improvement in UAS system failure rate would mean that the assessed levels for each of the three TPR indicators go a factor 10 down. For the Individual risk $\hat{R}_I^{UAS}(j)$ this would mean that the 10^{-6} contour would shrink to the location of the 10^{-5} contour in Figure 8. Similarly, the 10^{-5} contour would shrink to the location of the 10^{-4} contour in Figure 8. Hence, only five persons would have their housing within the novel 10^{-5} contour. For the zonal policy this would mean that these 5 persons have to give up their housing and a waiver has to be given for 13.9% of the population to continue living in their houses within the shrinked 10^{-6} contour (9.0 % of area). Even on this basis it will be difficult for Delft to welcome the parcel delivery service considered. In addition, the novel Collective ground risk per annum $\hat{R}_{Cground}^{UAS}$

would still be a factor 3.8 higher than allowed by standing TPR regulation for airports and hazardous installations.

Because the assessed TPR levels are based on models, instead of statistical data, there is a non-negligible level of uncertainty in these point estimates. Such uncertainties stem from the following model assumptions:

- Wind does not lead to significant deviation from the nominal flight path.
- There is no general aviation in the airspace used by the UAS flights.
- During uncoordinated descent to the ground other UA's are ignored.
- All crashes to the ground are outcomes of a ballistic descent.
- During ballistic descent there is no tumbling and no rotor wind-milling.
- Buildings and other infrastructure do not influence accident location.
- The Range Commanders Council adopted fatality probability model [44].
- The small size assumption of the crash impact area.
- The estimated percentage of the population that is not sheltered.

Of these model assumptions all except the latter have a similar effect on all three model based TPR assessments. Moreover the sheltering assumption has similar effects on the two Collective risk models. This means that the model assumptions do not have significant effect on the Monte Carlo simulation based comparison of the two novel TPR models versus the existing TPR model.

3.7 Conclusions

This paper has studied third party risk (TPR) that is posed by commercial use of a UAS operation that consists of a large number of UA flights per annum, e.g. UAS based parcel delivery in an urban area. Under current regulations such commercial UAS operations over an urban area is not allowed. However with the further development of reliable small UA these operations might prove to be sufficiently safe in future, as a result of which future regulations could allow small UA commercial operations over urban areas. From the literature review in Section 3.2 it has become clear that TPR literature has focussed on the risk posed to persons on the ground per UA flight hour. However to manage the future risk of commercial UAS operations over an urban area there is a need for TPR models that capture the risk posed to the population by a large number of UA flights per annum. For commercial aviation the latter has been established through the use of models for Collective ground risk and Individual risk posed to the persons on the ground. Similar model extensions in terms of Individual risk and Collective ground risk for UAS operations have been developed in Section 3.3. Subsequently, Section 3.4 has developed a MC simulation method to assess these TPR models.

In section 3.5 a scenario of a UAS based parcel delivery service for the city of Delft in The Netherland has been developed. This includes number of parcel deliveries, parcel weights, types of UAs to be used, wind effects, and flight profiles for the parcel deliveries. Subsequently in Section 6 this parcel delivery service scenario has been assessed using the TPR models developed in section 3.3 and the MC simulation steps of section 3.4.

The MC simulation results in Section 6 show that for the hypothetical UAS based parcel delivery service in the city of Delft the existing TPR requirement in terms of expected number of ground fatalities per UA flight hour will largely be satisfied. However the MC simulation results in Section 3.6 also show that the levels assessed for the two novel TPR models are an

order in magnitude higher than standing TPR requirements on airports and hazardous installations.

The overall conclusion is that the two novel TPR indicators fill a gap in understanding third party risk from a population perspective. The novel Collective ground risk per annum accumulates the risk contributions by a large number of UA flights in a rural area. The added value of Individual risk is that it identifies population areas which are posed to relatively high TPR; and therefore supports zonal policies.

The TPR evaluation of a hypothetical application to a UAS based parcel delivery service in the city of Delft shows that from a population perspective there is a need for substantial further developments in UAS operations. Recently, Petritoli et al. [47] has studied the development of a highly reliable UAS design; the overall reliability of this design is a factor 10 better than the UAS system failure rate assumed in the current simulation study. However overall reliability of a design covers only the technical share of UAS system failures; it does not cover non-technical issues such as human error, unexpected adverse weather, or collision with a bird, a building or with another UA. Hence to realize a factor 10 improvement in UAS system failure rate requires much more than the design by [47] alone. An important development is the mitigation of remaining TPR risks by safety management systems integrated on-board UAs [48,49] and ground-based support [50].

Because the assessed TPR levels are based on models, instead of statistical data, there is a non-negligible level of uncertainty in these point estimates. To reduce this level of uncertainty there is a need for further development in TPR submodels. Each of the uncertainties mentioned in subsection 3.6.5 are valuable candidates for follow-on research. This includes the development of further models for quadcopter non-ballistic descents as well as the development of submodels for non-technical hazards such as human error, unexpected weather change, and mid-air collisions. In [51] Multi-Body System (MBS) modelling and simulation is used to get insight in the validity of the human impact fatality model of [44]. A logical follow-up is to extend this MBS modelling and simulation to better understand the quantification in equation (2.8) of the product of the two right hand terms, i.e. size of the crash impact area multiplied by the human fatality probability. Another aspect that deserves further research is that TPR of UAS operations does not only address persons on the ground, though also persons on board of aircraft that are hit by a UA [8,52]. To gain a better understanding [53] has identified the extra TPR terms and which are covered by current regulation and which not. For the studied parcel delivery service in the city of Delft there is need to manage the third party risk posed by fly-away UAS to passengers onboard aircraft to and from Rotterdam The Hague airport, e.g. [54].

References

[1] ICAO, Unmanned Aircraft Systems (UAS), Circular 328-AN/190, International Civil Aviation Organization, 2011.

[2] FAA, "Operation and Certification of Small Unmanned Aircraft Systems," Department of Transportation, Washington, USA, 2016.

[3] JARUS, Guidelines on Specific Operation Risk Assessment (SORA), Joint Authorities Regulation Unmanned Systems, 2017.

[4] H. Bohnenblust, Risk-based decision making in the transportation sector, In: R.E. Jorissen, P.J.M. Stallen (Eds.), Quantified Societal Risk and Policy Making, Kluwer Academic Publishers, Dordrecht, 1998.

[5] B.J.M. Ale and M. Piers, The assessment and management of third party risk around a major airport, Journal of Hazardous Materials, Volume 71, Issues 1–3, January 2000, pp. 1-16.

[6] S.N. Jonkman, P.H.A.J.M. Van Gelder, J.K. Vrijling, An overview of quantitative risk measures for loss of life and economic damage, J. of Hazardous materials, Vol. A99 (2003), pp. 1-30.

[7] R.E. Weibel and R.J. Hansman Jr., "Safety Considerations for Operation of Different Classes of UAVs in the NAS," Unmanned Unlimited, Technical Conf., Workshop and Exhibit, 20-23 Sept. 2004, Chicago, IL, AIAA-2004-6421, pp. 1-11.

[8] R. Clothier and R. Walker, "Determination and Evaluation of UAV Safety Objectives," Proc. 21st Int. UAV Systems Conf., 2006, pp. 18.1-18.16.

[9] K. Dalamagkidis, K. Valavanis and L. Piegl, "On integrating unmanned aircraft systems into the National Airspace System, Springer, 2nd ed., 2012.

[10] C. Lum and B. Waggoner, "A Risk Based Paradigm and Model for Unmanned Aerial Systems in the National Airspace," AIAA Conf. , Seattle, 2010.

[11] R. Melnyk, D. Schrage, V. Volovoi and H. Jimenez, "A third-party casualty risk model for unmanned aircraft system operations," Reliability Engineering & System Safety, Vol. 124 (2014), pp. 105-116.

[12] E.S. Rudnick-Cohen, S. Azarm, J. Herrmann, Multi-objective design and path planning optimization of unmanned aerial vehicles (UAVs). 16th AIAA/ISSMO Multidisciplinary Analysis and Optimization Conf., 2015.

[13] E. Rudnick-Cohen, J.W. Herrmann, S. Azarm, Modeling Unmanned Aerial System (UAS) risks via Monte Carlo simulation, 2019 Int. Conf. on UAS (ICUAS2019), Atlanta, GA, USA, June 11-14, 2019.

[14] S. Bertrand, N. Raballand, F. Viguier, F. Muller, Ground risk assessment for long-range inspection missions of railways by UA's, Proc. 2017 Int. Conf. on Unmanned Aircraft Systems, Miami, FL.

[15] A. La Cour-Harbo, The value of step-by-step risk assessment for unmanned aircraft, Proc. 2018 International Conference on Unmanned Aircraft Systems (ICUAS),June 2018, Dallas, TX, USA, pp. 149-157.

[16] A. La Cour-Harbo, Quantifying risk of ground impact fatalities for small unmanned aircraft, J. of Intelligent and Robotic Systems, Vol. 93 (2019), pp. 367-384.

[17] J.V. Foster and D.C. Hartman, High fidelity unmanned aircraft system simulation development for trajectory prediction under off-nominal flight dynamics, 17th AIAA ATIO Conf., June 2017, Denver, Colorado.

[18] K. Cunningham, D.E. Cox, J.V. Foster, S.E. Riddick, S.A. Laughter, AirSTAR beyond visual range system description and preliminary test results, AIAA Sci. Tech Forum, January 2016.

[19] E. Ancel, F. Capristan, J. Foster and R. Condotta, Real-time risk assessment framework for UAS traffic management (UTM), 17th AIAA ATIO Conf., June 2017, Denver, Colorado, AIAA-2017-3273.

[20] A. La Cour-Harbo, Ground impact probability distribution for small unmanned aircraft in ballistic descent, Proc. ICUAS 2020, September 2020.

[21] S. Primatesta, A. Rizzo, A. La Cour-Harbo, Ground risk map for Unmanned Aircraft in urban environments, J. of Intelligent & Robotic Systems, May 2019, https://doi.org/10.1007/s10846-019-01015-z

[22] G.M.H. Laheij, J.G. Post, B.J.M. Ale, Standard methods for land-use planning to determine the effects on societal risk, J. of Hazardous Materials, Vol. 71 (2000), pp. 269–282.

[23] M. Christou, Z. Gyenes, M. Struckl, Risk assessment in support to land-use planning in Europe: Towards more consistent decisions? Journal of Loss Prevention in the Process Industries, Vol. 24 (2011). pp. 219-226.

[24] H. Smets, Frequency distribution of the consequences of accidents involving hazardous substances in OECD countries, 1996, Etudes et Dossiers, Geneva Association.

[25] C.W. Lum, K. Gauksheim, T. Kosel, T. McGeer, Assessing and estimating risk of operating Unmanned Aerial Systems in populated areas, 11th AIAA ATIO Conference, September 2011, AIAA-2011-6918.

[26] L.C. Barr, R.I. Newman, E. Ancel, C.M. Belcastro, J.V. Foster, J.K. Evans, D.H. Klyde, Preliminary risk assessment for small unmanned aircraft systems, 17th AIAA ATIO Conf., June 2017, Denver, Colorado.

[27] S.H. Kim, Third-Party risk of mid-air collision between small unmanned aircraft systems, Proc. AIAA Aviation Forum, June 2019, Dallas, Texas, DOI 10.25.14/6.2019-3052.

[28] S.H. Kim, Third-Party Risk Analysis of Small Unmanned Aircraft Systems Operations, J. of Aerospace Information Systems, Vol. 17 (2020), pp. 24-35.

[29] A. La Cour-Harbo, H. Schioler, Probability of low-altitude midair collision between general aviation and unmanned aircraft, Risk Analysis, Vol. 39 (2019), pp. 2499-2513.

[30] Y. Haartsen, R. Aalmoes, Y.S. Cheung. Simulation of unmanned aerial vehicles in the determination of accident locations. In 2016 IEEE Int. Conf. on UAS (ICUAS2016) , pp. 993-1002.

[31] R. Aalmoes, Y.S. Cheung, E. Sunil, J.M. Hoekstra, F. Bussink, A conceptual third party risk model for personal and unmanned aerial vehicles, Proc. Int. Conf. on UAS, ICUAS2015, June 2015.

[32] M. Abramowitz and I.A. Stegun (eds.), Handbook of Mathematical Functions, National Bureau of Standards, 10th printing, December 1972.

[33] W. Grimme, "Modelling and Monte Carlo simulation of third party risk of drones," MSc thesis Delft University of Technology, February 2018.

[34] P.H. Bottelberghs, Risk analysis and safety policy developments in The Netherlands, J. of Hazardous Materials, Vol. 71 (2000), pp. 59–84.

[35] V.M. Trbojevic, Risk criteria in EU, Proc. ESREL 2005, Poland, 27-30 June 2005.

[36] CBS, Wijk- en buurtkaart 2017, Centraal Bureau voor de Statistiek [Online].[Accessed 26 01 2019].

[37] M. Doole, J. Ellerbroek and J. Hoekstra, "Drone Delivery - Urban airspace traffic density estimation," TU Delft, Delft, 2018.

[38] KNMI, Uurgegevens van het weer in Nederland, KNMI, https://projects.knmi.nl/klimatologie/uurgegevens/selectie.cgi. [Accessed 26 01 2019].

[39] Microdrones, "md4-3000: The high-powered VTOL quadrocopter from Microdrones," https://www.microdrones.com/en/drones/md4-3000/. [Accessed 26 01 2019].

[40] E. Sunil, J. Ellerbroek and J. Hoekstra, "METROPOLIS – Urban Airspace Design - Scenario Definition Report (D 1.2)," TU Delft, 2014.

[41] Microdrones, "md4-1000: Robust and powerful – UAV / drone model from Microdrones," https://www.microdrones.com/en/drones/md4-1000/. [Accessed 26 01 2019].

[42] DJI, "Inspire 2 - Specs," [Online]. Available: https://www.dji.com/nl/inspire-2/specs. [Accessed 26 01 2019].

[43] DOD, "Global Positioning System Standard Position Service Performance Standard," Department of Defense, USA, Washington, 2008.

[44] Range Commanders Council, Range Safety criteria for Unmanned Air Vehicles, Rationale and methodology supplement; Supplement to Document 321-00, April 2000.

[45] D.I. Feinstein, W.F. Haugel, M.L. Kardatzke, A. Weinstock, Personnel casualty study. Tech. Rep. Project No. J 6067, Illinois Institute of Technology Research, July 1968.

[46] CBS, Traffic death toll up by 11 percent in 2018, Centraal Bureau voor de Statistiek, https://www.cbs.nl/en-gb/news/2019/16/traffic-death-toll-up-by--11-percent-in-2018

[47] E. Petritoli, F. Leccese, L. Ciani, Reliability and maintenance analysis of unmanned aerial vehicles, Sensors, Vol. 18 (2018), doi:10.3390/s18093171.

[48] C.A. Ippolito, Dynamic ground risk mitigating flight conyrol for autonomous small UAS in urban environments, AIAA-Aviation Forum, 17-21 June 2019, Dallas, Texas.

[49] E. Ancel, F.M. Capristan, J.V. Foster, R.C. Condotta, In-time non-participant casualty risk assessment to support onboard decision making for autonomous unmanned aircraft, AIAA-Aviation Forum, June 2019.

[50] B. Pang, Q. Tan, K.H. Low, A risk-based UAS traffic network model for adaptive urban airspace management, AIAA Aviation Forum, June 2020.

[51] B. Rattanagraikanakorn, H.A.P. Blom, A. Sharpanskykh, C. De Wagter, C. Jiang, M. Schuurman, D. Gransden, R. Happee, "Modeling and Simulating Human Fatality due to Quadrotor UAS Impact", AIAA Aviation Forum, June 2020.

[52] R.A. Clothier, B.P. Williams, K.J. Hayhurst, Modelling the risks remotely piloted aircraft pose to people on the ground, Safety Science, Vol. 101 (2018), pp. 33-47.

[53] C. Jiang, H.A.P. Blom, A. Sharphanskykh, Third Party Risk Indicators and Their Use in Safety Regulations for UAS Operations, AIAA Aviation Forum, June 2020.

[54] C.H.J. Wang, S.K. Tan, K.H. Low, Three-dimensional (3D) Monte-Carlo modelling for UAS collision risk management in restricted airport airspace, Aerospace Science and Technology, Vol. 105 (2020), 105964, pp. 1-13.

4

Joint Assessment of Impact Area and Human Fatality of Ground Crash by an Unmanned Aircraft System

Unmanned Aircraft System (UAS) flight imposes Safety Risk on ground population; this is also referred to as ground Third Party Risk (TPR). A commonly used ground TPR indicator is the expected number of ground fatalities per UAS flight hour. The in literature established model involves a product of impact area A_{impact} and probability of fatality $P\{F|impact\}$ for a person impacted by a crashing UAS. Although, in literature, various models have been developed for both terms, a validated model for the product $A_{impact} \times P\{F|impact\}$ is still missing. A promising direction is to conduct dynamical simulations of $P\{F|impact\}$ by making use of Finite Element (FE) or Multi-Body System (MBS) models of collision between a UAS and a human body. This dynamical modelling and simulation approach has been well developed for crash risk analysis in automotive industry; including model validation against measurements from controlled impacts with crash dummies and post-mortem human bodies. This paper develops a method to use this dynamical simulation approach for the joint assessment of the product $A_{impact} \times P\{F|impact\}$ in the ground TPR model. The key step in this development, is to show that in the ground TPR model, this product can be replaced by an integration over simulated risk values for different offsets between the UAS crash centre and the location of the impacted human. The subsequent step is to develop a method for the numerical evaluation of this enriched ground TPR model, by making use of a validated dynamical simulation model of a UAS impacting a human body under various offsets and geometries. Application of this novel approach is illustrated for a DJI Phantom III UAS crashing to the ground, including a comparison with existing models.

4.1 Introduction

Unmanned Aircraft System (UAS) technology has the potential to replace manned aircraft and aerial platforms. This potential is of particular interest for commercial UAS-based taxi services, parcel delivery services, medical aid services, etc. Advantages of commercial UAS-based services also come with third party risk (TPR) for overflown population on the ground. Especially challenging is that the imposed level of ground TPR typically increases linearly with the density of potential customers of UAS services. Therefore, a key factor in the further development of safe commercial UAS services are validated models of ground TPR posed by UAS flights.

A commonly adopted indicator for ground TPR is $E\{n_F\}$, i.e. the expected number of ground fatalities per UAS flight hour. In literature, e.g. [RCC, 2001; Weibel and Hansman, 2004; Melnyk et al. ,2014], the common model for this indicator reads as:

$$E\{n_F\} = \lambda_{system} \times \rho_{population} \times (1 - P_{shelter}) \times A_{impact} \times P\{F|impact\} \qquad (1.1)$$

where λ_{system} is the failure rate of the UAS system, $\rho_{population}$ is the population density of the overflown area, $P_{shelter}$ is the probability that a person on the ground is sheltered to the crashing UAS, A_{impact} is the size of the area on the ground that is impacted by the crashing UAS, and $P\{F|impact\}$ is the probability of Fatality (F) for a person on the ground that is impacted by a crashing UAS. The product of the first four terms yield the expected number of impacted persons on the ground per UAS flight hour. The last term $P\{F|impact\}$ is a measure for the consequences of a UAS impacting a person on the ground. Ground TPR eq. (1.1) has been extended for UAS flights over areas with non-homogeneous population densities and sheltering [Bertrand et al., 2017; la Cour-Harbo, 2019; Blom et al., 2021].

Regulation typically poses an upper bound on the expected number of ground fatalities per UAS flight hour, i.e. on $E\{n_F\}$ [ICAO, 2011; FAA, 2016; JARUS, 2017; EASA, 2021; EC, 2021]. Equation (1.1) shows that a commercial UAS service has three complementary directions in adhering to an upper bound on $E\{n_F\}$. The first direction is to reduce UAS system failure rate λ_{system} by improving the system design of the own UAS [Clothier et al., 2018; Petrioli et al., 2018] as well as the interaction with other UAS or other low flying object [Kim, 2019; la Cour-Harbo and Schioler, 2019]. The second direction is to reduce the effect of $\rho_{population} \times (1 - P_{shelter})$ by applying risk-aware UAS path planning and emergence landing strategies [Ippolito, 2019; Ancel et al., 2019; Primatesta et al., 2020; Hu et al., 2020, Oh et al., 2020; He et al., 2022]. The third direction is to reduce the effect of $A_{impact} \times P\{F|impact\}$ by improving physical UAS design in shape and material. In contrast to the former two directions, the physical UAS design direction has not yet received much attention; its further development asks for validated models to quantify effects of physical UAS design on $A_{impact} \times P\{F|impact\}$.

The ground TPR model for commercial aviation also involves the product $A_{impact} \times P\{F|impact\}$ [Ale and Piers, 2000]. In contrast to UAS operations, in commercial aviation sufficient accident data are available to quantify both terms. Unfortunately, accident data for different UAS types is too scarce to allow a similar statistical quantification. Hence, for ground TPR of UAS, non-statistical parametric models have been developed in literature.

Overviews [Melnyk et al., 2014; Washington et al., 2017] have shown that there is a significant diversity in the parametric models for A_{impact} and for P{$F|impact$}. Washington et al. [2017] argue that the current level of diversity leads to an undesired variability in the risk assessment outputs. An extra limitation of these existing models is that they do not take into account that the fatality for a person in the impact area may vary depending on the offset between the crash centre and the location of a human in the impact area.

To improve this situation, a recent development is to replace parametric models for P{$F|impact$} by a dynamical simulation of a finite-element (FE) or a Multi-Body-System (MBS) model of UAS collision with a human body [Koh et al., 2018; Arterburn et al, 2019; Rattanagraikanakorn et al., 2019, 2020a,b, 2022; Weng et al., 2021]. The basis for this dynamical simulation approach stems from car crash research in automotive industry [THUMS, 2015, 2018; MADYMO, 2017a,b]. For UAS impact on human body, validation of this dynamical simulation approach is accomplished by showing that detailed simulated results correspond with dynamical impact measurements under laboratory controlled UAS collisions with human dummies [Arterburn et al, 2017; Campolettano et al., 2017; Koh et al., 2018; Arterburn et al., 2019] and with human cadavers [Stark et al., 2019].

The objective of this paper is to further improve the situation by developing a method for using this dynamical simulation approach for the joint assessment of the product $A_{impact} \times$ P{$F|impact$} rather than P{$F|impact$} alone. A key step in this development is to show that ground TPR eq. (1.1) can be enriched through replacing the product $A_{impact} \times$ P{$F|impact$} by an integration over dynamically simulated risk values for various offsets between UAS crash centre and human location. The subsequent step is to capture this in a numerical evaluation process that makes use of a validated dynamical simulation model of a UAS impacting a human body.

The paper is organized as follows. Section 4.2 provides a literature overview of models for A_{impact} and for P{$F|impact$}, including an illustration of the large variety in resulting values for a UAS of 1.21 kg crashing to the ground. Section 4.3 develops the enrichment of eq. (1.1), and subsequently shows how this enriched model can be numerically evaluated by using dynamical simulations of a UAS collision with a human body. Section 4.4 evaluates the enriched model through the evaluation of a validated dynamical simulation model of the 1.21kg UAS, and compares the obtained results with existing models of section 4.2. Section 4.5 draws conclusions.

4.2 Existing Models for A_{impact} and P{$F|impact$}

Subsections 4.2.1 and 4.2.2 outline parametric models for A_{impact} and P{$F|impact$} respectively. Subsection 4.2.3 outlines dynamical simulation model for P{$F|impact$}. In subsection 4.2.4, these models are used to quantify and compare the product $A_{impact} \times$ P{$F|impact$} for the scenario of a vertical drop of a DJI Phantom III on the head of a standing human.

4.2.1 Parametric models for A_{impact}

From the overviews by [Melnyk et al., 2014; Washington et al., 2017] , there are three main types of parametric models for impact area A_{impact}: Planform area, Gliding area model, and Aircraft mass based model. The Gliding area model [RCC, 2001] satisfies:

$$A_{impact} = (Width_{UAS} + 2R_P) \times \left(Length_{UAS} + \frac{H_P}{\tan(\psi)} + 2R_P\right) \tag{2.1}$$

with R_P and H_P the diameter and height of person, and ψ the UAS descend angle. The planform area model [Weibel and Hansman, 2004] adopts (2.1) with values $R_P = H_P = 0$.

The aircraft mass based model satisfies [Ale and Piers, 2000]: $A_{impact} = c_{Fit} \times m_{MTOW}$, with m_{MTOW} the Maximum Take-Off Weight in kg, and the statistically fitted coefficient value $c_{Fit} = 0.2 \text{ m}^2/\text{kg}$.

4.2.2 Parametric models for $P\{F|impact\}$

From the overviews by [Melnyk et al., 2014; Washington et al., 2017], there are two main types of parametric models for $P\{F|impact\}$: the RCC [2001] model and the Blunt Criterion (BC) model.

RCC model

The RCC [2001] fatality risk curve is a function of kinetic energy of UAS at moment of impact of human body, and is based on a weighted average of the fatality risk curves that are obtained through statistical analysis of a military database of effects of blast, debris on human body parts [Feinstein et al., 1968]:

$$P\{F|impact\} = Z(\frac{\ln E_{imp} - \ln a}{b}) \tag{2.2}$$

where Z is the cumulative standard normal distribution [Dalamagkidis et al., 2011]. E_{imp} is the impact energy. Hence Z defines an S-shaped curve that starts at probability zero for $E_{imp} = 0$, reaches probability $1/2$ for $E_{imp} = a$ and asymptotically goes to probability 1 for large E_{imp}. The parameter values for a and b for a standard male human for different body parts as shown in Table 1.

Table 1. Model parameter values for a standard male human. Source: [RCC, 2000]

Parameter	Head	Thorax	Abdomen
a (Joules)	74.8	59.8	130.6
b	0.2802	0.3737	0.4335

BC model

[Magister, 2010] proposed to adopt the Blunt Criterion (BC) as basis for a human injury due to UAS impact. The basis for this approach stems from military kind of ballistic impacts on human [Sturdivan et al., 2004]. The BC injury level L_{BC} satisfies:

$$L_{BC} = \ln \frac{E_{imp}}{m_b^{1/3} l_b D_{imp}} \qquad (2.3)$$

where E_{imp} is the impact energy, m_b is the mass of the impacted body part, l_b is the thickness (in cm) of body wall of the impacted body part, D_{imp} is the diameter (in cm) of the impacting object, e.g. an impacting UAS. For thorax and abdomen, l_b depends on the body part mass:

$$l_b = m_b^{1/3} c_b \qquad (2.4)$$

where c_b is the thickness parameter of the body part considered. Table 2 gives the parameter values adopted for BC impacts of head [CASA, 2013], and of thorax and abdomen [Sturdivan et al., 2004].

Table 2. BC model values for impact on standard male

Parameter	Head	Thorax	Abdomen	Source
Mass ratio of body part	8%	21%	21%	[Sturdivan et al., 2004]
c_b	n.a.	0.711	0.711	[Sturdivan et al., 2004]
l_b (cm)	1.3	n.a.	n.a.	[CASA, 2013]

Values for P{$F|impact$} are obtained by applying two successive mappings. First, injury level L_{BC} is converted to AIS level L_{AIS} [Bir & Viano, 2004] using:

$$L_{AIS} = 1.33 \cdot L_{BC} + 0.6 \qquad (2.5)$$

Next, AIS level is converted to P{$F|impact$} by using the transformation curve of single injury AIS scale to probability of fatality [Gennarelli & Wodzin, 2006].

4.2.3 Dynamical Simulation models for P{$F|impact$}

Human injury modelling and simulation is a well-developed topic in automotive research; with emphasis on consequences for human involved in a car crash. As a result of this research dynamical simulation models have been developed and validated for collisions involving human and human crash dummies that are used in car crash testing. Examples of well-developed and validated simulation platforms are: [THUMS, 2015, 2018] and [MADYMO, 2017a, b]. The former makes use of Finite Element (FE) models of human body or crash dummy involved in a car collision, while the latter makes use of Multi-Body System (MBS) models. Dynamic simulation of a collision yields detailed acceleration curves over time of various parts of the human body or crash dummy involved. These results are subsequently translated into well-developed injury scales. The commonly used injury scales are Head Injury Criteria (HIC), Neck Injury Criteria (Nij) and Viscous Criteria (VC) for injuries to head, neck and other body parts respectively. HIC takes the effect of sudden head acceleration into account [Hutchinson et al., 1998; Schmitt et al., 2019]. Nij considers the consequences of head movements on neck forces and moments [Klinich et al., 1996; Parr et al., 2012]. VC takes into account that injury to soft tissue injury is compression and rate dependent [Lau and Viano, 1986; Viano et al. 1989].

For dynamical simulation of UAS collision with human body or a crash dummy, a validated model of the UAS type considered has to be developed and integrated in one of these platforms. In addition, there is need for a transformation of assessed injury levels to

P{$F|impact$} For integration in the THUMS (2015) platform, FE models have been developed by [Arterburn et al., 2019, Annex B] of UAS types: DJI Phantom III, Sensefly eBee+ and Precision Hawk MK III. These models have been validated against acceleration measurements of drop tests on a head of a human dummy. [Weng et al., 2021] developed and integrated an FE model of DJI Phantom III in [THUMS, 2018]; this model has been validated against acceleration measurements of the head of a human cadaver [Stark et al., 2019]. For integration in the MADYMO platform, [Rattanagraikanakorn et al., 2019, 2020a] developed the MBS model of DJI Phantom III. As is shown in Figure 1, this MBS model consists of multiple body part masses that are connected via restraint joints, with ellipsoid surface to realistically represent external surfaces.
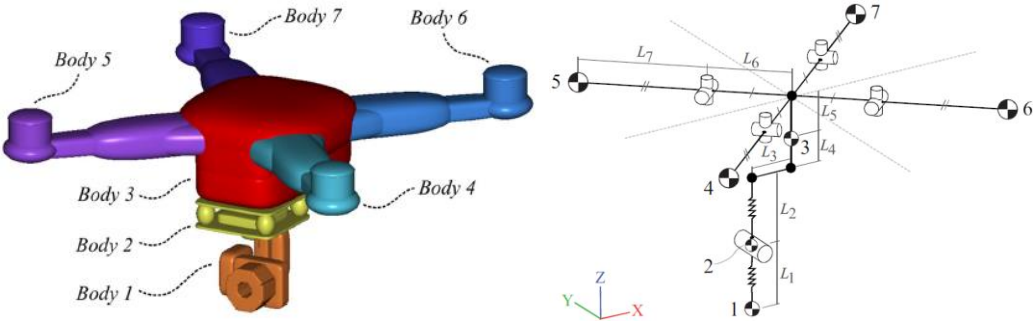
Figure 1. MBS model of the DJI Phantom III UAS. Source: [Rattanagraikanakorn et al., 2020a]

In [Rattanagraikanakorn et al., 2020a] this MBS model has been validated against head acceleration measurements of drop tests on a crash dummy [Arterburn et al., 2017]. In [Rattanagraikanakorn et al., 2022] also a comparison is made between MBS dynamical simulation of DJI Phantom III falling down on the head of a crash dummy versus the head of human body. This comparison showed significant differences both in HIC values and Nij values. Most significant is the finding that for a human body, Nij value is negligible relative to HIC value.

In [Rattanagraikanakorn, 2021, pp. 149-150] a systematic comparison has been made of MBS simulated HIC values for a human body and those measured during hittings of human cadavers by a DJI Phantom III [Stark et al., 2019]; this showed that the MBS model underestimated the measured HIC value on average by 11%. To compensate this estimation bias, in the sequel MBS dynamical simulation based HIC values are increased by 11%. Subsequently, the corresponding P{$F|impact$} value is obtained by a conversion of an unbiased HIC values to percentage of life-threatening injury [Touger et al., 1995]. For thorax and abdomen the VC (Viscous Criterion) injury level [Lau & Viano, 1986] is obtained during MBS dynamical simulation. The VC level is then converted to P{$F|impact$} in two steps: first a conversion curve from VC level to AIS level [Sturdivan et al., 2004], and then a conversion curve from AIS level to P{$F|impact$} [Gennarelli & Wodzin, 2006].

4.2.4 Comparison for a DJI Phantom III UAS

In this subsection we evaluate the existing models for A_{impact} and $\mathrm{P}\{F|impact\}$ and their products for a DJI Phantom III; a small UAS of weight 1.21 kg, width of 0.25 m; length of 0.25 m. Under a free fall, the final equilibrium descend speed is 18 m/s [Arterburn et al., 2019, Annex A].

Table 3 presents the calculated values for 3 models of A_{impact} and 3 models of $\mathrm{P}\{F|impact\}$ and their 3x3 products. For impact area A_{impact} , the evaluated models are: planform area [Weibel and Hansman, 2004], the extrapolation of the MTOW based area [Ale and Piers, 2000], and the gliding area at descend angle of 60 degree [Clothier et al., 2007]. These A_{impact} values are shown in the left column of Table 3.

For $\mathrm{P}\{F|impact\}$, the evaluated models are: the BC model, the dynamical simulation model, and the RCC model. In the dynamical simulation based assessment of $\mathrm{P}\{F|impact\}$, the scenario of [Koh et al., 2018] is followed, i.e. the DJI Phantom III makes a vertical drop in an upside-down attitude, on the centre of a head of a standing standard male human. The upside-down attitude avoids energy absorption by the camera gimbal. The $\mathrm{P}\{F|impact\}$ values obtained are shown in the top row of Table 3.

Table 3. Results of existing models for $A_{impact} \times \mathrm{P}\{F|impact\}$ of a DJI Phantom III UAS. The Dynamical Simulation result is obtained for a vertical drop on the centre of human head, with UAS in upside-down attitude to avoid energy absorption by the camera gimbal.

$\mathrm{P}\{F|impact\}$ / A_{impact} (m²)		BC	Dyn. Sim.	RCC
		0.188	0.706	1.0
Planform area	0.063	0.012	0.044	0.063
Extrapolated MTOW based area	0.242	0.045	0.171	0.242
Gliding area (descend angle of 60 degree)	0.984	0.186	0.696	0.984

The 9 estimated values for $A_{impact} \times \mathrm{P}\{F|impact\}$ in Table 3, range from $0.012 m^2$ to $0.984 m^2$, which is more than a factor 80. This factor is due to a factor 15.6 in estimated A_{impact} values, and a complementary factor 5.3 in the estimated $\mathrm{P}\{F|impact\}$ values. Of all results in Table 3, only the Dynamical Simulation based $\mathrm{P}\{F|impact\}$ value is from a validated model. This means that validation is lacking for each of the 9 estimated values for the product $A_{impact} \times \mathrm{P}\{F|impact\}$.

This DJI Phantom III example reveals that the range of estimated values for $A_{impact} \times \mathrm{P}\{F|impact\}$ from existing models may vary two orders in magnitude. Moreover, the true value may even fall outside this large range. This clearly illustrates the need of an improved method for quantifying the product $A_{impact} \times \mathrm{P}\{F|impact\}$ in ground TPR posed by a small UAS.

4.3 Enriched Ground TPR Model

This section starts by showing that in ground TPR eq. (1.1), the product $A_{impact} \times \mathrm{P}\{F|impact\}$ can be replaced by an integration of fatality probability values over different locations of the centre of a UAS relative to the human location. Subsequently, the effects of human face direction and drone state at impact are taken into account, and a numerical

integration procedure is presented for the evaluation of the enriched model using a dynamical simulation model.

4.3.1 Enriched ground TPR model

In [RCC, 2001], the term $P\{F|impact\}$ is characterized as a summation over fatality probabilities in case a horizontal moving object impacts different body parts of a human, i.e.:

$$P\{F|impact\} = \sum_B \left[P\{F|\text{hit on body part } B\} \times \frac{\text{Area of body part } B}{\text{Area of human body}} \right] \tag{3.1}$$

In case of a UAS crashing from the air to the ground, the impact location of UAS can be at any horizontal offset Δ relative to the location of a human. To capture this falling UAS situation, the summation over body parts in eq. (3.1) is replaced by an integration over all horizontal offsets Δ in the set $\{A_{impact}\}$, i.e.:

$$P\{F|impact\} = \int_{\{A_{impact}\}} P\{F|\Delta\} \frac{1}{A_{impact}} d\Delta \tag{3.2}$$

where $P\{F|\Delta\}$ is the conditional probability of fatality given horizontal offset Δ.

Taking into account that $P\{F|\Delta\} = 0$ for all $\Delta \notin \{A_{impact}\}$, eq. (3.2) implies:

$$P\{F|impact\} = \int_{\mathbb{R}^2} P\{F|\Delta\} \frac{1}{A_{impact}} d\Delta \tag{3.3}$$

Multiplying both sides in eq. (3.3) by A_{impact} yields:

$$A_{impact} \times P\{F|impact\} = \int_{\mathbb{R}^2} P\{F|\Delta\} d\Delta \tag{3.4}$$

Equation (3.4) captures the influence of possible offsets between human location and the centre of UAS crash. Hence, eq.(3.4) forms the mathematical characterization for estimating the product $A_{impact} \times P\{F|impact\}$ by an integration over $P\{F|\Delta\}$ estimates for all possible Δ offset values. The idea is to obtain these $P\{F|\Delta\}$ estimates by conducting dynamical simulations of a validated FE or MBS model of a UAS that falls at horizontal offset Δ from human location.

Finally, substitution (3.4) in eq. (1.1) yields the enriched ground TPR model:

$$\mathbb{E}\{n_F\} = \lambda_{System} \times \rho_{population} \times (1 - P_{Shelter}) \times \int_{\mathbb{R}^2} P\{F|\Delta\} d\Delta \tag{3.5}$$

4.3.2 Incorporating face direction and drone state at impact

MBS simulation studies [Rattanagraikanakorn et al., 2020a, 2022] show that human fatality depends on the face direction φ of the impacted human relative to the impact course of the UAS, on the 2-dimensional UAS velocity v (speed $|v|$ and descend angle ψ) and on the 3-dimensional UAS attitude θ (pitch θ_{pitch}, roll θ_{roll} and yaw θ_{yaw}). These parameters are shown in Figure 2.
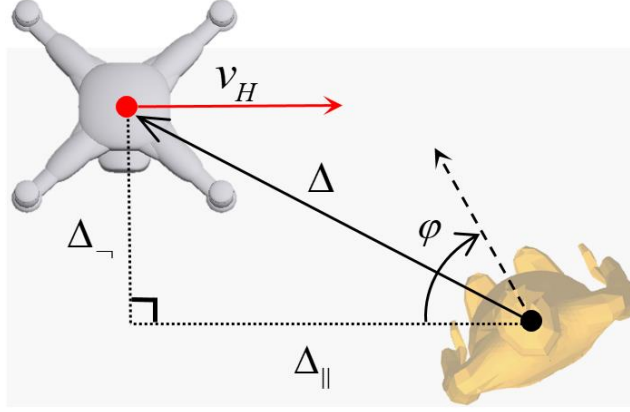
Figure 2. Top view of a standing human with face direction φ and a falling UAS, that passes human head at horizontal offset Δ relative to centre of human head. Δ is decomposed into components $\Delta_{\parallel}$ and $\Delta_{\neg}$, that are parallel and perpendicular to horizontal UAS velocity v_H.

From the law of total probability we can incorporating UA impact velocity v, UA attitude θ, and human face direction φ in $P\{F|\Delta\}$, as follows:

$$P\{F|\Delta\} = \int_{\mathbb{R}^+ \times [0,\pi/2] \times \Theta \times [0,2\pi]} P\{F|\Delta, v, \theta, \varphi\} \, p_{v,\theta}(v,\theta) p_\varphi(\varphi) dv d\theta d\varphi \tag{3.6}$$

where Θ the set of possible attitude values, $P\{F|\Delta, v, \theta, \varphi\}$ is the conditional probability of Fatality given $(\Delta, v, \theta, \varphi)$, $p_{v,\theta}(v,\theta)$ is the probability density of (v,θ), and $p_\varphi(\varphi)$ is the probability density of face direction φ.

Interchanging the sequence of integration in (3.5) and (3.6), i.e. start with integration over Δ, yields:

$$E\{n_F\} = \lambda_{System} \times \rho_{population} \times (1 - P_{Shelter}) \times \bar{Q} \tag{3.7}$$

with:

$$\bar{Q} = \int_{\mathbb{R}_+ \times [0,\pi/2] \times \Theta \times [0,2\pi]} Q(v,\theta,\varphi) \, p_{v,\theta}(v,\theta) p_\varphi(\varphi) dv d\theta d\varphi \tag{3.8}$$

$$Q(v,\theta,\varphi) = \int_{R^2} P\{F|\Delta, v, \theta, \varphi\} d\Delta \tag{3.9}$$

4.3.3 Numerical integration of the enriched ground tpr model

Eqs.(3.8-3.9) consider the full range of possible ways a human on the ground can be hit by a UAS. $Q(v,\theta,\varphi)$ is an integration of impact offset Δ-dependent human fatality $P\{F|\Delta, v, \theta, \varphi\}$ over all possible offsets Δ between UAS crash centre and the centre of human head. $\bar{Q}$ is the averaged $Q(v,\theta,\varphi)$ for possible variations in face direction φ, UAS velocity v, and UAS attitude θ.

By using a grid for offset Δ, eq. (3.9) is evaluated as:

$$Q(v,\theta,\varphi) = \sum_\iota \left[P\{F|\Delta_\iota, v, \theta, \varphi\} \left| G_\iota^\Delta \right| \right] \tag{3.10}$$

with $\left| G_\iota^\Delta \right|$ the size of the 2-dimensional Δ-grid.

Similarly, by using the grids for v, attitude θ and face direction φ, eq. (3.8) is evaluated as:

$$\bar{Q} = \sum_j \sum_k \sum_\ell \left[Q(v_j, \theta_k, \varphi_\ell) p_{v,\theta}(v_j, \theta_k) p_\varphi(\varphi) \left| G_j^v \right| \left| G_k^\theta \right| \left| G_\ell^\varphi \right| \right] \tag{3.11}$$

with $\left| G_j^v \right| \left| G_k^\theta \right| \left| G_\ell^\varphi \right|$ the product of the adopted grid sizes. For the numerical integration over UA velocity v, we use a 2D grid for UAS speed $|v|$ and UAS descend angle ψ.

A relevant alternative for the numerical integration of eq. (3.8) is to use Monte Carlo simulation:

$$\bar{Q} \simeq \frac{1}{N_{MC}} \sum_{i=1}^{N_{MC}} Q(v^i, \theta^i, \varphi^i) \tag{3.12}$$

where (v^i, θ^i) and φ^i, $i = 1, .., N_{MC}$, are independent random samples from the densities $p_{v,\theta}(v_j, \theta_k)$, and $p_\varphi(\varphi)$. For the generation of random samples from $p_{v,\theta}(v_j, \theta_k)$, use can be made of dynamical simulations of descending UAS under relevant event conditions [Foster and Hartman, 2017; Arterburn et al., 2019, Annex B]. The shape of $p_\varphi(\varphi)$ for human face direction depends on the situation. If persons on the ground are not aware of the falling UAS, then face direction will have a uniform distribution, i.e. $p_\varphi(\varphi) = \frac{1}{2\pi}$. If persons on the ground are watching the falling UAS, then face direction will be zero degree. For other situations, the quantification of $p_\varphi(\varphi)$ may require additional assessments, e.g. in case persons on the ground tend to turn their head upon being alerted by the noise of a falling UAS.

Accurate evaluation of eq. (3.12), typically asks for a very large number N_{MC} of MC runs. The same level of accuracy can be reached by making use of appropriate variance reduction technique, such as Latin Hypercube Sampling, e.g. [Helton and Davis, 2003].

4.4 Evaluation of Enriched Model through Dynamical Simulation

This section numerically evaluates the enriched model of section 4.3 for a DJI Phantom III impacting a standing 50th percentile male human body, and compares this to the results for the 9 existing model combinations in section 4.2 (Table 3). For the numerical evaluation use is made of the validated MBS dynamical simulation model of [Rattanagraikanakorn et al., 2020a,b] for a DJI Phantom III UAS.

4.4.1 Scenario A: vertical descend

MBS simulations are conducted with offsets $\Delta_\parallel$ and $\Delta_\neg$ varying over the Δ-grid, for face direction $\varphi = 0°$, for scenario A, of a pure vertical drop, i.e. descend angle $\psi = 90°$. Similar to section 2, the UA impact speed of DJI Phantom III is set at final equilibrium speed of $|v| = 18\ m/s$. Simulation results of $\mathbb{P}\{F | \Delta, v, \theta, \varphi\}$ for varying offsets $\Delta_\parallel$ and $\Delta_\neg$ are shown in Table 4, for pitch $\theta_{pitch} = 180°$, yaw $\theta_{yaw} = 0°$, roll $\theta_{roll} = 0°$, and face direction $\varphi = 0°$. Offset grid step is $0.02m$; due to face direction $\varphi = 0°$ results are symmetrical for positive and negative cross offset $\Delta_\neg$ values. Figure 3 shows, for scenario A, impact at the center of gravity of the human head, i.e. $\Delta = (0,0)$.

For scenario A, the head is always firstly contacted by the drone. In case of an initial hit of human head, a drone may start to tumble, as a result a second hit on thorax or abdomen could happen. Such drone tumbling is also captured in the simulations. The simulation results for scenario A show no hit (first or second) on thorax or abdomen. The maximum of $P\{F|\Delta, v, \theta, \varphi\}$ is at the center of the head. For off-centred combinations where head is first contacted by the drone arm, typically limited impact energy is transferred to the human, due to the bending of arm and subsequent tumbling of the drone. Integration of the $P\{F|\Delta, v, \theta, \varphi\}$ values in Table 4 yields $Q(v, \theta, \varphi) = 0.012 m^2$.

Figure 3. Scenario A impact at center of gravity of human head, i.e. $\Delta = (0,0)$

Table 4. Case A, $P\{F|\Delta, v, \theta, \varphi\}$ (%) as a function of cross offset $\Delta_\neg$ and along offset $\Delta_\parallel$. Pitch $\theta_{pitch} = 180°$, yaw $\theta_{yaw} = 0°$, roll $\theta_{roll} = 0°$, and face direction $\varphi = 0°$. Red line shows the boundary outside which the UAS does not touch human body. Integration yields $Q(v, \theta, \varphi) = 0.012 m^2$.

Along offset $\Delta_\parallel$ (m)	Cross offset $\Delta_\neg$ (m) 0.00	0.02	0.04	0.06	0.08	0.10	0.12	0.14	0.16	0.18	0.20	0.22
0.26												
0.24							0.00	0.00	0.00	0.00		
0.22						0.00	0.00	0.00	0.00	0.00	0.00	
0.20				0.00	0.00	0.00	0.00	0.00	0.00	0.00	0.00	
0.18			0.00	0.00	0.00	0.00	0.00	0.00	0.00	0.00	0.00	
0.16	0.33	1.15	1.01	0.68	0.24	0.00	0.00	0.00	0.00	0.00	0.00	
0.14	5.13	9.20	2.33	1.06	1.05	0.00	0.00	0.00	0.00	0.00	0.00	
0.12	15.54	17.68	12.05	1.91	1.13	0.82	0.00	0.00	0.00	0.00	0.00	
0.10	25.71	24.54	21.13	10.20	1.24	1.15	0.46	0.00	0.00	0.00	0.00	
0.08	41.39	34.92	28.41	18.04	8.03	1.14	1.04	0.00	0.00	0.00		
0.06	59.34	47.66	37.75	23.39	16.23	2.83	0.97	0.00				
0.04	68.18	58.65	49.78	30.98	23.41	10.92	1.15	0.00				
0.02	90.10	75.84	67.40	48.36	38.83	34.68	5.12	0.00				
0.00	70.60	57.65	50.90	35.71	23.30	10.32	1.13	0.00				
-0.02	51.04	37.58	31.96	21.38	15.42	4.00	0.96	0.00	0.00			
-0.04	40.44	29.73	25.03	18.56	10.61	1.23	0.96	0.00	0.00	0.00		
-0.06	26.01	22.25	20.28	13.42	2.15	1.14	0.86	0.00	0.00	0.00	0.00	
-0.08	17.96	17.48	16.99	5.23	1.12	1.09	0.17	0.00	0.00	0.00	0.00	
-0.10	8.56	12.71	7.04	1.22	1.14	0.58	0.00	0.00	0.00	0.00	0.00	
-0.12	1.88	2.76	1.22	0.93	0.94	0.00	0.00	0.00	0.00	0.00	0.00	
-0.14	0.00	0.00	0.27	0.45	0.00	0.00	0.00	0.00	0.00	0.00	0.00	
-0.16			0.00	0.00	0.00	0.00	0.00	0.00	0.00	0.00	0.00	
-0.18				0.00	0.00	0.00	0.00	0.00	0.00	0.00	0.00	
-0.20					0.00	0.00	0.00	0.00	0.00	0.00		
-0.22												

4.4.2 Scenario B: non-vertical descend

The following non-vertical scenario B is considered: Descend angle $\psi = 60°$, pitch $\theta_{pitch} = 180°$, yaw $\theta_{yaw} = 0°$, roll $\theta_{roll} = 0°$, final equilibrium speed of $|v| = 18\ m/s$. MBS

simulations are conducted with offsets $\Delta_{\parallel}$ and $\Delta_{\neg}$ varying over the Δ-grid, for face direction $\varphi = 0°$. Simulation results of $P\{F|\Delta, v, \theta, \varphi\}$ for varying offsets $\Delta_{\parallel}$ and $\Delta_{\neg}$ are shown in Table 5. Figure 4 shows, for scenario B, impact at the center of gravity of human head, i.e. $\Delta = (0,0)$.

Table 5. Scenario B, $P\{F|\Delta, v, \theta, \varphi\}$ (%) as a function of cross offset $\Delta_{\neg}$ and along offset $\Delta_{\parallel}$. Outside the red line, the UAS does not touch human body. Offset combinations that lead to second hit (on thorax or abdomen) are marked by a black border. Integration yields $Q(v, \theta, \varphi) = 0.010 m^2$.

Along offset $\Delta_{\parallel}$ (m) vs. Cross offset $\Delta_{\neg}$ (m)

$\Delta_{\parallel}$ \ $\Delta_{\neg}$	0.00	0.02	0.04	0.06	0.08	0.10	0.12	0.14	0.16	0.18	0.20	0.22	0.24	0.26	0.28	0.30	0.32
0.26																	
0.24						0.00	0.00	0.00	0.00								
0.22					0.00	0.00	0.00	0.00	0.00	0.00							
0.20				0.00	0.00	0.00	0.00	0.00	0.00	0.00							
0.18			0.00	0.00	0.00	0.00	0.00	0.00	0.00	0.00	0.00						
0.16		0.00	0.18	0.13	0.44	0.00	0.00	0.00	0.00	0.00	0.00						
0.14	0.97	1.23	1.45	1.12	0.85	0.75	0.00	0.00	0.00	0.00	0.00						
0.12	1.43	2.14	3.79	3.14	1.15	0.95	0.60	0.00	0.00	0.00	0.00						
0.10	4.41	5.11	6.63	6.72	3.50	1.11	0.86	0.20	0.00	0.00	0.00						
0.08	10.39	10.04	10.51	9.51	8.59	1.82	0.95	0.65	0.00	0.00	0.00						
0.06	13.72	15.35	16.41	12.35	10.20	6.60	1.10	0.36	0.00	0.00	0.00						
0.04	24.63	25.03	26.18	21.29	15.77	11.19	1.26	0.08	0.00	0.24	0.00						
0.02	25.26	26.02	27.31	22.72	14.81	6.18	2.43	0.00	0.00	0.00	0.00						
0.00	35.53	32.99	32.61	28.21	16.48	2.21	0.49	0.00	0.00	0.00							
-0.02	38.67	37.49	37.15	29.70	10.50	1.19	1.12	0.00	0.00	0.00							
-0.04	46.61	39.00	37.50	22.69	2.17	1.70	0.69	0.00	0.00	0.00							
-0.06	51.06	40.06	33.86	10.49	1.79	1.28	0.18	0.00	0.00	0.00	0.00						
-0.08	50.20	37.72	24.81	2.51	1.92	0.96	0.00	0.01	0.48	0.23	0.00						
-0.10	49.81	35.86	12.64	1.31	1.63	0.41	0.00	0.68	0.55	0.27	0.00						
-0.12	47.11	31.47	3.71	1.24	1.17	0.00	0.57	0.68	0.47	0.20	0.00						
-0.14	26.25	18.72	1.44	1.21	0.67	0.00	0.73	0.59	0.36	0.10	0.00						
-0.16	3.50	4.20	1.09	1.03	0.05	0.07	0.66	0.47	0.23	0.00	0.00						
-0.18	1.26	2.98	1.15	0.55	0.00	0.19	0.54	0.33	0.09	0.00	0.00						
-0.20	2.33	1.20	0.66	0.05	0.00	0.10	0.38	0.16	0.00	0.00	0.00						
-0.22	1.05	1.25	0.64	0.80	0.00	0.00	0.16	0.00	0.00	0.00	0.00						
-0.24	0.73	1.79	0.00	0.00	0.00	0.00	1.63	0.16	0.00	0.00	0.00						
-0.26	0.69	0.71	0.00	0.00	0.00	0.00	0.00	1.55	1.14	1.39							
-0.28	0.65	0.61	1.35	2.35	1.83	1.65	1.28	0.78	0.76	0.00	0.00	0.00	0.00	0.00	0.00		
-0.30	0.63	0.61	0.98	0.00	0.00	2.35	0.00	0.00	0.00	0.00	0.00	0.00	0.00	0.00	0.00		
-0.32	0.63	0.60	0.74	0.00	0.00	0.00	0.00	0.00	0.00	0.00	0.00	0.00	0.00	0.00	0.00		
-0.34	0.70	0.62	0.67	0.00	0.00	0.00	0.00	0.00	0.00	0.00	0.00	0.00	0.00	0.00	0.00		
-0.36	0.74	0.92	1.01	0.00	0.00	0.00	0.00	0.00	0.00	0.00	0.00	0.00	0.00	0.00	0.00		
-0.38	0.96	0.00	0.00	0.00	0.00	0.00	0.00	0.00	0.00	0.00	0.00	0.00	0.00	0.00	0.00		
-0.40	0.00	0.00	0.00	0.00	0.00	0.00	0.00	0.00	0.00	0.00	0.00	0.00	0.00	0.00	0.00		
-0.42	0.00	0.00	0.00	0.00	0.00	0.00	0.00	0.00	0.00	0.00	0.00	0.00	0.00	0.00	0.00		
-0.44	0.00	0.00	0.00	0.00	0.00	0.00	0.00	0.00	0.00	0.00	0.00	0.00	0.00	0.00	0.00		
-0.46	0.00	0.00	0.00	0.00	0.00	0.00	0.00	0.00	0.00	0.00	0.00	0.00	0.00	0.00	0.00		
-0.48	0.00	0.00	0.00	0.00	0.00	0.00	0.00	0.00	0.00	0.00	0.00	0.00	0.00	0.00	0.00		
-0.50	0.00	0.00	0.00	0.00	0.00	0.00	0.00	0.00	0.00	0.00	0.00	0.00	0.00	0.00	0.05		
-0.52	0.00	0.00	0.00	0.00	0.00	0.00	0.00	0.00	0.00	0.00	0.00	0.00	0.00	0.00	0.00		
-0.54	0.00	0.00	0.00	0.00	0.00	0.00	0.00	0.00	0.00	0.00	0.00	0.00	0.00	0.00	0.00		
-0.56	0.00	0.00	0.00	0.00	0.00	0.00	0.00	0.00	0.00	0.00	0.00	0.00	0.00	0.00	0.00		
-0.58	0.00	0.00	0.00	0.00	0.00	0.00	0.00	0.00	0.00	0.00	0.00	0.00	0.00	0.00	0.00		
-0.60	0.00	0.00	0.00	0.00	0.00	0.00	0.00	0.00	0.00	0.00	0.00	0.00	0.00	0.00			
-0.62	0.00	0.00	0.00	0.00	0.00	0.00	0.00	0.00	0.00	0.00	0.00	0.00	0.00				
-0.64	0.00	0.00	0.00	0.00	0.00	0.00	0.00	0.00	0.00	0.00	0.00	0.00	0.00				
-0.66	0.00	0.00	0.00	0.00	0.00	0.00	0.00	0.00	0.00	0.00	0.00	0.00					
-0.68			0.00	0.00	0.00	0.00	0.00	0.00	0.00	0.00	0.00	0.00	0.00				
-0.70																	

Scenario B simulations include first and second hits of thorax or abdomen. Most hits are first hits; offset combinations where second hit happens on thorax/abdomen are marked by thick borders in Table 5. This shows that second hits happen at a few offset combinations only, and their contributions to $P\{F|\Delta, v, \theta, \varphi\}$ are very small relative to the first hit contributions.
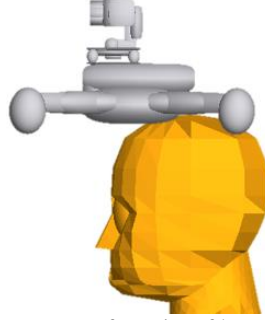
Figure 4. Scenario B impact at center of gravity of human head, i.e. $\Delta = (0,0)$

Due to hits on thorax and abdomen in scenario B, $P\{F|\Delta, v, \theta, \varphi\}$ contributions to $Q(v, \theta, \varphi)$ come from a much larger area than for Scenario A (Table 4). Another difference is that the $P\{F|\Delta, v, \theta, \varphi\}$ values near the central area of the head are for scenario B (Table 5) significantly lower than for scenario A (Table 4). The explanation is that for central hit under a descent angle of 60 degrees the drone starts to tumble instead of the bouncing back that happens under a descent angle of 90 degrees. Start of tumbling after first contact leads to less energy transfer to the head than bouncing back. Integration of the $P\{F|\Delta, v, \theta, \varphi\}$ values through eq. (3.10) yields $Q(v, \theta, \varphi) = 0.010m^2$ for scenario B, which is slightly lower compared to the $Q(v, \theta, \varphi) = 0.012m^2$ for scenario A. This means that for scenario B, the additional risk contributions from hits on thorax and abdomen, do not compensate the significant smaller $P\{F|\Delta, v, \theta, \varphi\}$ contributions to $Q(v, \theta, \varphi)$ from hits around the centre of the head.

4.4.3 Varying UAS attitude

Figure 5 presents $Q(v, \theta, \varphi)$ as a function of varying pitch, for four descend angles, i.e. $\psi = 60°, 70°, 80°, 90°$, with the other parameters the same as in scenarios A and B. The $Q(v, \theta, \varphi)$ values vary from $0.013m^2$ to $0.001m^2$; with highest values for $\theta_{pitch} = 150°$ and $180°$ and lowest values for $\theta_{pitch} = 0°$ and $330°$. At pitches halfway, i.e. at $\theta_{pitch} = 90°$ or $\theta_{pitch} = 270°$, the $Q(v, \theta, \varphi)$ values also are halfway. Figure 5 shows that variation in descend angle ψ yields a significantly lower variation in $Q(v, \theta, \varphi)$ than the variation in pitch does. Due to the symmetrical shape of DJI Phantom III, the effect of varying roll on $Q(v, \theta, \varphi)$ is similar to the effect of varying pitch.

For a better understanding of the much lower $Q(v, \theta, \varphi)$ value when UAS pitch is zero, Table 6 shows the map of $P\{F|\Delta, v, \theta, \varphi\}$ for pitch $\theta_{pitch} = 0°$ in vertical descend scenario A.

Figure 6 illustrates both a centered and an off-centred impact situation in Table 6. Comparison of results in Table 6 with those in Table 4, shows that for areas where Δ is close to 0, $P\{F|\Delta, v, \theta, \varphi\}$ values are significantly lower under $\theta_{pitch} = 0°$ than under $\theta_{pitch} = 180°$. The physical explanation is that for centred hit at pitch $\theta_{pitch} = 0°$, the first contact is between camera and human head (e.g. in Figure 6.a). In such case, the camera gimbal, at the bottom of the drone, absorbs significant part of the impact energy. Such absorption of energy is avoided when the drone is flipped upside down. The peak values for $P\{F|\Delta, v, \theta, \varphi\}$ appear to be in an off-center area; i.e. where the drone firstly contacts head with its main body and therefore transfers more impact energy directly to the head (e.g. in Figure 6.b). For other offset

combinations, either camera or drone arm contacts head first, which reduces impact energy to be absorbed by human head.
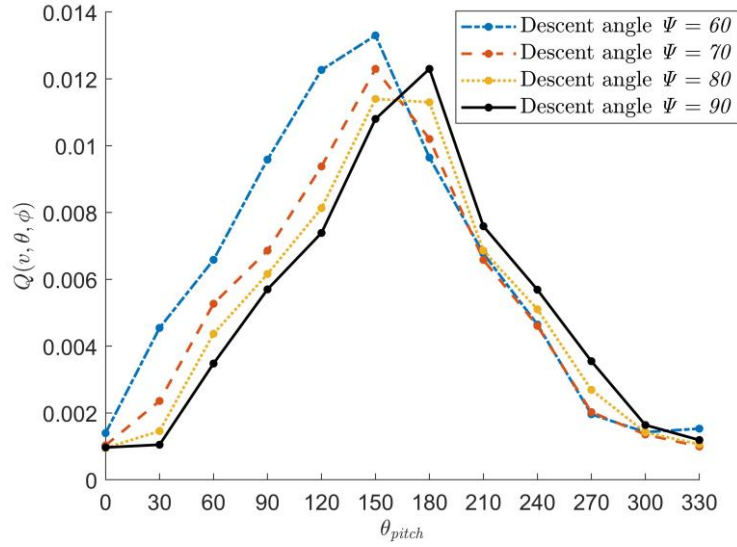
Figure 5. $Q(v, \theta, \varphi)$ as a function of pitch for four descend angles at face direction $\varphi = 0°$, $|v| = 18m/s$, zero roll and yaw

Table 6. Scenario A for pitch $\theta_{pitch} = 0°$; $P\{F|\Delta, v, \theta, \varphi\}$ (%) as a function of cross offset $\Delta_\neg$ and along offset $\Delta_\parallel$. Red line shows the boundary outside which the UAS does not touch human body. Integration yields $Q(v, \theta, \varphi) = 0.001m^2$

		Cross offset $\Delta_\neg$ (m)										
		0.00	0.02	0.04	0.06	0.08	0.10	0.12	0.14	0.16	0.18	0.20	0.22
	0.28											
	0.26											
	0.24						0.00	0.00	0.00	0.00			
	0.22					0.00	0.00	0.00	0.00	0.00	0.00		
	0.20				0.00	0.00	0.00	0.00	0.00	0.00	0.00	0.00	
	0.18	0.00	0.00	0.00	0.00	0.00	0.00	0.00	0.00	0.00	0.00	0.00	
	0.16	0.69	0.66	0.88	0.70	0.06	0.00	0.00	0.00	0.00	0.00	0.00	
	0.14	1.02	1.00	0.98	1.15	0.80	0.50	0.00	0.00	0.00	0.00	0.00	
	0.12	1.37	1.31	1.14	1.14	1.18	0.78	0.06	0.00	0.00	0.00	0.00	
	0.10	0.99	1.02	1.14	1.23	1.83	1.04	0.53	0.00	0.00	0.00	0.00	
	0.08	0.86	0.96	1.03	1.11	3.55	1.20	0.69	0.00	0.00	0.00	0.00	
	0.06	0.82	0.87	0.92	0.71	1.34	1.95	0.98	0.00	0.00	0.00		
	0.04	0.95	0.95	0.99	0.81	0.69	9.63	1.08	0.00				
	0.02	1.00	1.01	1.02	0.92	0.43	16.24	1.56					
	0.00	1.03	1.01	1.04	1.01	0.74	7.92	1.10	0.00				
	-0.02	1.02	0.98	1.04	1.00	0.70	3.78	1.04	0.00	0.00			
	-0.04	1.00	0.94	1.02	1.00	0.69	1.63	0.90	0.00	0.00	0.00		
	-0.06	0.99	0.96	1.02	0.99	0.00	1.24	0.74	0.00	0.00	0.00	0.00	
	-0.08	0.95	0.95	0.99	0.88	0.97	0.97	0.56	0.00	0.00	0.00	0.00	
	-0.10	0.86	0.86	0.84	0.26	1.14	0.86	0.00	0.00	0.00	0.00	0.00	
	-0.12	0.00	0.00	0.63	1.09	0.77	0.02	0.00	0.00	0.00	0.00	0.00	
	-0.14		0.00	0.00	0.00	0.00	0.00	0.00	0.00	0.00	0.00	0.00	
	-0.16				0.00	0.00	0.00	0.00	0.00	0.00	0.00	0.00	
	-0.18					0.00	0.00	0.00	0.00	0.00	0.00	0.00	
	-0.20					0.00	0.00	0.00	0.00	0.00			
	-0.22												

The vertical axis label is: Along offset $\Delta_\parallel$ (m)

a. Centre impact, $\Delta = (0,0)$ b. Off-centre: $\Delta_\neg = 0.1m$, $\Delta_\parallel = 0$

Figure 6. Examples of impacts for scenario A with pitch $\theta_{pitch} = 0°$

Figure 7.a-b show the relative contributions to $Q(v, \theta, \varphi)$ of first and second hits on thorax/abdomen for $\psi = 60°$ and $\psi = 70°$ respectively. For descend angle $\psi = 60°$, the contribution of first and second hits on thorax and abdomen is on average 5.8% and 1.9% respectively, though with peaks of 20.5% and 12.3% respectively.
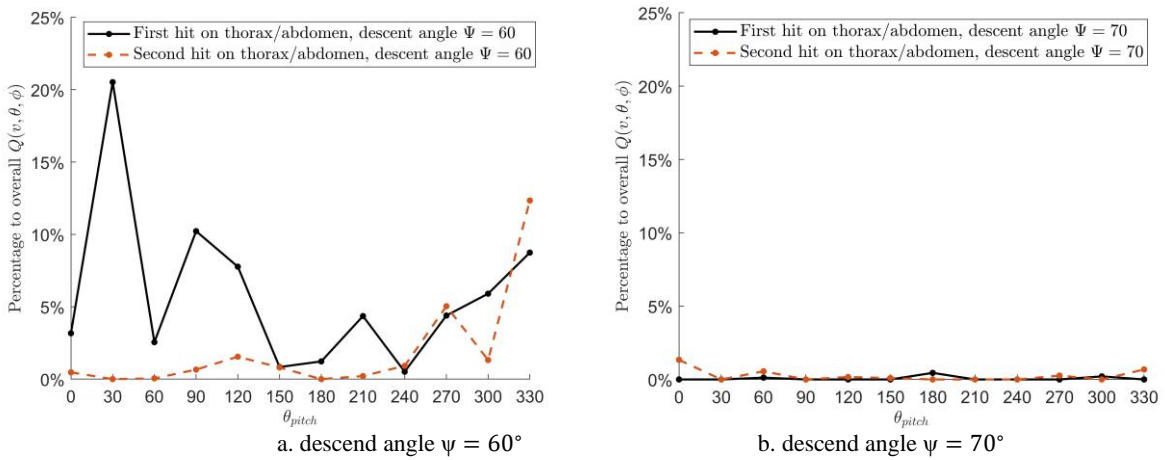
a. descend angle $\psi = 60°$ b. descend angle $\psi = 70°$

Figure 7. Relative contribution of first and second hit on thorax and abdomen

Due to the symmetrical shape of DJI Phantom III, the effect of varying roll on $Q(v, \theta, \varphi)$ is similar to the effect of varying pitch. Figure 8 shows examples of two specific combinations of roll and pitch during centered hits of human head, under vertical descend: a) Pitch $\theta_{pitch} = 90°$ and roll $\theta_{roll} = 0°$; b) Pitch $\theta_{pitch} = 90°$ and roll $\theta_{roll} = 90°$. In Figure 9.b arm absorbs significant part of impact energy compared to Figure 8.a, which results in a much lower central impact value, i.e. $P\{F | \Delta, v, \theta, \varphi\} = 23.5\%$ in Figure 8.b versus $P\{F | \Delta, v, \theta, \varphi\} = 92.9\%$ in Figure 9.a.

a. $\theta_{roll} = 0°$, resulted $P\{F | \Delta, v, \theta, \varphi\} = 92.9\%$ b. $\theta_{roll} = 90°$, resulted $P\{F | \Delta, v, \theta, \varphi\} = 23.5\%$

Figure 8. Examples of energy absorption by UAS arms for combinations of pitch and roll of UAS at descent angle $\psi = 90°$ (scenario A), pitch $\theta_{pitch} = 90°$ and no offset, i.e. $\Delta = (0,0)$

4.4.4 Varying face direction

Figure 9 presents the simulation results of $Q(v, \theta, \varphi)$ as a function of face direction, for the four descend angles, and for $\theta_{pitch} = 150°$, i.e. the pitch value that yields the highest risk under non-vertical descends.
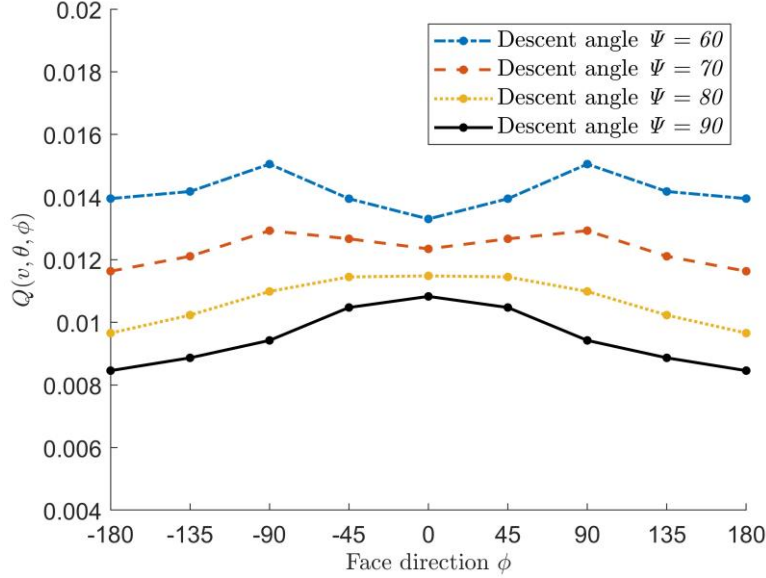
Figure 9. $Q(v, \theta, \varphi)$ as a function of face direction and descent angle at $\theta_{pitch} = 150°$, $|v| = 18m/s$

The results in Figure 9 show that $Q(v, \theta, \varphi)$ is symmetrical for face direction [0, 180] and [-180, 0] degrees. They also shows that varying face direction leads to less than a factor 1.3 variation in $Q(v, \theta, \varphi)$.

Remark: Whereas the MBS dynamical simulation model of [Rattanagraikanakorn et al., 2020a,b, 2022] can handle head impacts under any face direction, it can only handle impacts on thorax and abdomen for zero face direction. Therefore, to obtain Figure 9, it is assumed that contributions to $Q(v, \theta, \varphi)$ from hits on thorax and abdomen are for all face directions the same as for face direction $\varphi = 0°$.

4.4.5 Results for $\bar{Q}$ and comparison versus existing models

Now we illustrate the evaluation of $\bar{Q}$ using the grid version (3.11) of eq. (3.8). For this, we assume that $p_\varphi(\varphi)$ is uniform on face direction grid points $\{0°, 45°, 90°, 135°, 180°, 225°, 270°, 315°\}$, and $p_{v,\theta}(v_j, \theta_k)$ is uniform on pitch grid points $\{0°, 30°, 60°, 90°, 120°, 150°, 180°, 210°, 240°, 270°, 300°, 330°\}$, and has concentrated probability mass at speed $|v| = 18m/s$, at descend angle $\psi = 60°$ or $\psi = 90°$, zero roll and zero yaw. Then, the obtained values for $Q(v, \theta, \varphi)$ can be integrated using eq. (3.11) to a value for $\bar{Q}$; this yields $\bar{Q} = 0.0047m^2$ for $\psi = 90°$ and $\bar{Q} = 0.0062m^2$ for $\psi = 60°$. Table 7 collects these $\bar{Q}$ values together with the assessed $Q(v, \theta, \varphi)$ values for scenarios A and B.

Table 7. Values obtained for $Q(v, \theta, \varphi)$ and $\bar{Q}$ under descend angles of $\psi = 90°$ and $\psi = 60°$. The $Q(v, \theta, \varphi)$ values have been obtained for scenarios A and B (Tables 4 and 5)

Descend angle	$Q(v, \theta, \varphi)$ (m^2)	$\bar{Q}$ (m^2)
$\psi = 90°$	0.012	0.0047
$\psi = 60°$	0.010	0.0062

Comparison of these $Q(v, \theta, \varphi)$ values to the $A_{impact} \times P\{F|impact\}$ values, obtained in Table 3 for the 3x3 combinations of existing models show:

73

- For Scenario A, the $Q(v, \theta, \varphi) = 0.012 m^2$ obtained by dynamical simulation of a validated MBS model is equal to the lowest value obtained for $A_{impact} \times P\{F|impact\}$. This is for the existing model combination of planform area and BC model. The explanation is that $P\{F|impact\}$ for a central hit is much higher than it is for most non-zero offset values. It is pure coincidence that the BC model underestimates the central hit probability so much that, in combination with Planform area, this yields a correct value.

- For Scenario B, the $Q(v, \theta, \varphi) = 0.010 m^2$ obtained is lower than all 9 values ($0.012 m^2$ to $0.984 m^2$) obtained for $A_{impact} \times P\{F|impact\}$ in Table 3. This is in sharp contrast to the existing models, where a decrease in descend angle is expected to significantly increase $A_{impact} \times P\{F|impact\}$. By comparing the results in Table 4 and Table 5, one can see that for Scenario B there is significant lower central head impact values $P\{F|\Delta, v, \theta, \varphi\}$ than for Scenario A. This decrease in central peak values is not compensated by the significant larger impact area for Scenario B than for Scenario A.

- The weighted $\bar{Q}$ values are about 2 times lower compared to the $Q(v, \theta, \varphi) = 0.012 m^2$ and $Q(v, \theta, \varphi) = 0.010 m^2$ obtained for scenarios A and B. This factor 2 reduction is largely due to energy absorption by the camera gimbal in case the camera hits human head first.

4.4.6 Discussion of results

With the results obtained for the enriched ground TPR model of section 4.3 through dynamical simulations of a validated MBS model, two key shortcomings of the existing ground TPR models are resolved. Firstly, the developed approach does no longer need a separate model for the crash impact area. Secondly, the developed approach takes into account that off-centre fatality probabilities $P\{F|\Delta, v, \theta, \varphi\}$ may have quite different values than the central $P\{F|\Delta, v, \theta, \varphi\}$. Thirdly, the results for the DJI Phantom III UAS shows that the existing models overestimate the product $A_{impact} \times P\{F|impact\}$ up to two orders in magnitude. The best estimate from existing models appears to be provided by the combination of the Planform area model for A_{impact}, and the BC model for $P\{F|impact\}$ The finding also is that this similarity is rather coincidental. A complementary finding is that, in contrast to existing model expectation, the risk does not always increase if the UAS descent angle ψ decreases.

Also in contrast to existing models, the proposed approach is able to take the effect of UAS attitude and human face direction into account. The simulation results for the DJI Phantom III show that the effect of face direction $\wp$ appears to be relatively low, i.e. less than a factor 1.3 between highest and lowest $Q(v, \theta, \varphi)$ values. The simulation results also show that UAS attitude has the largest effect on the $Q(v, \theta, \varphi)$ values. Of these, the effect of varying drone pitch θ_{pitch} is by far the largest. The physical explanation is that under zero pitch and near-centre hits, the camera gimbal has a strong damping effect on the contribution to $Q(v, \theta, \varphi)$. Also, when the camera gimbal is not involved in the impact, e.g. pitch 90° - 270°, the variation remains significant. This illustrates well that material and shape design of a UAS may have significant impact on the rate and the amount of energy that is transferred to the human body during impact.

4.5 Conclusions

The existing model of ground TPR posed by UAS flight to persons on the ground asks for a quantification of the product $A_{impact} \times P\{F|impact\}$. Recently, for the estimation of

$P\{F|impact\}$, dynamical simulation models of small UAS types have been developed, validated and integrated with validated dynamical simulation models of human bodies for estimating injury risk in a car crash.

Section 4.2 showed, for a well studied UAS of 1.21 kg, that despite such validated dynamical simulation model, the existing models for the product $A_{impact} \times P\{F|impact\}$ provide a large range of possible values, though also leaves the question unanswered which of these values is correct.

In section 4.3, an enriched ground TPR model for UAS has been developed that replaces the product $A_{impact} \times P\{F|impact\}$ by an integration of values for over possible horizontal offsets between the centre of UAS crash location and centre of human head. This integration approach supports a joint assessment of the two terms, and also has been extended to incorporate effects of human face directions and UAS attitudes and velocities.

In section 4.4, the enriched ground TPR model is evaluated using a validated MBS dynamical simulation model of a DJI Phantom III UAS. Subsections 4.4.1 and 4.4.2 showed how $P\{F|\Delta, v, \theta, \varphi\}$ depends on the offset Δ between the UAS centre relative to the centre of the human head, for vertical and non-vertical descends. Subsections 4.4.3 and 4.4.4 showed the influences of attitude of the descending drone and of human face direction on these results. Subsection 4.4.5 compared the results obtained for the proposed approach to those from the existing 9 model combinations of section 4.2. This showed that the true risk value for a DJI Phantom III falls outside the range of risk values from these 9 existing models. Subsection 4.4.6 explained the main findings based on the simulation results. Firstly, the proposed approach resolves three key shortcomings of the existing ground TPR models. Secondly, it resolves the need of a separate model for the crash impact area. Thirdly, it resolves the large range of uncertainty that the existing models define for the product $A_{impact} \times P\{F|impact\}$. Fourthly, the proposed approach is able to take the effect of possible offsets between UAS crash centre and human location into account, as well as possible variation in UAS attitude and human face direction.

For the DJI Phantom III, the effect of face direction φ appears to be relatively low, i.e. less than a factor 1.3 between highest and lowest $Q(v, \theta, \varphi)$ values. The effect of varying drone pitch θ_{pitch} on $Q(v, \theta, \varphi)$ values is much larger. The physical explanation is that under zero pitch and near-centre hits, the camera gimbal has a strong damping effect on the contribution to $Q(v, \theta, \varphi)$. Also, when the camera gimbal is not involved in the impact, e.g. pitch 90° - 270°, the variation remains significant. The latter finding illustrates well that material and shape design of a UAS may have significant impact on the rate and the amount of energy that is transferred to the human body during impact.

The dynamical simulation model used in section 4.4 is a validated MBS model of the UAS considered integrated in the MADYMO platform. It also is possible to use a validated FE model of the UAS considered integrated in the THUMS platform. Use of an FE-based model may yield a slightly higher level of precision than an MBS-based model [Fahlstedt et al., 2016]. To manage the significantly higher computational demand of an FE model, a valid approach is to take advantage of variance reduction through the use of Latin Hypercube sampling [Helton and Davis, 2003].

So far, common practice is to consider UAS collision with a 50-percentile male human. However, higher injury levels are expected for UAS collision with woman and children. Because both the MADYMO platform and the THUMS platform include validated dynamical simulation models of woman and children, this extension is relative straightforward once a

validated MBS or FE model of the UAS considered has been integrated in the corresponding platform.

References

Ale, B., Piers, M. (2000). *The assessment and management of third party risk around a major airport*. Journal of Hazardous Materials*, 71*(1-3), 1-16.

Ancel, E., Capristan, F.M., Foster, J.V., Condotta, R.C. (2017). *Real-time Risk Assessment Framework for Unmanned Aircraft System (UAS) Traffic Management (UTM)*. Proceedings of 17th AIAA ATIO Conference. pages: 1-17. Denver, Colorado. AIAA 2017-3273.

Ancel, E., Capristan, F. M., Foster, J. V., & Condotta, R. C. (2019). In-time non-participant casualty risk assessment to support onboard decision making for autonomous unmanned aircraft. In Aiaa aviation 2019 forum (p. 3053).

Arterburn, D., M. Ewing, R. Prabhu, F. Zhu, D. Francis (2017). UAS Ground Collision Severity Evaluation, ASSURE Task A4 Final Report. FAA UAS Center of Excellence. , URL: https://www.assureuas.org/projects/completed/a4/ASSURE_A4

Arterburn, D., G. Olivares, J. Bolte, R. Prabhu and S. Duma (2019). UAS Ground Collision Severity Evaluation 2017-2019, ASSURE Task A14 Final Report. FAA, Atlamtic City, NJ, URL:

https://www.assureuas.org/projects/completed/a14/ASSURE_A14

Bertrand, S., Raballand, N., Viguier, F., & Muller, F. (2017). *Ground Risk Assessment for Long-Range Inspection Missions of Railways by UAVs*. Proceedings of 2017 International Conference on Unmanned Aircraft Systems. pages: 1343-1351. Miami, FL.

Bir, C., & Viano, D.C. (2004). *Design and injury assessment criteria for blunt ballistic impacts*. Journal of Trauma and Acute Care Surgery*, 57*(6), 1218-1224.

Blom, H.A.P., Jiang, C., Grimme, W.B., Mitici, M., & Cheung, Y.S. (2021). *Third party risk modelling of Unmanned Aircraft System operations, with application to parcel delivery service*. Reliability Engineering & System Safety, 107788.

Campolettano, E.T., M.L. Bland, R.A. Gellner, D.W. Sproule, B. Rowson, A.M. Tyson, S.M. Duma and S. Rowson (2017). Ranges of injury risk associated with impact from unmanned aircraft systems, Ann. Biomed. Eng. Vol. 45, pp. 2733-2741. doi:10.1007/s10439-017-1921-6

CASA (2013). *Human injury model for small unmanned aircraft impacts*. Australian Civil Aviation Safety Authority.

Clothier, R., Walker, R., Fulton, N., & Campbell, D. (2007). *A casualty risk analysis for unmanned aerial system (UAS) operations over inhabited areas*. Proceedings of Proceedings of AIAC12: 2nd Australasian Unmanned Air Vehicles Conference. pages: 1-16.

Clothier, R.A., Williams, B.P., & Hayhurst, K.J. (2018). *Modelling the risks remotely piloted aircraft pose to people on the ground*. Safety science*, 101*, 33-47. doi:10.1016/j.ssci.2017.08.008

Dalamagkidis, K., Valavanis, K. P., & Piegl, L. A. (2011). *On integrating unmanned aircraft systems into the national airspace system: issues, challenges, operational restrictions, certification, and recommendations* (Vol. 54): springer science & Business Media.

EASA, 2021, Study on the societal acceptance of Urban Air Mobility in Europe, 19th May 19, 2021

EC, 2021, Commision implementing regulation on a regulatory framework for the U-Space, 22nd April 2021.

FAA, 2016, "Operation and Certification of Small Unmanned Aircraft Systems," Department of Transportation, Washington, USA.

Fahlstedt, M., Halldin, P. and Kleiven, S. (2016). Comparison of multibody and finite element human body models in pedestrian accidents with the focus on head linematics, Traffic Injury Prevention, Vol. 17, pp. 320-327.

Feinstein, D.I., Heugel, W.F., Kardatzke, M.L., & Weinstock, A. (1968). *Personnel casualty study*. IIT Research Institute, Chicago, IL.

Foster, J.V., & Hartman, D. (2017). *High-Fidelity Multi-Rotor Unmanned Aircraft System (UAS) Simulation Development for Trajectory Prediction Under Off-Nominal Flight Dynamics*. Proceedings of 17th AIAA ATIO Conference. pages: 1-17. Denver, Colorada.

Gennarelli, T. A., & Wodzin, E. (2006). *AIS 2005: a contemporary injury scale*. Injury, *37*(12), 1083-1091.

He, X., Jiang, C., Li, L., & Blom, H. A. P. (2022). A Simulation Study of Risk-Aware Path Planning in Mitigating the Third-Party Risk of a Commercial UAS Operation in an Urban Area. Aerospace, 9(11), 682.

Helton, J.C., and Davis, F.J. (2003), Latin hypercube sampling and the propagation of uncertainty in analyses of complex systems. Reliability Engineering and System Safety, Vol.81, pp. 23-69.

Hu, X., Pang, B., Dai, F., & Low, K. H. (2020). Risk assessment model for UAV cost-effective path planning in urban environments. IEEE Access, 8, 150162-150173.

Hutchinson, J., M.J. Kaiser, and M. Lankarani (1998), The Head Injury Criterion (HIC) functional, J. of Applied Mathematics and Computation, Vol. 96, pp. 1-16.

ICAO, 2011, Unmanned Aircraft Systems (UAS), Circular 328-AN/190, International Civil Aviation Organization.

Ippolito, C. A. (2019). Dynamic ground risk mitigation for autonomous small uas in urban environments. In AIAA Scitech 2019 Forum (p. 0961).

JARUS, 2017, Guidelines on Specific Operation Risk Assessment (SORA), Joint Authorities Regulation Unmanned Systems.

Kim, S. H. (2019). Third-party risk of mid-air collision between small unmanned aircraft systems. In AIAA Aviation 2019 Forum, p. 3052.

Klinich, K.D., R.A. Saul, G. Auguste, S. Backaitis and M. Kleinberger (1996), Techniques for developing child dummy protection reference values, measurement, Report 00819638, National Highway Traffic Safety Administration, https://doi.org/10.21949/1403104

Koh, C. H., Low, K. H., Li, L., Zhao, Y., Deng, C., Tan, S. K., Chen, Y., Yeap, B. C., & Li, X. (2018). *Weight threshold estimation of falling UAVs (Unmanned Aerial Vehicles) based on impact energy*. Transportation Research Part C: Emerging Technologies, *93*, 228-255. doi:https://doi.org/10.1016/j.trc.2018.04.021

la Cour-Harbo, A. (2019). *Quantifying Risk of Ground Impact Fatalities for Small Unmanned Aircraft*. Journal of Intelligent & Robotic Systems, *93*(1), 367-384. doi:10.1007/s10846-018-0853-1

la Cour-Harbo, A., & Schiøler, H. (2019). Probability of Low-Altitude Midair Collision Between General Aviation and Unmanned Aircraft. Risk Analysis, 39(11), 2499-2513.

Lau, I.V., & Viano, D.C. (1986). *The viscous criterion—bases and applications of an injury*

severity index for soft tissues. SAE transactions, 672-691.

MADYMO (2017a). MADYMO Human body models manual, Release 7.7, TASS International.

MADYMO (2017b). MADYMO Theory manual Version 7.7, MADYMO utility manual, TASS International.

Magister, T. (2010). *The small unmanned aircraft blunt criterion based injury potential estimation*. Safety science*, 48*(10), 1313-1320.

Melnyk, R., Schrage, D., Volovoi, V., & Jimenez, H. (2014). *A third-party casualty risk model for unmanned aircraft system operations*. Reliability Engineering & System Safety*, 124*, 105-116.

Oh, S., J. Cho, N. Kim, Y. Yoon (2020), Preliminary impact assessment of restricting airspace over populated areas for sUAS operations, The Transportation Research Board (TRB) 99th Annual Meeting, 14th January 2020. http://hdl.handle.net/10203/276236

Parr, M.J.C., M.E. Miller, N.R. Bridges, J.R. Buhrman, C.E. Perry and N.L. Wright (2012), Evaluation of the Nij neck injury criteria with human response data for use in future research on helmet mounted display mass properties, Proc. Human Factors Ergon. Soc., pp. 2070-2074, doi:10.1177/1071181312561439.

Petritoli, E., Leccese, F., & Ciani, L. (2018). Reliability and maintenance analysis of unmanned aerial vehicles. Sensors, 18(9), 3171.

Primatesta, S., Rizzo, A., & la Cour-Harbo, A. (2020). *Ground risk map for unmanned aircraft in urban environments*. Journal of Intelligent & Robotic Systems*, 97*(3), 489-509.

Rattanagraikanakorn, B. (2021), Modelling collision consequences of unmanned aircraft systems on human, PhD Thesis, Delft University of Technology, November 2021, Delft, Netherlands.

Rattanagraikanakorn, B., Schuurman, M., Gransden, D.I., Happee, R., De Wagter, C., Sharpanskykh, A., & Blom, H.A.P. (2019). Modelling Head Injury due to Unmanned Aircraft Systems Collision: Crash Dummy vs Human Body, Proc. 19th AIAA ATIO Conf., June 2019, Dallas, TX, 10.2514/6.2019-2835.

Rattanagraikanakorn, B., Gransden, D. I., Schuurman, M., De Wagter, C., Happee, R., Sharpanskykh, A., & Blom, H.A.P. (2020a). *Multibody system modelling of unmanned aircraft system collisions with the human head*. International Journal of Crashworthiness*, 25*(6), 689-707.

Rattanagraikanakorn, B., Blom, H.A.P., Sharpanskykh, A., De Wagter, C., Jiang, C., Schuurman, M. J., Gransden, D. I., & Happee, R. (2020b). *Modeling and Simulating Human Fatality due to Quadrotor UAS Impact*. Proc. AIAA AVIATION 2020 FORUM. June 2020, 10.2514/6.2020-2902.

Rattanagraikanakorn B, Schuurman M, Gransden D I, Happee R., De Wagter C., Sharpanskykh A., Blom H.A.P. (2022). Modelling head injury due to unmanned aircraft systems collision: Crash dummy vs human body. International Journal of Crashworthiness, 27(2): 400-413.

RCC (2000). *Common risk criteria for National test ranges; Inert debris, Supplement to Standard 321-00*. Range Commanders Council.

RCC (2001). *Range Safety criteria for Unmanned Air Vehicles, Rationale and methodology supplement*. Supplement to Document 323-99, Range Commanders Coucil, April 2001.

Schmitt, K.-U., P.F. Niederer, D.S. Cronin, B. Morrison III, M.H. Muser and F. Walz (2019), Trauma Biomechanics: An Introduction to Injury Biomechanics, 5th Edition, Springer.

Stark, D.B., A.K. Willis, Z. Eshelman, Y.S. Kang, R. Ramachandra, J.H. Bolte, M. McCrink (2019). Human response and injury resulting from head impacts with unmanned aircraft systems, Stapp Car Crash Journal, Vol. 63, pp. 29-64. doi:10.4271/2019-22-0002.

Sturdivan, L. M., Viano, D. C., & Champion, H. R. (2004). *Analysis of injury criteria to assess chest and abdominal injury risks in blunt and ballistic impacts*. Journal of Trauma and Acute Care Surgery, *56*(3), 651-663.

Touger, M., Gallagher, E. J., & Tyrell, J. (1995). *Relationship between venous and arterial carboxyhemoglobin levels in patients with suspected carbon monoxide poisoning*. Annals of emergency medicine, *25*(4), 481-483.

THUMS (2015), Documentation Total Human Model for Safety (THUMS), AM50 occupant model academic version 5.0_20150527, Toyota Motor Corporation.

THUMS (2018), Documentation Total Human Model for Safety (THUMS), AM50 pedestrian/occupant model academic version 4.02_20181226, Toyota Motor Corporation.

Viano, D.C., I.V. Lau, C. Ashbury, A.I. King, P. Begeman (1989), Biomechnaics of the human chest, abdomen and pelvis in lateral impact, Accident analysis and prevention, Vol. 21, pp. 553-574.

Washington, A, Clothier, R.A., Silva, J. (2017), A review of unmanned aircraft system ground risk models, Progress in Aerospace Sciences, Vol. 95, pp. 24-44.

Weibel, R., & Hansman, R. J. (2004). *Safety considerations for operation of different classes of UAVs in the NAS*. Unmanned Unlimited, Technical Conf., Workshop and Exhibit, 20-23 Sept. 2004, Chicago, IL, AIAA-2004-6421, pp. 1-11.

Weng, Y. B. Bian, K. Gunasekaran, J. Gholipour, C. Vidal and H. Mao (2021). Modelling Small Remotely Piloted Aircraft System to Head Impact for Investigating Craniocerebral Response, J. of Biomechanics, doi:https://doi.org/10.1016/j.jbiomech.2021.110748

5

Effect of Parachute and Airbag in Reducing Safety Risk Posed by Small UAS to People on the Ground

To reduce the safety risk posed by small UAS posed to overflown persons on the ground, one of the mitigating measures is to equip the UAS with an airbag in combination with a parachute, both of which function in case of an uncontrolled descent. The in literature developed methods for the evaluation of this safety risk apply only if a UAS is equipped with a parachute alone. This paper develops a method to assess the safety risk for persons on the ground posed by a UAS that is both equipped with an airbag and a parachute. The developed method conducts complementary dynamical simulations for the UAS descent to the ground, and the effect of the UAS impacting a human on the ground. For the human impact simulation, use is made of Multi Body System (MBS) simulations for the UAS and the human; in combination with Finite Element (FE) model of the airbag. This method is applied for a specific parcel delivery UAS, of 15 kg weigh, for cases with and without airbag. The latter results are also compared to results obtained using the existing methods.

5.1 Introduction

The use of Unmanned Aircraft System (UAS) [ICAO, 2011] is of high interest for services like medical aid, surveillance, parcel delivery and air taxi. As has been identified in [EASA, 2021], the advantages of commercial UAS-based services may come with negative issues for overflown population. One of the main negative issues identified is the ground Third Party Risk (TPR), i.e. the safety risk posed by UAS flights to people and property on the ground [Clothier et al., 2018]. The development of these commercial UAS-based services encounters a yet unresolved gap: many potential customers live in urban and metropolitan areas where these issues play a key role. In line with this, standing safety regulations typically consider UAS not (yet) safe enough to be allowed to fly to potential customers in urban areas [FAA, 2016; JARUS, 2017; Oh et al., 2020]. To abridge this safety gap further UAS developments are ongoing, such as designing more reliable UAS, e.g. [Petrioli et al., 2018], and the use of risk mitigating measures like equipping a UAS with a parachute [DJI, 2022; Flyfire, 2022; Antwork, 2022] and airbag [Cawthorne, 2016; Disney, 2016; DJI, 2019], or both [Manta Air, 2023]. Other developments are risk-aware path planning, e.g. [Ancel et al. 2019; Ipolito, 2019; Primatesta et al., 2020;], as well as introduction of an Urban Air Mobility (UAM) framework, e.g. [EASA, 2021; EC, 2021].

An important complementary role in these UAS developments is to assess their effects in terms of ground TPR. The requirement posed by acceptable ground TPR on the reliability of a UAS has been studied by [Melnyk et al., 2014; Blom et al., 2021]. The effect of UAS weight has been studied by [Koh etal., 2018]. The effect of risk-aware path planning on ground TPR has been studied by [Pang et al., 2022; He et al., 2022]. The effect of parachute descend on ground TPR has been studied by [la Cour-Harbo, 2019; Bertrand et al., 2017]. The objective of the current study is to evaluate the ground TPR effect of the combined use of parachute and airbag.

In the above mentioned studies, ground TPR per UAS flight hour is quantified as a product of the following five terms: i) Failure rate of the overall UAS system; ii) Population density on the ground; iii) Probability that a person on the ground is not sheltered; iv) UAS crash impact area around an unsheltered person on the ground; and v) Probability of fatality if an unsheltered person is hit by a crashing UAS. The above mentioned ground TPR studies implicitly assume that the terms iv) and v) are independent. Recently, [Jiang et al., 2023] developed a method to assess the product of terms iv) and v) in a way that takes their dependence into account. The key step was to prove that the product of terms iv) and v) can be replaced by a systematic assessment and integration of probability of human fatality over all possible offsets between centre locations of human and crashing UAS. Jiang et al. [2023] has also shown that this assessment can be accomplished by conducting simulations of a dynamical model of a collision between a UAS and a human body. This type of dynamical simulation has been well developed for assessing human injury levels in case of a car crash, using Finite Element (FE) models [THUMS, 2018] or Multi Body System (MBS) models [MADYMO, 2023]. In support of this dynamical modelling and simulation approach for UAS collision with human body, FE models have been developed by [Koh et al., 2018; Weng et al. 2021]; and MBS models by [Rattanagraikanakorn, 2021].

In [Jiang et al., 2023] this novel ground TPR assessment method has also been applied to a UAS of 1.5 kg without parachute and airbag, using the MBS model of [Rattanagraikanakorn et al., 2020]. The objective of the current research is to address the relevant changes in applying this dynamical simulation approach to a parcel delivery UAS that is equipped with a parachute and airbag. The first relevant change is that the weight of a parcel delivery drone typically is an order in magnitude higher than the 1.5 kg UAS. Secondly, the parachute reduces the impact

velocity of the UAS on the human body. Thirdly, the dynamical simulation model for a collision between UAS and human body has to be extended with a dynamical model for the influence of the airbag.

The effect of these changes is demonstrated through conducting a ground TPR assessment for a 15 kg delivery UAS, that is equipped with parachute and airbag. By making a comparison with ground TPR for the same UAS without airbag, it is shown that a combination of parachute and airbag may provide effective risk mitigation for use of a 15 kg delivery UAS.

The paper is organized as follows. Section 5.2 provides the background of ground TPR model and the enrichment by [Jiang et al., 2023]. Section 5.3 shows the development of the dynamical simulation model for the airbag equipped parcel delivery UAS. Section 5.4 evaluates fatality risk conducting simulations with this dynamical model for a delivery UAS of 15 kg for different cases with/without airbag and/or parachute, and compares the results with fatality risks evaluated using in literatures developed models. Section 5.5 draws conclusions.

5.2 Background of Ground TPR Assessment

This section provides an overview of the background in ground TPR assessment, with focus on the product of the terms iv) and v). Subsection 5.2.1 starts with the widely accepted ground TPR equation which covers the five terms mentioned in the Introduction, and its use by Bertrand et al. (2017) and la Cour-Harbo (2019) for a parcel deliver drone of 15 kg. Subsections 5.2.2 and 5.2.3 explain the dynamical simulation approach to numerically assess the product of terms iv) and v).

5.2.1 Ground TPR model

The widely accepted risk indicator for TPR posed by a UAS flight to people on the ground is the expected number of fatalities $E\{n_F\}$ per UAS flight hour. The common model for the assessment of this TPR indicator satisfies [RCC, 2001; Weibel and Hansman, 2004; Melnyk et al., 2014]:

$$E\{n_F\} = \lambda_{system} \times \rho_{population} \times (1 - P_{shelter}) \times A_{impact} \times P\{F|impact\} \qquad (2.1)$$

where λ_{system} is the failure rate of the UAS system; $\rho_{population}$ is the population density of the overflown area; $P_{shelter}$ is the probability that a person on the ground is sheltered to the crashing UAS; A_{impact} is the size of the area on the ground that is impacted by the crashing UAS; and $P\{F|impact\}$ is the probability of fatality in case the UAS impacts a human in the impact area.

Common practice, e.g. [Melnyk et al., 2014; Primatesta et al., 2020], is to assume that the terms A_{impact} and $P\{F|impact\}$ are independent. However as shown by [Jiang et al., 2023], taking this dependency into account may have significant impact on the ground TPR assessment. The next subsection explains the novel approach by [Jiang et al., 2023] in assessing the product $A_{impact} \times P\{F|impact\}$.

5.2.2 Dynamical simulation based evaluation of $A_{impact} \times P\{F|impact\}$

[Jiang et al., 2023] developed a method to assess the product $Q \triangleq A_{impact} \times P\{F|impact\}$ in (2.1), through conducting simulations of an MBS model of a UAS that collides with human body model. The key step in this development is to prove that the product in (2.1) satisfies the following equality:

$$Q \triangleq A_{impact} \times \mathrm{P}\{F|impact\} = \int_{\mathbb{R}^2} \mathbb{P}\{F|\Delta\}d\Delta \qquad (2.2)$$

where $\mathrm{P}\{F|\Delta\}$ is the conditional probability of fatality given horizontal offset Δ between the centre of the UAS impact location relative to the location of an impacted human.

The derivation of eq. (2.2) by [Jiang et al., 2023] worked as follows. In [RCC, 2001], the term $\mathrm{P}\{F|impact\}$ is characterized as a summation over fatality probabilities in case a horizontal moving object impacts different body parts of a human, i.e.:

$$\mathrm{P}\{F|impact\} = \sum_B \left[\mathrm{P}\{F|\text{hit on body part } B\} \times \frac{\text{Area of body part } B}{\text{Area of human body}} \right] \qquad (2.3)$$

In case of a UAS crashing from the air to the ground, the impact location of UAS can be at any horizontal offset Δ relative to the location of a human. To capture this falling UAS situation, the summation over body parts in eq. (2.3) is replaced by an integration over all horizontal offsets Δ in the set $\{A_{impact}\}$, i.e.:

$$\mathrm{P}\{F|impact\} = \int_{\{A_{impact}\}} \mathrm{P}\{F|\Delta\} \frac{1}{A_{impact}} d\Delta \qquad (2.4)$$

where $\mathrm{P}\{F|\Delta\}$ is the conditional probability of fatality given horizontal offset Δ.

Taking into account that $\mathrm{P}\{F|\Delta\} = 0$ for all $\Delta \notin \{A_{impact}\}$, eq. (2.4) implies:

$$\mathrm{P}\{F|impact\} = \int_{\mathbb{R}^2} \mathrm{P}\{F|\Delta\} \frac{1}{A_{impact}} d\Delta \qquad (2.5)$$

Multiplying both sides in eq. (2.5) by A_{impact} yields eq. (2.2).

Equation (2.2) implies the following numerical evaluation of the product $A_{impact} \times \mathrm{P}\{F|impact\}$. Firstly, quantify $\mathrm{P}\{F|\Delta\}$ through conduct dynamical simulations for all horizontal offsets Δ. Subsequently, the solution $Q \triangleq A_{impact} \times \mathrm{P}\{F|impact\}$ of eq. (2.2) can be numerically evaluated by an integration of the assessed $\mathrm{P}\{F|\Delta\}$ values over all horizontal offsets Δ.

5.2.3 Dynamical simulation phases

Dynamical simulation of a crashing UAS involves two subsequent simulation parts. The first part is the dynamical simulation of the descent until reaching the top of the human body in Figure 1. The second part is the dynamical simulation of a collision of the UAS with the human body, and transforming this into implied injury levels. The aim of the first part is to assess the UAS speed and angle of descent at the end of the descent to the ground. The aim of the second part is to assess $Q \triangleq A_{impact} \times \mathrm{P}\{F|impact\}$ given the UAS impact speed and angle of descent. Methods for the dynamical simulation of the first part range from detailed simulation of UAS dynamical behavior including UAS rotation, e.g. [Foster and Hartman, 2017], to ballistic kind of UAS descent simulation, e.g. [la Cour-Harbo, 2020]. Dynamical simulation of a collision between a UAS and a human body is in need of a well-developed Finite Element (FE) model or a well-developed Multi Body System (MBS) model of the specific UAS, the human body type, and their contact behavior. The latter simulated contact events have to be mapped to relevant injury levels and to probability of fatality.
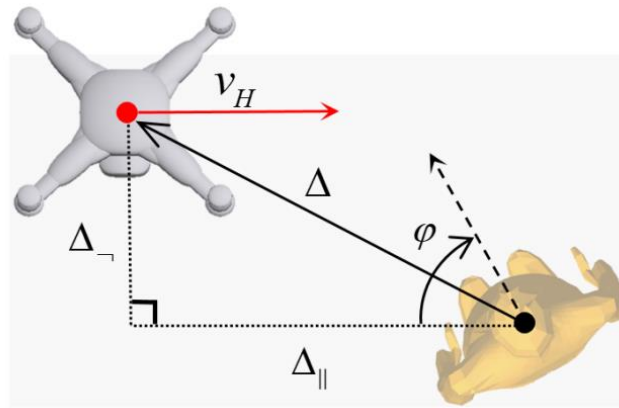
Figure 1. Top view of a standing human with face direction φ and a UAS at position Δ relative to human when it passes a horizontal plane on top of human head. Offset Δ is decomposed into components $\Delta_{\parallel}$ and $\Delta_{\neg}$, that are parallel and perpendicular to horizontal UAS velocity v_H.

Dynamical simulation of collisions with human, and capturing this in injury levels is a well-developed topic in automotive research; with emphasis on consequences for human involved in a car crash. As a result of this research, dynamical simulation models have been developed and validated for collisions involving human and human crash dummies that are used in car crash testing. Examples of well-developed and validated simulation platforms are: [THUMS, 2015, 2018] and [MADYMO, 2017a,b]. The former makes use of Finite Element (FE) models of human body or crash dummy involved in a car collision, while the latter makes use of Multi-Body System (MBS) models. Dynamic simulation of a collision yields detailed acceleration curves over time of various parts of the human body or crash dummy involved. These results are subsequently translated into well-developed injury scales. The commonly used injury scales are Head Injury Criteria (HIC), Neck Injury Criteria (Nij) and Viscous Criteria (VC) for injuries to head, neck and other body parts respectively. HIC takes the effect of sudden head acceleration into account [Hutchinson et al., 1998; Schmitt et al., 2019]. Nij considers the consequences of head movements on neck forces and moments [Klinich et al., 1996; Parr et al., 2012]. VC takes into account that injury to soft tissue injury is compression and rate dependent [Lau and Viano, 1986; Viano et al. 1989].

For dynamical simulation of UAS collision with human body or a crash dummy, a validated model of the UAS type considered has to be developed and integrated in one of these platforms. In addition, there is need for a transformation of assessed injury levels to probability of fatality. For integration in the THUMS (2015) platform, FE models have been developed by [Arterburn et al., 2019, Annex B] of UAS types: DJI Phantom III, Sensefly eBee+ and Precision Hawk MK III. These models have been validated against acceleration measurements of drop tests on a head of a human dummy. [Weng et al., 2021] developed and integrated an FE model of DJI Phantom III in [THUMS, 2018]; this model has been validated against acceleration measurements of the head of a human cadaver [Stark et al., 2019].

For integration in the MADYMO platform, [Rattanagraikanakorn et al., 2019, 2020] developed an MBS model of DJI Phantom III, and has validated this model against head acceleration measurements of drop tests on a crash dummy [Arterburn et al., 2017] and those measured during hittings of human cadavers [Stark et al., 2019]. In [Rattanagraikanakorn et al., 2022] a comparison is made between MBS dynamical simulation of DJI Phantom III falling down on the head of a crash dummy versus the head of human body. This comparison showed significant differences both in HIC values and Nij values. Most significant is the finding that for this scenario, Nij effect on human injury level is negligible relative to HIC effect. For the mapping of HIC values to corresponding probability of fatality values, use is made of the conversion curve by [Touger et al., 1995] of HIC value to percentage of life-threatening injury.

For thorax and abdomen the VC (Viscous Criterion) injury level [Lau & Viano, 1986] is obtained during MBS dynamical simulation. The VC level is then converted to P{$F|impact$} in two steps: first a conversion curve from VC level to AIS level [Sturdivan et al., 2004], and then a conversion curve from AIS level to probability of fatality [Gennarelli & Wodzin, 2006].

In Jiang et al. (2023) this dynamical simulation model of DJI Phantom III collision with human body, has been used for the assessment of $Q \triangleq A_{impact} \times P\{F|impact\}$ The next section explains how this dynamical modelling approach is extended for a specific parcel delivery UAS that is equipped with a parachute and an airbag.

5.3 Dynamical Simulation Modelling

5.3.1 Descent modelling

The specific parcel delivery UAS studied is the RA3 [Antwork, 2020], which UAS is able to carry a parachute system for emergency descent. The parachute system consists of a parachute, parachute box, canopy and gas trigger that are embedded on top of the mainframe [Antwork, 2020]. As shown in Figure 2, four ropes connect four corners of the expanded parachute to four corners of the parachute carrying box part of the RA3 UAS. Distance between nearby parachute corners is 1.65m. During descent, the parachute decelerates the descending velocity and helps the UAS to keep an upright attitude to land with its bottom touching the ground. For the impact modelling, it is assumed that a deployed parachute reduces the impact velocity, though does not play a further role during human impact.

Figure 2. RA3 UAS with parachute deployed.

For the modelling of descent to the ground by a failing UAS, there are analytical models [la Cour-Harbo, 2020], and dynamical simulation models, including ballistic descent models with and without parachute [la Cour-Harbo, 2019] and high fidelity models [Forster and Hartman, 2017; Sun and Visser, 2019]. In this paper, the following ballistic descent model is adopted:

$$\dot{s}_t = v_t \tag{3.1}$$

$$\dot{v}_t = Col[0,0,g] - \frac{1}{2}(A_S^d C_D^d + A_S^p C_D^p)\|v_t - w_t\|(v_t - w_t)\rho/m \tag{3.2}$$

where s_t is the UAS 3D position at moment t, v_t and w_t are the UAS 3D ground velocity and 3D wind velocity at moment t, g is gravitational constant, C_D^d and C_D^p are the drag coefficient

of drone and parachute respectively, A_S^d and A_S^p are the reference surface areas of the drone and parachute respectively, ρ is air density, m is mass of the system. $A_S^p = 0$ if the parachute is not deployed.

Two types of descents are considered: descent of RA3 UAS with parachute, and descent of RA3 without parachute, i.e. $A_S^p = 0$. The RA3 relevant parameter values for eq. (3.2) are shown in Table 1. Drag coefficient C_D^d and C_D^p are obtained through Computational Fluid Dynamics analysis of RA3 UAS and parachute for angle of attack 90 degrees (i.e. vertical descent with 0 degrees of pitch) [Antwork, 2022].

Table 1. Parameter values for eq. (3.2); mass of parachute and airbag are assumed to be negligible.

Parameter	Definition	Value
A_S^d	Reference area of RA3 drone	0.12 m²
A_S^p	Reference area of parachute	2.72 m²
C_D^d	Drag coefficient of RA3 drone	0.73
C_D^p	Drag coefficient of parachute	1.54
m	Mass of RA3 drone	15.0 kg
ρ	Air density	1.23 kg/m³
g	Gravitational constant	9.81m/s²

5.3.2 MBS model of RA3 UAS

The first step in MBS model development is the identification of the relevant multiple bodies; this is shown in Figure 6.b, with the true RA3 UAS shown in Figure 3a. The propeller blades are not modelled assuming that the propellers are fully stopped during crash. The MBS model involves seven such bodies, one for the main body and one for each of the six arms. The main body includes the mainframe, cargo box, avionic system and battery that are lumped into Body 0. Motors at the end of each arm are lumped into Bodies 1-6. In the MBS model, each of these seven bodies is considered to be a rigid body, the shape of which is defined by a set of ellipsoid surfaces. The latter enables MBS contact detection and MBS contact effect evaluation. MBS model details and properties (i.e. weight, dimension, etc.) of the RA3 UAS is presented in Appendix A.
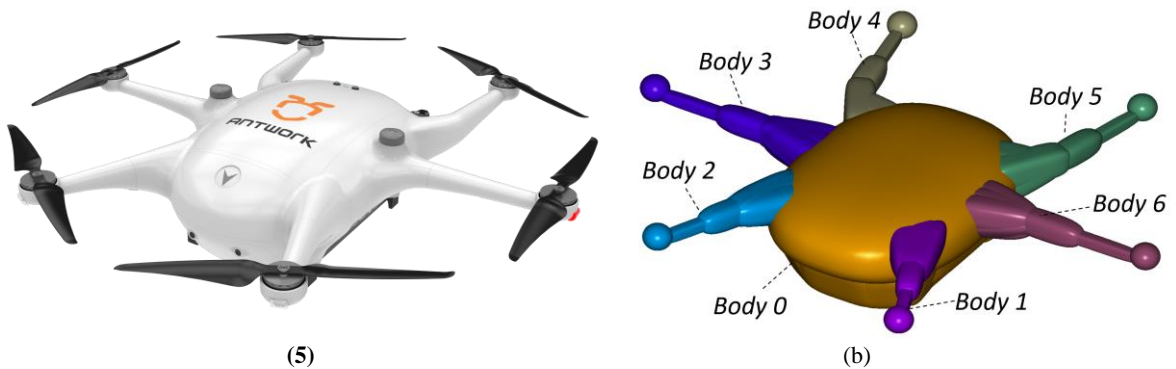
(5)   (b)
Figure 3. Identifying relevant bodies. (a) RA3 system. (b) Bodies in MBS model.

As shown in Figure 4, the RA3 UAS consists of two types of materials. The main frame and drone arms are made from carbon fiber. The cargo box on bottom of the UAS is made from EPP foam.
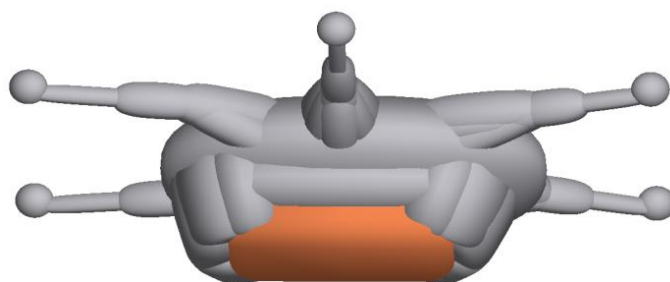
Figure 4. Materials of RA3 UAS, body and arm made from carbon fiber (in grey);
foam cargo box made from EPP foam (in orange)

Per local body it is assumed that there is no breakage of the body parts during impact. During impact, bending deformation on arms of RA3 UAS is determined by the torsional stiffness of the arm joint. The stiffness of the arm joints is obtained through quasi-static compression test of the RA3 UAS body. Details of the compression test the stiffness curve of arms are also presented in Appendix A.

5.3.3 UAS impact on human

The MBS model of the human body adopted is a representative model for a mid-size (50th percentile) male human [Happee et al., 1998, 2000]. This human body MBS model (Figure 5) is available in Madymo (filename: h_occ50fc, version 5.2) and is used to simulation the impact of UAS on a 50th percentile male human.

Upon hitting a human body, the type of contacting UAS material is taken into account in the Madymo model. The contact for the carbon fiber of the main frame and arms of RA3 with human body is modelled using the Hertz elastic contact model [Brake, 2012]. The contact for the EPP foam cargo box of the RA3 is modelled using the ellipsoid-foam contact model [Chou et al., 1994]. Material properties and measured contact compliance curves are presented in Appendix B.

(5)   (b)
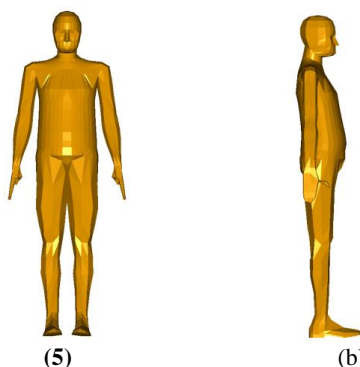
Figure 5. 50th percentile human male body model. (a) front view, (b) side view.

The effect of UAS impact on human body is evaluated according to the following three injury criteria:

- Head Injury Criterion (HIC) for head injuries;
- Neck Injury Criteria N_{ij} for neck injuries;
- Viscous Criterion (VC) for thorax and abdomen injuries.

All three injury criteria models are available within the dynamical simulation platform MADYMO. Head Injury Criterion (HIC) is an integrated value of head acceleration curve and represent the peak average power delivered to the head [Hutchinson et al., 1998]. HIC is widely adopted in car crash research, e.g. by the National Highway Traffic Safety Administration (NHTSA). Neck injury criteria N_{ij} are also widely adopted in car crash

research. N_{ij} capture four types of neck loading N_{TF}, N_{TE}, N_{CF}, and N_{CE} [Eppinger et al., 1999]. The first subscript refers to Tension (i=T) and Compression (i=C) in axial direction. The second subscript refers to Flexion (j=F) and Extension (j=E) bending moments in the sagittal plane. Viscous Criterion (VC) is an injury criterion that has been developed for soft tissues [Lar et al., 1986], and therefore suitable for the evaluation of injury on thorax and abdomen.

5.3.4 Finite Element (FE) model of airbag

In normal condition, the airbag is folded in the mainframe. During parachute descend, the airbag will be fully inflated. In the airbag system designed by [Manta Air, 2023], the inflation starts to work if the parachute has been deployed; this design is adopted for the RA3 UAS. The airbag for RA3 UAS is assumed to be similar to the airbag that is FE modelled in [MADYMO version 2.1, 2020] under filename: a_driver_airbag_scaled_inc. This FE airbag consists of two flat circular pieces sewed together that forms a closed chamber. Within the airbag, four straps are used to connect the two circular fabrics to limit the deployment range of airbag. As shown in Figure 6, the airbag is placed on bottom of the drone and is scaled to cover the bottom area of the mainframe.
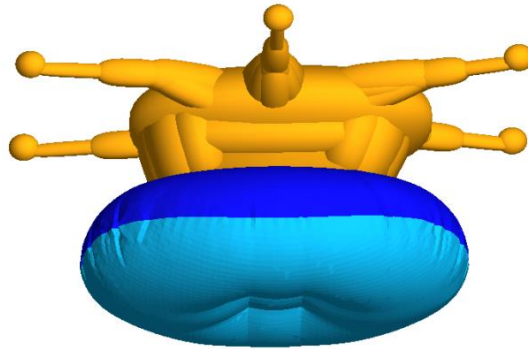
Figure 6. Airbag on bottom of the RA3 UAS

Upon inflation, the tension on fabric skin is determined by the material properties, with shear stiffness for woven fabric as shown in Figure 7. The FE model captures the stressing and wrinkling of the inflated airbag fabric, and the caused tension on the airbag fabric skin and internal air pressure. The internal air pressure of an inflated airbag depends on the amount of air pumped into the airbag during inflation, the airbag chamber size and the temperature. It is assumed that the pressure and temperature within airbag is uniform throughout the chamber, and there is no leakage of air to the environment.
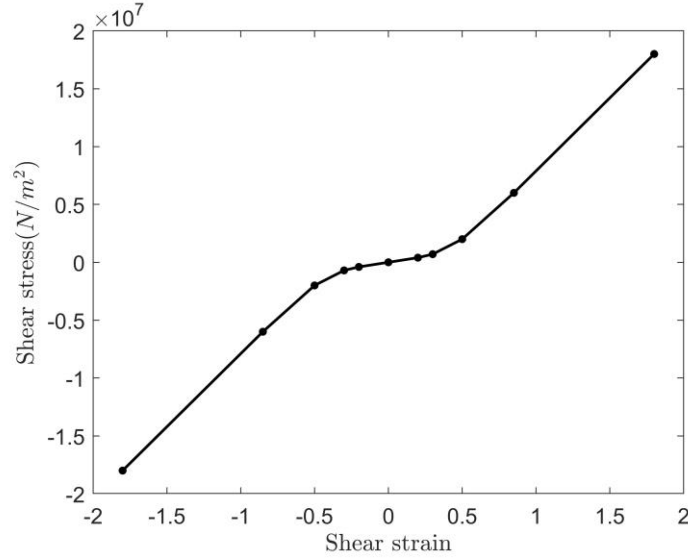
Figure 7. Fabric shear stiffness [Madymo, 2020]

5.3.5 Conversion of injury criteria to probability of fatality

The result of a dynamical simulation of a UAS collision with a human yields seven quantified injury levels: one for HIC, four for Nij, and two for VC. These seven injury levels typically depend on the horizontal offset Δ So we need to convert, for each Δ, the seven assessed injury levels to a single value for $P(F|\Delta)$. Such conversion is done in two steps.

During the first step, the HIC value is transformed to a corresponding probability of fatality $P(F_{HIC}|\Delta)$. The four Nij values are transformed to a single probability of fatality $P(F_{NI}|\Delta)$. The two VC injury values are transformed to a single probability of fatality $P(F_{VC}|\Delta)$. These first step transformations are explained in Appendix C, with transformation curves in Figures C1, C2 and C6 respectively.

During the second step, the three probabilities of fatality $P(F_I|\Delta)$, for $I \in \{HIC, NI, VC\}$, are probabilistically fused to the overall $P(F|\Delta)$. For this fusion it is assumed that a human is not fatally injured if it is not fatally injured by Head injury, not by Neck injury, and not by VC injury. By assuming independence of these three events, we get:

$$P(F|\Delta) = 1 - \prod_{I \in \{HIC, NI, VC\}} [1 - P(F_I|\Delta)] \qquad (3.3)$$

The latter result forms input to the enriched model of ground TPR equation (2.2).

5.4 Dynamical Simulation Results

This section conducts dynamical simulations of RA3 UAS collision with a human for the following three cases:

- Case A: UAS with parachute and airbag;
- Case B: UAS with parachute, no airbag;
- Case C: UAS without parachute or airbag.

For each of these three cases, a dynamical simulation consists of two phases: the descent phase, and the collision with human. For the descent phase, equations (3.1-3.2) are simulated. The outcomes of this first phase simulation are used as starting conditions for the MBS/FE model based simulation collision of UAS with a human. Subsection 4.1 presents the phase 1

results for cases A-C. Subsection 4.2 provides Q results for cases B and C that are based on analytical models. Subsection 4.3 provides Q results for A-C under zero wind, and face direction $\varphi = 0°$. Subsection 4.4 extends these results to non-zero horizontal wind speeds. Subsection 4.5 considers the effect of increasing airbag pressure and adding an front airbag. Subsection 4.6 discusses the results obtained.

5.4.1 Simulation of descent phase

For case B (RA3 with parachute, no airbag) and case C (RA3 without parachute or airbag), simulations of eqs. (3.1-3.2) are conducted for a UAS that starts to descent due to a failure at an altitude of 120m under horizontal wind speed ranging from 0 to 10 m/s. In both cases, during its descent, the attitude of UAS is assumed to be the same; i.e. pitch $\theta_{pitch} = 0°$, roll $\theta_{roll} = 0°$, yaw $\theta_{yaw} = 0°$. The resulting impact speeds and descent angles are shown in Table 2. The assumption adopted is that the inflated airbag does not influence the descent; hence results for case B also apply to case A.

Table 2. Descent simulation results for cases A/B and C

Wind speed (m/s)	Case A/B		Case C	
	Impact speed $\lvert v \rvert$ (m/s)	Descent angle ψ (degrees)	Impact speed $\lvert v \rvert$ (m/s)	Descent angle ψ (degrees)
0	7.5	90.0	40.6	90.0
2	7.8	75.1	40.6	89.0
4	8.5	62.0	40.6	88.0
6	9.6	51.5	40.5	86.9
8	11.0	43.3	40.5	85.8
10	12.5	37.0	40.4	84.7

For case C, the results in Table 2 show that the influence of wind on impact velocity is negligible. The influence on descend angle is also quite limited, varying from $\psi = 90°$ for zero wind to $\psi = 84.7°$ for 10m/s wind. However, for case B, the results in Table 2 show that due to the drag of parachute, the impact velocities and the descent angles are significantly lower than in case C, and these also vary in a large range with increasing horizontal wind.

5.4.2 Analytical model based assessment of $Q = A_{impact} \times \mathrm{P}\{F \lvert impact\}$

This subsection evaluates $Q = A_{impact} \times \mathrm{P}\{F \lvert impact\}$ for RA3 UAS using analytical models for crash impact area A_{impact} and impact probability of fatality $\mathrm{P}\{F \lvert impact\}$. The numerical results obtained from these analytical models are presented in Table 3a for cases B and C. Table 3 also makes clear that there are no such analytical models for case A.

For impact probability of fatality $\mathrm{P}\{F \lvert impact\}$, [la Cour-Harbo, 2019] adopts the Area Weight Kinetic Energy (AWKE) model [Arterburn, 2017] for case B, and the Blunt Criterion (BC) model [Magister, 2010] for case C. For the RA3 UAS weight of 15kg and impact velocities in Table 2, yields $\mathrm{P}\{F \lvert impact\} = 1$ for both case B and case C.

For crash impact area A_{impact}, four analytical models are considered: Person area, Planform area, Gliding area, and a Maximum Take Off Weight (MTOW) based area. For a fixed wing UAS with similar mass as the RA3 UAS, [la Cour-Harbo, 2019, Table 4] proposes to use the person area $A_{impact} = 0.3\ m^2$, both for cases B and C. The planform area model [Weibel and Hansman, 2004] adopts $A_{impact} = Width_{UAS} \times Length_{UAS}$; for RA3 UAS this equals $A_{impact} = 1.43m^2$ ($1.1m \times 1.3m$). The Gliding area model [RCC, 2001] also takes the UAS descend angle and the size of human (height $1.73m$, diameter $0.2m$) into account; for RA3

UAS this yields $A_{impact} = 2.55m^2$ at descent angle of 90 degrees for no wind condition. Under 10 m/s horizontal wind: $A_{impact} = 6.45m^2$ at a descend angle of 37 degrees (case B) and $A_{impact} = 2.81m^2$ at a descend angle of 85 degrees (case C). The MTOW based area satisfies [Ale and Piers, 2000]: $A_{impact} = c_{Fit} \times m_{MTOW}$, with m_{MTOW} the Maximum Take-Off Weight in kg, and the statistically fitted coefficient value $c_{Fit} = 0.2$ m²/kg; for RA3 UAS this yields $A_{impact} = 3.00m^2$.

For impact probability of fatality P{$F|impact$}, the RCC model [RCC, 2001] and the Blunt Criterion (BC) model [Magister, 2010] are evaluated. For a UAS weighting 15kg and at impact velocity $46m/s$, both methods yield P{$F|impact$} = 1. The evaluated results for the product $A_{impact} \times$ P{$F|impact$} are shown in Table 3a. Under zero wind, the Q estimates range from $0.30m^2$ to $3.00m^2$, which is a factor 10. Such large range makes it difficult to select one of these analytical models. Table 3a also shows that the Q estimates for case B (UAS with parachute) and case C (UAS without parachute) are the same, with exception of the results in the right column. Due to the gliding effect under $10m/s$ wind, the product $A_{impact} \times$ P{$F|impact$} is for a parachute (case B) more than twice as high than without parachute (case C). Based on the outcomes from the analytical models the expectation is that the risk would remain the same, or could even increase, by using a parachute. This forms another indication that the analytical models fall short in a proper estimation of the product $A_{impact} \times$ P{$F|impact$}.

Table 3a. Conventional assessments of $Q \triangleq A_{impact} \times$ P{$F|impact$}

Case	$A_{impact} \times$ P{$F|impact$}				
	Person	Planform	MTOW	Gliding 0 m/s wind	Gliding 10 m/s wind
A	-	-	-	-	-
B	$0.30m^2$	$1.43\,m^2$	$3.00\,m^2$	$2.55\,m^2$	$6.45\,m^2$
C	$0.30m^2$	$1.43\,m^2$	$3.00\,m^2$	$2.55\,m^2$	$2.81\,m^2$

5.4.3 Dynamical simulation of Q under zero wind

For each of the three case A-C, MBS simulations are conducted, under zero wind conditions, to assess $P(F|\Delta)$ values for various offsets Δ for human impact, and human face direction $\varphi = 0°$. The MBS assessed P{$F|\Delta$} values are shown in Table 4, Table 5 and Table 6 for cases A, B and C respectively, under descent angle $\psi = 90°$ and face direction $\varphi = 0°$. Note that due to face direction $\varphi = 0°$, results are symmetrical for positive and negative cross offset $\Delta_{\neg}$ values, therefore results are only shown for positive cross offsets. The obtained P{$F|\Delta$} values are subsequently integrated over various offsets Δ values, using eq. (2.2), to assess the corresponding Q value. The assessed Q values are given in the captions of Tables 4-6, and are collected in Table 3b.

Table 3b. Assessed Q values for cases A, B and C, under zero wind and face direction $\varphi = 0°$.

Case	Q
A	$0.031m^2$
B	$0.256m^2$
C	$0.849m^2$

The results in Table 3b show that at zero wind, the equipped airbag and parachute (case A) reduces $Q = A_{impact} \times$ P{$F|impact$} by a factor 8 relative to parachute only (case B), while the parachute alone reduces Q by another factor 3.3 relative to an unequipped RA3. Hence the combination parachute and airbag reduce ground TPR by a factor 25 relative to an unequipped RA3 delivery UAS.

Remark: The Q values in Table 3b in comparison to $A_{impact} \times$ P{$F|impact$} in Table 3a show: The dynamical simulation based estimate of $Q = 0.256$ m² for cases B and C, under zero wind, in Table 3b, corresponds quite well with the analytical model-based estimate of $Q = 0.30\ m^2$ in Table 3a. However, under a horizontal wind of $10\ m/s$, our estimated $Q = 0.858\ m^2$ is a factor 3 as high.

Comparison of $P(F|\Delta)$ results in Tables 4 and 5 show that the offset area of non-zero $P(F|\Delta)$ contributions is similar, and that the difference is largely due to reduce $P(F|\Delta)$ values in this area. Comparison of $P(F|\Delta)$ results in Tables 5 and 6 also show that the offset area of non-zero $P(F|\Delta)$ contributions is similar, and that the difference is largely due to reduce $P(F|\Delta)$ values in this area.

Table 4. $P(F|\Delta)$ (%), for case A, as a function of cross offset $\Delta_\neg$ and along offset $\Delta_\parallel$, under zero wind. Impact speed $|v| = 7.5 m/s$, descent angle $\psi = 90°$, face direction $\varphi = 0°$. Red line shows the boundary outside which the UAS does not touch human body. Integration, using eq. (2.2), yields $Q = 0.031 m^2$.

$\Delta_\parallel$ \ $\Delta_\neg$	0.00	0.05	0.10	0.15	0.20	0.25	0.30	0.35	0.40	0.45	0.50	0.55	0.60	0.65	0.70	0.75
0.70																
0.65						2.7	3.1	2.8								
0.60						3.0	4.2	3.7	0.0							
0.55						3.5	4.5	3.8	0.0							
0.50						3.9	4.6	3.9	0.0							
0.45	3.7	3.7	3.3	2.7	2.7	4.8	5.1	0.6								
0.40	4.6	4.7	4.1	3.6	3.9	5.9	5.7	3.8								
0.35	13.4	16.5	8.2	4.5	4.3	5.4	6.8	3.8								
0.30	20.7	10.8	20.9	55.8	5.1	5.5	21.7	3.6								
0.25	7.4	6.7	9.2	24.2	7.1	3.5	4.6	0.0								
0.20	6.4	5.7	5.8	21.8	16.9	3.2	4.4									
0.15	6.9	5.9	4.9	5.0	4.8	3.1	2.8									
0.10	6.0	5.6	4.8	4.0	3.5	3.0	3.0	6.4	4.6	4.3	3.6	3.2	3.0	2.9	0.0	
0.05	4.8	4.2	4.0	3.7	3.5	3.1	5.2	24.7	6.7	5.8	5.0	4.6	3.8	3.8	0.0	
0.00	5.3	4.7	4.2	3.8	3.6	3.2	4.6	40.8	10.8	7.5	5.4	4.4	3.6	3.7	0.2	
-0.05	5.0	4.7	4.3	4.0	3.6	3.3	3.3	5.3	5.9	4.4	4.2	4.0	3.4	3.3	0.0	
-0.10	4.9	4.7	4.3	5.3	3.8	3.3	3.0	3.9	0.0	2.8	0.0	0.0	0.0	0.0		
-0.15	4.7	4.5	5.1	6.2	9.0	3.2	2.9									
-0.20	5.6	5.8	6.9	8.4	21.1	3.1	2.9									
-0.25	30.5	28.4	15.6	45.4	4.8	3.4	3.5									
-0.30	18.1	26.0	10.8	4.7	4.0	5.9	9.0									
-0.35	4.5	4.5	4.3	4.7	5.5	18.5	4.3									
-0.40	4.6	4.4	4.5	4.0	4.5	6.8	4.2									
-0.45						3.9	4.4	4.2	3.0							
-0.50						4.1	3.6	3.6	0.0							
-0.55						3.5	4.0	3.5	0.0							
-0.60						2.7	3.4	3.1	0.0							
-0.65						0.0										
-0.70																

Table 5. $P(F|\Delta)$ (%), under zero wind velocity for case B, as a function of cross offset $\Delta_\neg$ and along offset $\Delta_\parallel$. Impact speed $|v| = 7.5m/s$, descent angle $\psi = 90°$, face direction $\varphi = 0°$. Red line shows the boundary outside which the UAS does not touch human body. Integration yields $Q = 0.256m^2$.

Along offset $\Delta_\parallel$ (m) \ Cross offset $\Delta_\neg$ (m)	0.00	0.05	0.10	0.15	0.20	0.25	0.30	0.35	0.40	0.45	0.50	0.55	0.60	0.65	0.70	0.75
0.70																
0.65						2.7	3.1	2.8								
0.60						3.0	4.2	3.7	0.0							
0.55						3.5	4.5	3.8	0.0							
0.50						3.9	4.6	3.9	0.0							
0.45					2.8	4.9	5.3	0.7								
0.40	5.2	5.2	5.1		4.1	6.3	6.0	3.8								
0.35	32.5	37.8	38.8	5.1	7.6	10.7	7.7	3.9								
0.30	78.5	94.1	91.8	43.1	5.5	85.9	35.7	3.8								
0.25	75.3	97.0	83.7	93.1	78.3	54.4	70.8	0.0								
0.20	73.4	97.8	98.9	100.0	93.4	14.3	32.0									
0.15	19.5	54.9	100.0	91.6	66.1	5.2	4.5									
0.10	43.3	39.8	27.2	52.5	81.5	6.8	63.3	19.6	4.8	4.3	3.7	3.2	3.0	2.9	0.0	
0.05	58.3	52.8	42.2	34.7	94.3	9.6	90.4	73.8	7.8	6.2	5.2	4.6	3.8	3.8	0.0	
0.00	63.7	58.0	46.1	37.6	94.3	10.7	89.1	88.9	15.1	8.9	5.8	4.4	3.6	3.7	0.2	
-0.05	54.1	50.3	40.1	29.3	89.8	8.8	97.6	61.7	6.7	4.5	4.2	4.0	3.4	3.3	0.0	
-0.10	37.3	34.4	46.7	61.7	52.0	8.7	36.1	3.7	0.0	2.9	0.0	0.0	0.0	0.0		
-0.15	32.0	64.6	97.3	100.0	60.8	37.2										
-0.20	60.2	87.7	80.0	100.0	91.0	6.7	2.9									
-0.25	81.5	99.1	98.0	62.5	46.2	79.5	4.6									
-0.30	57.0	87.4	89.7	15.4	16.5	81.3	9.9									
-0.35	10.7	10.2	32.7	15.9	85.6	23.3	4.3									
-0.40	10.1	8.9	5.2	3.9	4.7	6.9	4.3									
-0.45					3.9	4.4	4.3	3.0								
-0.50						4.1	3.7	3.7	0.0							
-0.55						3.5	4.0	3.5	0.0							
-0.60						2.7	3.4	3.1	0.0							
-0.65						0.0										
-0.70																

Table 6. $P(F|\Delta)$ (%) , under zero wind for case C, as a function of cross offset $\Delta_\neg$ and along offset $\Delta_\parallel$. Impact speed $|v| = 40.6m/s$, descent angle $\psi = 90°$, face direction $\varphi = 0°$. Red line shows the boundary outside which the UAS does not touch human body. Integration yields $Q = 0.849m^2$.

Along offset $\Delta_\parallel$ (m) \ Cross offset $\Delta_\neg$ (m)	0.00	0.05	0.10	0.15	0.20	0.25	0.30	0.35	0.40	0.45	0.50	0.55	0.60	0.65	0.70	0.75
0.70																
0.65						12.7	100	100								
0.60						100	100	100	1.0							
0.55						100	100	100	8.6							
0.50				0		100	100	100	0							
0.45				0		100	100	100								
0.40	100	100	100		100	100	100	100								
0.35	100	100	100	100	100	100	100	100								
0.30	100	100	100	100	100	100	100	93.9								
0.25	100	100	100	100	100	100	100	0								
0.20	100	100	100	100	100	100	100									
0.15	100	100	100	100	100	100	100									
0.10	100	100	100	100	100	100	100	100	100	100	100	100	100	100	0	
0.05	100	100	100	100	100	100	100	100	100	100	100	100	100	100	100	
0.00	100	100	100	100	100	100	100	100	100	100	100	100	100	100	100	
-0.05	100	100	100	100	100	100	100	100	100	100	100	100	100	100	85.9	
-0.10	100	100	100	100	100	100	100	26.1	81.2	43.0	0	0	0	0.7		
-0.15	100	100	100	100	100	100										
-0.20	100	100	100	100	100	100	0.4									
-0.25	100	100	100	100	100	100	100									
-0.30	100	100	100	100	100	100	100									
-0.35	100	100	100	100	100	100	100									
-0.40	100	100	100	29.4	100	100	100									
-0.45						100	100	100	100							
-0.50						100	100	100	1.0							
-0.55						100	100	100	3.0							
-0.60						100	100	100	0							
-0.65						1.3										
-0.70																

5.4.4 Dynamical simulation of Q under horizontal wind

For each of the three case A-C, dynamical simulations are conducted, under non-zero wind conditions, to assess $P(F|\Delta)$ values for various offsets Δ for human impact, and human face direction $\varphi = 0°$. As identified in subsection 5.4.1, the descend phase for case A is the same as it is for case B; which implies similarity in initial conditions of the dynamical simulation of the UAS impact with human. The key difference, between cases A and B, is the effect of the airbag during the human impact simulation. For case A the airbag is placed on bottom of UAS with standard atmospheric inner pressure, i.e. 101325 Pa. Figure 8a,b depict the effect of the airbag during hitting of the human under 0 m/s and 10 /s horizontal wind, both for zero offset.
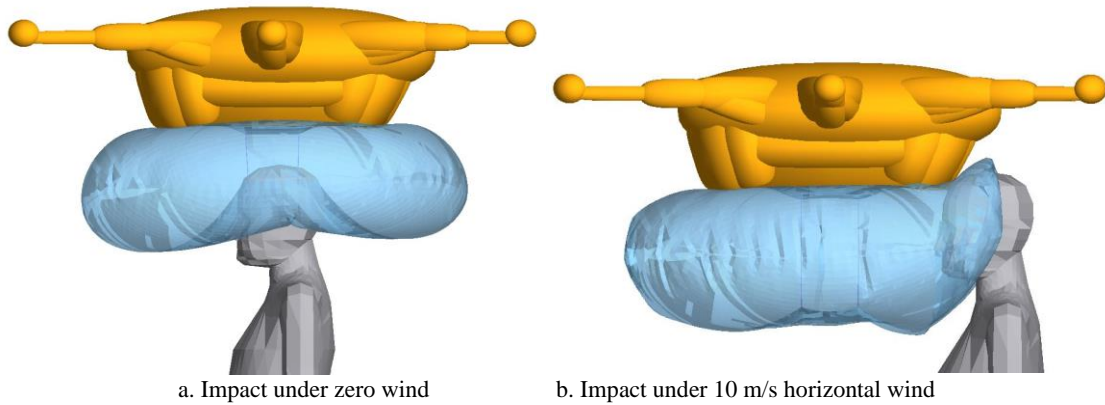
a. Impact under zero wind   b. Impact under 10 m/s horizontal wind
Figure 8. Case A impact at zero offset, i.e. $\Delta = (0,0)$

Dynamical simulations, using the MBS or FE/MBS models, have been conducted to evaluate $P(F|\Delta)$ for various offset values; these results are presented in Tables 7, 8 and 9 for 10 m/s horizontal wind. The obtained $P(F|\Delta)$ values are subsequently integrated over various offsets Δ values, using eq. (2.2); the resulting Q values are given in the captions of Tables 7, 8 and 9.

Subsequently, these MBS or FE/MBS model simulations have been repeated for horizontal wind of 2, 4, 6 and 8 m/s. The resulting Q values are depicted in Figure 9 as for cases A, B and C as a function of horizontal wind speed.

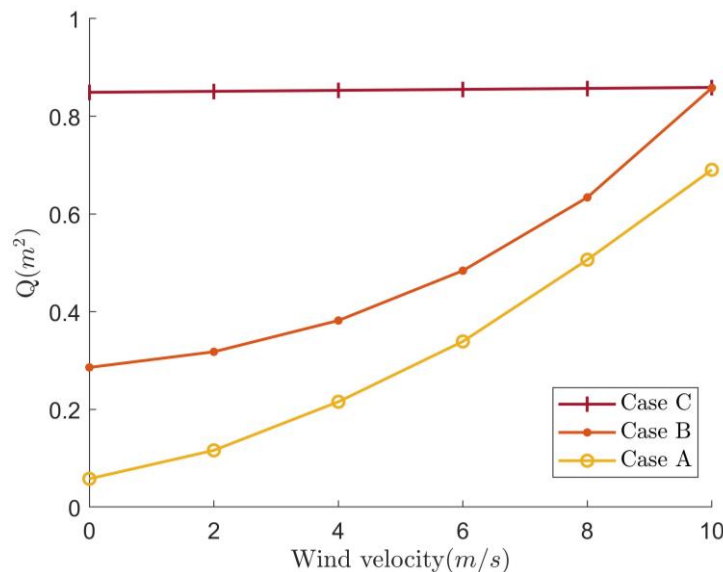**Figure 9**. Q for case A (parachute and airbag), case B (parachute, no airbag), and case C (no parachute, no airbag) as a function of horizontal wind velocity, for face direction $\varphi = 0°$.

The curve for case C in Figure 9 shows that horizontal wind up to 10 m/s has no effect on Q. In line with this, the $P(F|\Delta)$ results for case C in Tables 6 and 9 are almost the same. This similarity does not apply to cases A and B. The curve for cases A and B show that the protecting effects of parachute and bottom airbag systematically decrease if the horizontal wind speed increases. At a horizontal wind speed of 10 m/s the reduction of Q by the parachute is almost gone, while the reduction of Q by the parachute and airbag is marginalized to 20% only.

Table 7. $P(F|\Delta)$ (%) , for case A, as a function of cross offset $\Delta_\neg$ and along offset $\Delta_\parallel$, under $10m/s$ horizontal wind. Impact speed $|v| = 12.5m/s$, descent angle $\psi = 37°$, face direction $\varphi = 0°$. Red line shows boundary outside which the UAS does not touch human body. Integration yields $Q = 0.677m^2$.

$\Delta_\parallel$ \ $\Delta_\neg$	0	0.05	0.1	0.15	0.2	0.25	0.3	0.35	0.4	0.45	0.5	0.55	0.6	0.65	0.7	0.75	0.8
0.75																	
0.7							3.3	2.7									
0.65	0.0	0.0				4.5	14.2	4.6									
0.6	0.0	0.0	0.0	0.0		0.0	1.1	1.5	0.0								
0.55	0.0	0.0	0.0	0.0	0.0	0.0	0.0	1.1	0.0								
0.5	0.0	0.0	0.0	0.0	0.0	0.0	0.0	1.2	0.0								
0.45	0.0	0.0	0.0	0.0	0.0	0.0	0.0	1.1	0.0								
0.4	0.0	1	1	1	0.0	0.0	0.0	1.8									
0.35	1	4	21	19.2	1.4	0.0	0.0	1.6									
0.3	13	9	80	50.1	21	0.6	0.0	1.2									
0.25	100	100	97	96.4	58	1.3	0.0	0.2									
0.2	100	100	62	100	10.4	5.6	13.3	0.0									
0.15	91	81	100	100	88.2	16.3	100	99	9.9	2.3	4.7	4.2	3.8	3.4			
0.1	100	100	100	100	100	48.8	100	100	49.5	38.8	5.8	4.5	4.4	4.0	2.9		
0.05	100	100	100	100	100	1	100	100	89.7	51.8	11.9	6.1	4.4	4.1	3.7		
0	100	100	100	100	100	46	100	100	97.8	66.3	16.4	6.1	4.8	4.2	1.1		
-0.05	100	100	100	100	100	100	100	100	97.5	68.4	16.2	7.5	4.9	4.3	1.1		
-0.1	100	100	100	100	100	100	100	100	89.3	46.1	11.9	5.0	4.2	1.4	0.8		
-0.15	100	100	100	100	100	100	100	100	83.1	44.4	3.9	3.8	1.0	1.0			
-0.2	100	100	100	100	100	100	12.4										
-0.25	100	100	100	100	100	60.0	7.4										
-0.3	100	100	100	100	88.0	85.5	60.7										
-0.35	100	100	100	100	93.8	100	9.8										
-0.4	100	100	100	100	100	30.2	5.2	3.0									
-0.45	100	100	100	100	100	4.9	19.4	17.6									
-0.5	100	100	100	100	76.7	20.8	95.3	100	2.9								
-0.55	88.4	84.3	24.0	24.1	90.8	58.6	100	100	19.5								
-0.6	2.7	16.0	18.0	11.0	49.6	88.6	100	100	40.5			0.0	0.0	0.0	0.0		
-0.65	11.1	15.8	15.7	21.5	7.6	89.7	100	100	93.4	0.0	0.0	0.0	0.0	0.0	0.0	0.0	
-0.7	14.4	15.3	13.0	18.8	18.3	100	100	100	27.6	0.0	0.0	0.0	0.0	0.0	0.0	0.0	
-0.75	15.0	20.1	15.3	17.8	26.7	73.7	100	100	0.0	0.0	0.0	0.0	0.0	0.0	0.0	0.0	
-0.8	12.6	13.0	8.0	3.2	8.1	12.4	97.0	59.8	0.0	0.0	0.0	0.0	0.0	0.0	0.0	0.0	
-0.85	9.0	8.1	3.0	2.1	5.7	3.3	7.9	2.0	0.0	0.0	0.0	0.0	0.0	0.0	0.0	0.0	
-0.9	6.9	5.4	2.4	0.0	5.4	1.0	1.1	0.8	0.0	0.0	0.0	0.0	0.0	0.0	0.0	0.0	
-0.95	4.0	3.3	1.7	0.0	0.8	0.9	1.8	1.5	1.8	0.7	0.0	0.0	0.0	0.0	0.0	0.0	
-1	3.6	2.4	1.1	0.0	0.0	1.1	3.6	3.8	3.9	1.1	0.0	0.0	0.0	0.0	0.0	0.0	
-1.05	7.1	4.4	1.9	0.0	1.1	2.3	6.4	6.6	5.8	1.9	0.0	0.0	0.0	0.0	0.0	0.0	
-1.1	7.6	5.0	1.1	0.0	1.0	3.4	7.7	9.5	9.7	3.4	0.8		0.0	0.0	0.0	0.0	
-1.15	6.9	3.0	1.6	0.0	0.7	1.6	6.6	5.0	6.3	0.9			0.0	0.0			
-1.2	10.4	4.4	2.5	0.8	0.0	0.9	2.7	3.8	3.2	1.4							
-1.25	5.4	3.8	1.9	0.8	0.0	0.8	2.4	2.9	2.6	1.0							
-1.3	1.5	1.3	0.9	1.1	0.0	0.8	2.5	3.6	2.1	0.9							
-1.35	1.9	1.6	1.1	2.1	0.8	1.1	2.9	3.4	3.4	3.6							
-1.4	2.7	1.6	0.0	0.0	2.5	4.6	6.6	8.4	6.8	3.2							
-1.45			0.0	0.0	0.8	1.1	3.8	3.9	4.5	2.8							
-1.5				0.7	3.7	1.9	4.3	4.2	5.4	12.8							
-1.55					0.8	1.9	2.8	3.4	1.3	0.0							
-1.6																	

Comparison of Table 7 to the results in Table 8 learns that the airbag reduces the Q value by less than a factor 1.3 only. The explanation for this low factor is that, due to the low descent angle of $\psi = 37°$, the airbag only works for part of the offset locations. The $P(F|\Delta)$ values for along offset values between $\Delta_\parallel = 0.35 - 0.65m$ are largely decreased. However for the other offset values, the effect of airbag is negligible.

Table 8. $P(F|\Delta)$ (%), under horizontal wind velocity $10m/s$ for case B, as a function of cross offset $\Delta_\neg$ and along offset $\Delta_\parallel$. Impact speed $|v| = 12.5m/s$, descent angle $\psi = 37°$, face direction $\varphi = 0°$. Red line shows boundary outside which UAS does not touch human body. Integration yields $Q = 0.858m^2$.

$\Delta_\parallel$ (m)	Cross offset $\Delta_\neg$ (m)																
	0	0.05	0.1	0.15	0.2	0.25	0.3	0.35	0.4	0.45	0.5	0.55	0.6	0.65	0.7	0.75	0.8
0.75																	
0.7							3.3	2.7									
0.65	20.5	8.4				4.5	14.2	4.6									
0.6	100	100	100	53.5		4.4	6.8	26.8	0.0								
0.55	100	100	100	100	3.6	5.5	18.6	4.6	0.0								
0.5	100	100	100	100	86.9	19.6	13.4	4.7	0.0								
0.45	100	100	100	100	97.9	53.3	38.5	4.2	3.6								
0.4	100	100	100	100	100	22.5	84.7	5.4									
0.35	100	100	100	60.7	99.4	21.3	100	5.0									
0.3	100	100	100	70.3	100	5.8	100	3.9									
0.25	100	100	100	52.1	100	12.5	100	5.2									
0.2	100	100	100	100	14.1	25.8	62.7	3.0									
0.15	100	100	100	100	90.1	36.3	100	100	14.8	6.3	4.7	4.2	3.8	3.4			
0.1	100	100	100	100	100	70.7	100	100	54.2	25.2	5.8	4.5	4.4	4.0	2.9		
0.05	100	100	100	100	100	100	100	100	91.9	55.0	11.9	6.1	4.4	4.1	3.7		
0	100	100	100	100	100	100	100	100	98.7	69.0	16.4	6.1	4.8	4.2	1.1		
-0.05	100	100	100	100	100	100	100	100	98.5	70.7	16.2	7.5	4.9	4.3	1.1		
-0.1	100	100	100	100	100	100	100	100	89.3	46.1	11.9	5.0	4.2	1.4	0.8		
-0.15	100	100	100	100	100	100	100	100	83.1	44.4	3.9	3.8	1.0	1.0			
-0.2	100	100	100	100	100	100	12.4										
-0.25	100	100	100	100	100	60.0	7.4										
-0.3	100	100	100	100	88.0	85.5	60.7										
-0.35	100	100	100	100	93.8	100	9.8										
-0.4	100	100	100	100	100	30.2	5.2	3.0									
-0.45	100	100	100	100	100	4.9	19.4	17.6									
-0.5	100	100	100	100	76.7	20.8	95.3	100	2.9								
-0.55	88.4	84.3	24.0	24.1	90.8	58.6	100	100	19.5								
-0.6	2.7	16.0	18.0	11.0	49.6	88.6	100	100	40.5			0.0	0.0	0.0	0.0		
-0.65	11.1	15.8	15.7	21.5	7.6	89.7	100	100	93.4	0.0	0.0	0.0	0.0	0.0	0.0	0.0	
-0.7	14.4	15.3	13.0	18.8	18.3	100	100	100	27.6	0.0	0.0	0.0	0.0	0.0	0.0	0.0	
-0.75	15.0	20.1	15.3	17.8	26.7	73.7	100	100	0.0	0.0	0.0	0.0	0.0	0.0	0.0	0.0	
-0.8	12.6	13.0	8.0	3.2	8.1	12.4	97.0	59.8	0.0	0.0	0.0	0.0	0.0	0.0	0.0	0.0	
-0.85	9.0	8.1	3.0	2.1	5.7	3.3	7.9	2.0	0.0	0.0	0.0	0.0	0.0	0.0	0.0	0.0	
-0.9	6.9	5.4	2.4	0.0	5.4	1.0	1.1	0.8	0.0	0.0	0.0	0.0	0.0	0.0	0.0	0.0	
-0.95	4.0	3.3	1.7	0.0	0.8	0.9	1.8	1.5	1.8	0.7	0.0	0.0	0.0	0.0	0.0	0.0	
-1	3.6	2.4	1.1	0.0	0.0	1.1	3.6	3.8	3.9	1.1	0.0	0.0	0.0	0.0	0.0	0.0	
-1.05	7.1	4.4	1.9	0.0	1.1	2.3	6.4	6.6	5.8	1.9	0.0	0.0	0.0	0.0	0.0	0.0	
-1.1	7.6	5.0	1.1	0.0	1.0	3.4	7.7	9.5	9.7	3.4	0.8		0.0	0.0	0.0		
-1.15	6.9	3.0	1.6	0.0	0.7	1.6	6.6	5.0	6.3	0.9			0.0	0.0			
-1.2	10.4	4.4	2.5	0.8	0.0	0.9	2.7	3.8	3.2	1.4							
-1.25	5.4	3.8	1.9	0.8	0.0	0.8	2.4	2.9	2.6	1.0							
-1.3	1.5	1.3	0.9	1.1	0.0	0.8	2.5	3.6	2.1	0.9							
-1.35	1.9	1.6	1.1	2.1	0.8	1.1	2.9	3.4	3.4	3.6							
-1.4	2.7	1.6	0.0	0.0	2.5	4.6	6.6	8.4	6.8	3.2							
-1.45			0.0	0.0	0.8	1.1	3.8	3.9	4.5	2.8							
-1.5				0.7	3.7	1.9	4.3	4.2	5.4	12.8							
-1.55					0.8	1.9	2.8	3.4	1.3	0.0							
-1.6																	

In Table 8, the integrated $Q = 0.858m^2$ is 3.3 times higher than the $0.256m^2$ in Table 5. The explanation for this to happen is that the horizontal wind of 10 m/s has two risk increasing effects: i) it increases the impact velocity ($12.5m/s$ compared to $7.5m/s$); and ii) it lowers the descent angle ($37°$ compared to $90°$). In Table 8, the larger impact velocity results in higher probability of fatality for different impact locations, whereas the lower descent angle of $37°$ results in larger impact area for human head and now also includes human thorax and abdomen.

The results in Tables 5 and 8 show that horizontal wind speed plays a significant role on the ground risk posed by case B, i.e. UAS RA3 descends with parachute deployed. To make this more specific, additional MBS simulations have been conducted for horizontal wind velocities ranging from 0 to $10m/s$, and the obtained $P(F|\Delta)$ values have been integrated to Q. The obtained results are shown in Figure 10.

Table 9. $P(F|\Delta)$ (%), under 10 m/s horizontal wind for case C, as a function of cross offset $\Delta_\neg$ and along offset $\Delta_\parallel$. Impact speed $|v| = 40.4 m/s$, descent angle $\psi = 84.7°$, face direction $\varphi = 0°$. Red line shows boundary outside which UAS does not touch human body. Integration yields $Q = 0.859 m^2$.

Along offset $\Delta_\parallel$ (m)	Cross offset $\Delta_\neg$ (m)															
	0.00	0.05	0.10	0.15	0.20	0.25	0.30	0.35	0.40	0.45	0.50	0.55	0.60	0.65	0.70	0.75
0.70																
0.65						10.7	100	98.3								
0.60						100	100	100	3.3							
0.55						100	100	100	6.9							
0.50						100	100	100	3.5							
0.45					2.8	100	100	100								
0.40	100	100	100		100	100	100	100								
0.35	100	100	100	100	100	100	100	100								
0.30	100	100	100	100	100	100	100	98.9								
0.25	100	100	100	100	100	100	100	3.4								
0.20	100	100	100	100	100	100	100									
0.15	100	100	100	100	100	100	100									
0.10	100	100	100	100	100	100	100		100	100	100	100	100	100		
0.05	100	100	100	100	100	100	100	100	100	100	100	100	100	100	100	
0.00	100	100	100	100	100	100	100	100	100	100	100	100	100	100	100	
-0.05	100	100	100	100	100	100	100	100	100	100	100	100	100	100	89.7	
-0.10	100	100	100	100	100	100	100	100	100	100	9.9	8.1	3.5	3.8		
-0.15	100	100	100	100	100	100										
-0.20	100	100	100	100	100	100	3.0									
-0.25	100	100	100	100	100	100	100									
-0.30	100	100	100	100	100	100	100									
-0.35	100	100	100	100	100	100	100									
-0.40	100	100	100	53.8	100	100	100									
-0.45						100	100	100								
-0.50						100	100	100	4.1							
-0.55						100	100	100	13.1							
-0.60						100	100	100								
-0.65							4.4	5.0								
-0.70																
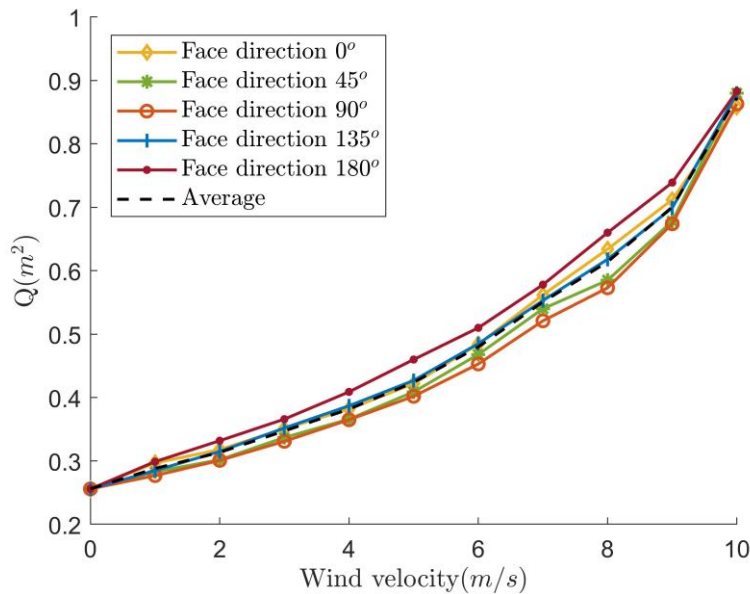
Figure 10. Q , for case B, as a function of horizontal wind velocity, for face direction $\varphi \in \{0°, 45°, 90°, 135°, 180°\}$, where $\varphi = 0°$ stands for face in the wind.

The results in Figure 10 show that risk value increases as wind velocity increases, while the effect of human face direction φ is quite limited. The Q values range from $0.256 m^2$ under zero wind, up to $0.874 m^2$ under 10 m/s wind.

Comparison of the Q results obtained for case B to those obtained for case C, shows that under $10 m/s$ horizontal wind, the obtained Q values are the same; i.e. $Q = 0.858 m^2$ in Table

8 versus $Q = 0.859 m^2$ in Table 9. However, under zero wind, the parachute reduces Q by a factor 3.3.

5.4.5 Dynamical simulation of airbag modifications

In this subsection we evaluate the effect of the following three airbag cases, in combination with a deployed parachute:

A. Bottom airbag at 1 atmosphere pressure, i.e. equal to environment;

A1. Bottom airbag at 1.1 atmosphere pressure;

A2. Bottom airbag and front airbag, both at 1.1 atmosphere pressure.

The change from case A to case A1 is accomplished by changing the atmospheric pressure setting parameter in the FE airbag model in MADYMO. The change from case A1 to case A2 involves the inclusion of a front airbag in the FE/MBS model. To accomplish this, the front airbag is assumed to be of similar design as the bottom airbag; this made it possible to also use the FE airbag model in MADYMO for the front airbag. Furthermore, we assume that under influence of wind, the front airbag captures more wind as a result of which the front of the RA3 UAS will reach human body first. For cases A1,A2, the initial hitting of the airbag(s) under 10 m/s horizontal wind are depicted in Figure 11a,b.

a. with bottom 1.1x atm airbag   b. with bottom and front 1.1x atm airbag
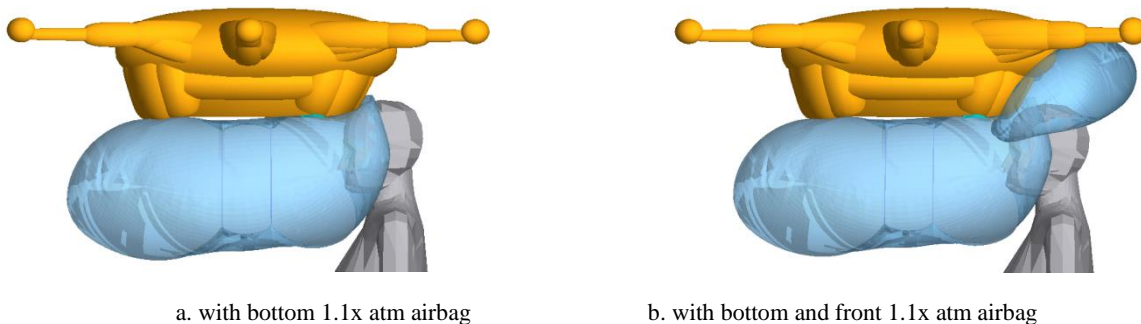
Figure 11. Case A impact at zero offset, i.e. $\Delta = (0,0)$ with 10m/s horizontal wind

For cases A1 and A2, dynamical simulations have been conducted to assess $P(F|\Delta)$ values for horizontal wind ranging from 0 m/s to 10 m/s; this is shown in Tables 10 and 11.

Table 10. $P(F|\Delta)$ (%) , for case A2 (1.1x atmosphere in bottom and side airbag), as a function of cross offset $\Delta_\neg$ and along offset $\Delta_\parallel$, under $10m/s$ horizontal wind. Impact velocity $|v| = 12.5m/s$, descent angle $\psi = 37°$, face direction $\varphi = 0°$. Red line shows the boundary outside which the UAS does not touch human body. Integration, using eq. (2.2), yields $Q = 0.452m^2$.

Along \ Cross	0.00	0.05	0.10	0.15	0.20	0.25	0.30	0.35	0.40	0.45	0.50	0.55	0.60	0.65	0.70	0.75	0.80
0.75																	
0.70							3.3	2.7									
0.65	7.8	7.3				3.8	3.6	0.0									
0.60	6.5	6.4	6.4	5.3			3.6	3.4	2.7	0.0							
0.55	5.4	5.4	5.6	4.7	3.9	3.3	3.1	2.7	0.0								
0.50	4.4	5.9	5.0	4.6	4.0	3.0	2.9	2.8	0.0								
0.45	4.4	4.4	4.3	4.2	3.8	3.2	3.0	2.8	0.0								
0.40	4.7	4.7	4.6	4.3	3.8	3.3	3.0	2.8									
0.35	5.2	5.0	4.9	4.5	4.0	3.5	3.1	2.8									
0.30	6.8	7.0	6.9	5.2	4.1	3.6	3.1	2.8									
0.25	10.1	13.0	9.2	13.9	4.0	3.6	3.1	2.8									
0.20	11.6	16.8	83.1	71.8	4.8	3.5	3.3	5.7									
0.15	10.5	10.9	100	100	91.7	3.4	19.8	89.3	9.9	2.3	4.7	4.2	3.8	3.4			
0.10	35.8	47.3	100	100	100	4.0	100	100	49.5	38.8	5.8	4.5	4.4	4.0	2.9		
0.05	100	100	100	100	100	6.2	100	100	89.7	51.8	11.9	6.1	4.4	4.1	3.7		
0.00	100	100	100	100	100	11.4	100	100	97.8	66.3	16.4	6.1	4.8	4.2	1.1		
-0.05	32.2	84.8	86.7	100	100	99.7	100	100	97.5	68.4	16.2	7.5	4.9	4.3	1.1		
-0.10	5.6	9.8	8.8	9.9	31.9	91.9	100	100	89.3	46.1	11.9	5.0	4.2	1.4	0.8		
-0.15	6.7	13.9	10.3	6.5	6.8	21.4	12.2	51.8	83.1	44.4	3.9	3.8	1.0	1.0			
-0.20	9.5	13.1	6.9	5.0	50.8	54.7	9.1	12.4									
-0.25	9.8	8.2	5.7	5.3	68.3	41.4	7.4										
-0.30	7.1	6.4	5.4	70.1	66.8	85.5	60.7										
-0.35	5.9	5.6	5.0	78.0	86.4	100	9.8										
-0.40	5.3	5.1	4.8	32.6	100	30.2	5.2	3.0									
-0.45	4.7	4.8	4.5	4.6	100	4.9	19.4	17.6									
-0.50	4.3	4.3	3.9	3.9	76.7	14.5	95.3	100	2.9								
-0.55	4.0	3.9	3.6	3.4	76.3	58.4	100	100	19.5								
-0.60	2.7	3.6	3.3	3.2	34.0	88.6	100	100	40.5			0.0	0.0	0.0	0.0		
-0.65	11.1	15.8	15.7	21.5	7.6	89.7	100	100	93.4	0.0	0.0	0.0	0.0	0.0	0.0	0.0	
-0.70	14.4	15.3	13.0	18.8	18.3	100	100	100	27.6	0.0	0.0	0.0	0.0	0.0	0.0	0.0	
-0.75	15.0	20.1	15.3	17.8	26.7	73.7	100	100	0.0	0.0	0.0	0.0	0.0	0.0	0.0	0.0	
-0.80	12.6	13.0	8.0	3.2	8.1	12.4	97.0	59.8	0.0	0.0	0.0	0.0	0.0	0.0	0.0	0.0	
-0.85	9.0	8.1	3.0	2.1	5.7	3.3	7.9	2.0	0.0	0.0	0.0	0.0	0.0	0.0	0.0	0.0	
-0.90	6.9	5.4	2.4	0.0	5.4	1.0	1.1	0.8	0.0	0.0	0.0	0.0	0.0	0.0	0.0	0.0	
-0.95	4.0	3.3	1.7	0.0	0.8	0.9	1.8	1.5	1.8	0.7	0.0	0.0	0.0	0.0	0.0	0.0	
-1.00	3.6	2.4	1.1	0.0	0.0	1.1	3.6	3.8	3.9	1.1	0.0	0.0	0.0	0.0	0.0	0.0	
-1.05	7.1	4.4	1.9	0.0	1.1	2.3	6.4	6.6	5.8	1.9	0.0	0.0	0.0	0.0	0.0	0.0	
-1.10	7.6	5.0	1.1	0.0	1.0	3.4	7.7	9.5	9.7	3.4	0.8		0.0	0.0	0.0	0.0	
-1.15	6.9	3.0	1.6	0.0	0.7	1.6	6.6	5.0	6.3	0.9			0.0	0.0			
-1.20	10.4	4.4	2.5	0.8	0.0	0.9	2.7	3.8	3.2	1.4							
-1.25	5.4	3.8	1.9	0.8	0.0	0.8	2.4	2.9	2.6	1.0							
-1.30	1.5	1.3	0.9	1.1	0.0	0.8	2.5	3.6	2.1	0.9							
-1.35	1.9	1.6	1.1	2.1	0.8	1.1	2.9	3.4	3.4	3.6							
-1.40	2.7	1.6	0.0	0.0	2.5	4.6	6.6	8.4	6.8	3.2							
-1.45			0.0	0.0	0.8	1.1	3.8	3.9	4.5	2.8							
-1.50				0.7	3.7	1.9	4.3	4.2	5.4	12.8							
-1.55					0.8	1.9	2.8	3.4	1.3	0.0							
-1.60																	

Cross offset $\Delta_\neg$ (m) — Along offset $\Delta_\parallel$ (m)

Table 11. $P(F|\Delta)$ (%) , for case A1 (1.1x atmosphere in bottom airbag), as a function of cross offset $\Delta_\neg$ and along offset $\Delta_\parallel$, under $10m/s$ horizontal wind. Impact velocity $|v| = 12.5m/s$, descent angle $\psi = 37°$, face direction $\varphi = 0°$. Red line shows the boundary outside which the UAS does not touch human body. Integration, using eq. (2.2), yields $Q = 0.638m^2$.

Along offset $\Delta_\parallel$ (m)	Cross offset $\Delta_\neg$ (m) 0.00	0.05	0.10	0.15	0.20	0.25	0.30	0.35	0.40	0.45	0.50	0.55	0.60	0.65	0.70	0.75	0.80
0.75																	
0.70							3.3	2.7									
0.65	7.8	7.3	6.2	5.2	4.3	3.8	3.6	0.0									
0.60	6.5	6.4	6.4	5.3	4.1	3.6	3.4	2.7	0.0								
0.55	5.4	5.4	5.6	4.7	3.9	3.3	3.1	2.7	0.0								
0.50	4.4	5.9	5.0	4.6	4.0	3.0	2.9	2.8	0.0								
0.45	4.4	4.4	4.3	4.2	3.8	3.2	3.0	2.8	0.0								
0.40	4.7	4.7	4.6	4.3	3.8	3.3	3.0	2.8									
0.35	5.2	5.0	4.9	4.5	4.0	3.5	3.1	2.8									
0.30	6.8	7.0	6.9	5.2	4.1	3.6	3.1	2.8									
0.25	10.1	13.0	9.2	13.9	4.0	3.6	3.1	2.8									
0.20	11.6	16.8	83.1	71.8	4.8	3.5	3.3	5.7									
0.15	100	100	100	100	91.7	3.4	19.8	89.3	9.9	2.3	4.7	4.2	3.8	3.4			
0.10	100	100	100	100	100	4.0	100	100	49.5	38.8	5.8	4.5	4.4	4.0	2.9		
0.05	100	100	100	100	100	6.2	100	100	89.7	51.8	11.9	6.1	4.4	4.1	3.7		
0.00	100	100	100	100	100	11.4	100	100	97.8	66.3	16.4	6.1	4.8	4.2	1.1		
-0.05	100	100	100	100	100	100	100	100	97.5	68.4	16.2	7.5	4.9	4.3	1.1		
-0.10	100	100	100	100	100	100	100	100	89.3	46.1	11.9	5.0	4.2	1.4	0.8		
-0.15	100	100	100	100	100	100	12.2	51.8	83.1	44.4	3.9	3.8	1.0	1.0			
-0.20	100	100	100	100	100	89.5	9.1	12.4									
-0.25	100	100	100	100	100	60.0	7.4										
-0.30	100	100	100	100	88.0	85.5	60.7										
-0.35	100	100	100	100	93.8	100	9.8										
-0.40	100	100	100	100	100	30.2	5.2	3.0									
-0.45	100	100	100	100	100	4.9	19.4	17.6									
-0.50	100	100	100	100	76.7	20.8	95.3	100	2.9								
-0.55	88.4	84.3	24.0	24.1	90.8	58.6	100	100	19.5								
-0.60	2.7	16.0	18.0	11.0	49.6	88.6	100	100	40.5			0.0	0.0	0.0	0.0		
-0.65	11.1	15.8	15.7	21.5	7.6	89.7	100	100	93.4	0.0	0.0	0.0	0.0	0.0	0.0	0.0	
-0.70	14.4	15.3	13.0	18.8	18.3	100.0	100	100	27.6	0.0	0.0	0.0	0.0	0.0	0.0	0.0	
-0.75	15.0	20.1	15.3	17.8	26.7	73.7	100	100	0.0	0.0	0.0	0.0	0.0	0.0	0.0	0.0	
-0.80	12.6	13.0	8.0	3.2	8.1	12.4	97.0	59.8	0.0	0.0	0.0	0.0	0.0	0.0	0.0	0.0	
-0.85	9.0	8.1	3.0	2.1	5.7	3.3	7.9	2.0	0.0	0.0	0.0	0.0	0.0	0.0	0.0	0.0	
-0.90	6.9	5.4	2.4	0.0	5.4	1.0	1.1	0.8	0.0	0.0	0.0	0.0	0.0	0.0	0.0	0.0	
-0.95	4.0	3.3	1.7	0.0	0.8	0.9	1.8	1.5	1.8	0.7	0.0	0.0	0.0	0.0	0.0	0.0	
-1.00	3.6	2.4	1.1	0.0	0.0	1.1	3.6	3.8	3.9	1.1	0.0	0.0	0.0	0.0	0.0	0.0	
-1.05	7.1	4.4	1.9	0.0	1.1	2.3	6.4	6.6	5.8	1.9	0.0	0.0	0.0	0.0	0.0	0.0	
-1.10	7.6	5.0	1.1	0.0	1.0	3.4	7.7	9.5	9.7	3.4	0.8		0.0	0.0	0.0	0.0	
-1.15	6.9	3.0	1.6	0.0	0.7	1.6	6.6	5.0	6.3	0.9			0.0	0.0			
-1.20	10.4	4.4	2.5	0.8	0.0	0.9	2.7	3.8	3.2	1.4							
-1.25	5.4	3.8	1.9	0.8	0.0	0.8	2.4	2.9	2.6	1.0							
-1.30	1.5	1.3	0.9	1.1	0.0	0.8	2.5	3.6	2.1	0.9							
-1.35	1.9	1.6	1.1	2.1	0.8	1.1	2.9	3.4	3.4	3.6							
-1.40	2.7	1.6	0.0	0.0	2.5	4.6	6.6	8.4	6.8	3.2							
-1.45			0.0	0.0	0.8	1.1	3.8	3.9	4.5	2.8							
-1.50			0.7	3.7	1.9	4.3	4.2	5.4	12.8								
-1.55				0.8	1.9	2.8	3.4	1.3	0.0								
-1.60																	

The obtained $P(F|\Delta)$ values are subsequently integrated to Q. The results are shown in Figure 12 for cases A1 and A2, jointly with the curves obtained for cases A and B.

The comparison between case B (no airbag) and case A (1x atm bottom airbag) shows the effectiveness of bottom airbag under low wind conditions. However as wind increases, the effectiveness of airbag decreases rapidly. The increased risk stems from 2 types of impact: the non-central impact on the bottom airbag with offset; and the impact on the front of UAS that is not covered by airbag. The curve for case A1 shows that the increased risk can partly be mitigated by using a bottom airbag with 1.1 atmosphere pressure. This mitigation is not effective for possible collision of the front of the RA3 UAS with human body. The curve for case A2 shows that this risk is further mitigated by the additional front airbag at 1.1 atmosphere pressure.
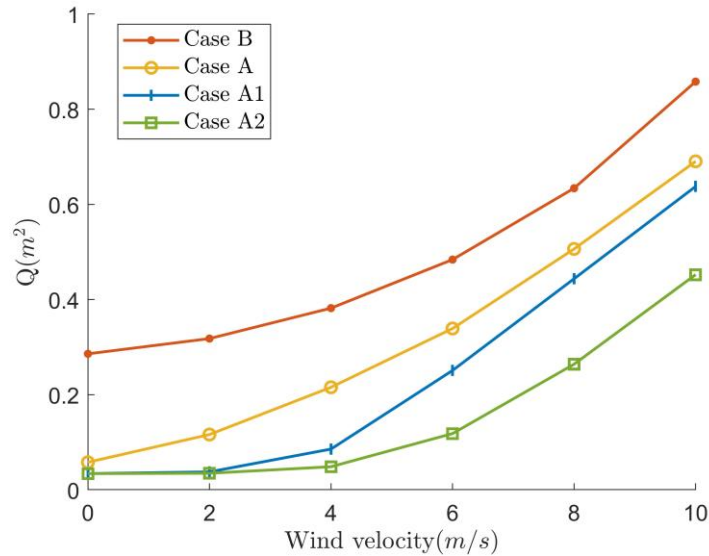
Figure 12. Q as a function of horizontal wind velocity, for case B (no airbag), case A (bottom airbag, 1x atm.), case A1 (bottom airbag, 1.1x atm.) and A2 (bottom and front airbags, 1.1 atm.)

Even for case A2, the risk still increase to a relative high level if wind velocity increases. The higher wind velocity leads to higher impact velocity and lower descent angle. The increased impact velocity results in higher risk for impact on drone arms that are not covered by airbag. The lower descent angle leads to non-vertical and non-central impacts on airbag that results in higher risk, as the airbag is not designed for such types of impact. This can be seen from the $P(F|\Delta)$ values in Table 10 for case A2 and 10m/s horizontal wind velocity. The high risk areas are for those drone arm impacts and non-central impacts on bottom and side airbags.

5.4.6 Discussion of results

Comparison of the Q assessment results in Tables 3a and 3b, using existing analytical models and the novel dynamical simulation approach respectively, showed two disadvantages of the existing analytical models: i) They fall short in evaluating the effect of an airbag; and ii) They leave a large range of uncertainty in the assessed Q value.

Table 12 collects the assessed Q values for cases C, B, A, A1, and A2 under zero and 10 m/s wind.

Table 12. Q for cases C, B, A, A1, and A2

Case	0 m/s wind	10 m/s wind
C	0.849 m^2	0.859 m^2
B	0.256 m^2	0.858 m^2
A	0.031 m^2	0.677 m^2
A1	0.026 m^2	0.638 m^2
A2	0.025 m^2	0.452 m^2

The Q results in Table 12 show that under zero wind, parachute deployment (case B) reduces Q by a factor 3.3. The additional use of a bottom airbag with a pressure of 1 atmosphere (case A) reduces Q by a complementary factor 8.2. By increasing the pressure of the bottom airbag to 1.1 atmosphere (case A1), there is a further reduction by 20%. Adding a front airbag (case A2) does not help under zero wind.

However, under horizontal wind of 10 m/s, the above positive effects of parachute and airbag reduce to a large extend, while without parachute (case C) the influence of 10 m/s horizontal wind is negligible. For parachute alone (case B), Q is hardly reduced. The

explanation is that although the parachute still significantly decreases impact velocity (from 40m/s to below 12.5m/s), under 10 m/s horizontal wind the parachute also reduces the descent angle to as low as 37 degrees, resulting in larger impact area on human head, thorax and abdomen. Because an airbag placed at the bottom of the UAS does not really protect for these impact geometry, the latter also explains why for case A (parachute and bottom airbag), Q is reduced by 21% only. Increasing the pressure of the bottom airbag by a factor 1.1 (case A1), yields a small extra reduction of 5%. The latter impact geometry is better addressed by adding a front airbag (case A2); this yields an extra reduction of 21%, i.e. 48% reduction in total.

5.5 Conclusion

This paper has developed a simulation based method in evaluating the effect of parachute and airbag in reducing ground Third Party Risk (TPR), i.e. safety risk posed by small UAS to people on the ground. Existing ground TPR methods and models do not cover the combined effect of parachute and airbag. In section 5.2 it is shown that the existing model for ground TPR assessment includes the product $A_{impact} \times \mathrm{P}\{F|impact\}$, with A_{impact} the size of the area on the ground that is impacted by the crashing UAS; and with $\mathrm{P}\{F|impact\}$ the probability of fatality in case the UAS impacts a human in the impact area. Recently, [Jiang er al, 2023] have shown that this product is equal to the following integral:

$$A_{impact} \times \mathrm{P}\{F|impact\} = \int_{\mathbb{R}^2} \mathrm{P}\{F|\Delta\}d\Delta$$

where $\mathrm{P}\{F|\Delta\}$ is the conditional probability of fatality given horizontal offset Δ between the centre of the UAS impact location relative to the location of an impacted human. Moreover, [Jiang et al, 2023] have shown that $\mathrm{P}\{F|\Delta\}$ can be assessed through conducting dynamical simulations for two subsequent phases: i) Dynamical simulation of a differential equation model of the uncontrolled fall of the UAS considered; and ii) Dynamical simulation of a FE or MBS model of the subsequent collision of the falling UAS with a human on the ground.

In section 5.3, dynamical simulation models for both phases have been developed for a RA3 UAS [Antwork, 2023], which is a package delivery drone of 15 kg weight. The descent simulation model takes effect of parachute into account. To simulate a collision with human body, a Multi Body System (MBS) model has been developed following the steps of [Ratagraikanakorn et al., 2020a]. This includes the development of an MBS model for the RA3 UAS, the integration of this MBS model with the human body models and airbag models available in a platform for the simulation of human injury impacts of car collisions [MADYMO, 2023], and development of a conversion of human injury criteria to probability of fatality.

In section 5.4, ground TPR has been evaluated for the following three cases: A) UAS with parachute and bottom airbag (at 1 atmosphere pressure); B) UAS with parachute only; and C) UAS without parachute or airbag. In contrast to case A, cases B and C could be assessed using the existing methods. The results show that the existing methods fall short in a providing a valid assessment of the risk mitigating effect of a parachute. Dynamical simulation of the collision phase has also been conducted for each of these three cases. These results show that at zero wind ground TPR is reduced by a factor 3.3 due to parachute alone (case b), and by more than a factor 25 due to parachute and airbag (case A). Dynamical simulation results also show that these reduction factors steadily deteriorate when horizontal wind is increased. At 10 m/s horizontal wind the effect of parachute alone (case B) is gone, while the risk reduction effect of parachute and airbag (case A) is marginalized to 20%.

In order to further mitigate ground TPR under non-zero horizontal wind, for the case with parachute and airbag, two additional cases have been evaluated: Case A1: parachute and bottom airbag at 1.1 atmospheric pressure; and Case A2: parachute and bottom and side airbag, both at 1.1 atmospheric pressure. The simulation results obtained show that the risk reducing effect of case A2 in particular is similar to case A as long as the horizontal wind remains below 4 m/s. For higher horizontal wind values the risk reducing effect steadily goes down to 50% at 10 m/s.

Main conclusions:

- Existing ground TPR assessment methods for UAS fall short in reliably assessing risk mitigating effects of parachute and airbag.
- Proposed dynamical simulation approach allows to assess and learn understanding the risk mitigating effects of equipping a UAS with parachute and airbag(s)
- Ground TPR posed by UAS RA3 can be reduced by an order in magnitude by proper equipment by parachute and airbag, and by restricting its operational use to horizontal wind up to 4 m/s.

In this paper risk mitigating effect of parachute and airbag are investigated using dynamical simulation approach. This method can be further extended to other types of UAS, such as fixed wing UAS, e.g. [Zipline, 2023] and VTOL systems, e.g. [Ehang, 2023; Wing, 2023]. The results show that the evaluated risk is highly dependent of the initial impact conditions of the UAS, which is determined by the dynamical simulation of failure descent of the UAS. Currently for failure descent model use is made of ballistic descent model of three Degrees of Freedom (DoF), i.e. the 3D location of the descent trajectory. Further improvements can be applied to the failure descent model of six DoF [Foster & Hartman, 2017; Sun and Visser, 2019] that furtherly takes into consideration the 3D attitude of the UAS. This will provide more accurate impact location and initial impact condition of the UAS.

Appendix 5A. MBS model of RA3

Body masses and segments

The 7 rigid masses and their connections in the RA3 MBS model are shown in Figure A1.a. Bodies 1-6 are connected with Joints 1-6 to Body 0 as shown in Figure A1.b. Joints 1-6 are universal joints, for which Cardan restraints (torsional spring parallel with a damper) are used to account for force deflections from structure deformations.
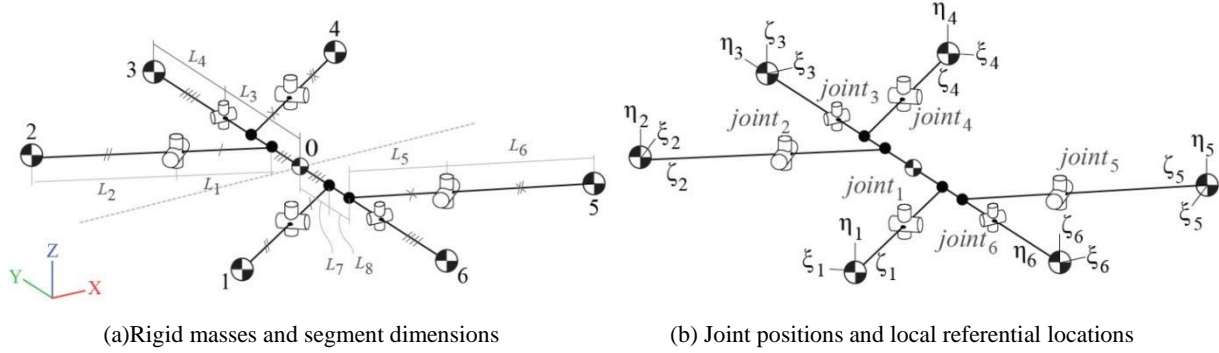

(a)Rigid masses and segment dimensions   (b) Joint positions and local referential locations
Figure A1. Skeleton of the MBS model of RA3 UAS showing rigid masses, joints and restraints.

In Tables A1 and A2, RA3 UAS model segment dimensions, masses and moment of inertia are given. Geometrical dimensions and masses are obtained from physical measurements of the UAS parts. Moment of inertia of each body parts are measured using bifilar test.

Table A1. Geometrical dimensions of the RA3 UAS

Segment	Length(m)	Segment	Length(m)
L1	0.181	L5	0.143
L2	0.409	L6	0.412
L3	0.173	L7	0.089
L4	0.456	L8	0.141

Table A2. Mass and moment of inertial of each body

Body part	Mass (g)		Moment of inertia (kg*m^2)					
Body 0 (Main frame)	m0	11974.4	$I_{XX}0$	0.499	$I_{YY}0$	0.382	$I_{ZZ}0$	0.771
Body 1 (Arm 1)	m1	502	$I_{XX}1$	0.002	$I_{YY}1$	0.001	$I_{ZZ}1$	0.003
Body 2 (Arm 2)	m2	502	$I_{XX}2$	0.002	$I_{YY}2$	0.001	$I_{ZZ}2$	0.003
Body 3 (Arm 3)	m3	515.5	$I_{XX}3$	0.003	$I_{YY}3$	0.001	$I_{ZZ}3$	0.004
Body 4 (Arm 4)	m4	522.5	$I_{XX}4$	0.003	$I_{YY}4$	0.001	$I_{ZZ}4$	0.004
Body 5 (Arm 5)	m5	522.5	$I_{XX}5$	0.003	$I_{YY}5$	0.001	$I_{ZZ}5$	0.004
Body 6 (Arm 6)	m6	515.5	$I_{XX}6$	0.003	$I_{YY}6$	0.001	$I_{ZZ}6$	0.004

Arm stiffness measurement

The stiffness of an RA3 arm is quantified as the moment M as a function of angular displacement θ. Using quasi-static compression test (Figure A2), force F – displacement d curve is firstly obtained, and the moment M - angular displacement θ curve (Figure A3) is subsequently generated using $M = F \times L$ and $\theta = d/L$, where L is the length of arm. Due to that arms 1-6 use the same carbon fiber material and same type of aluminium connector to the mainframe, they have the same torsional stiffness.

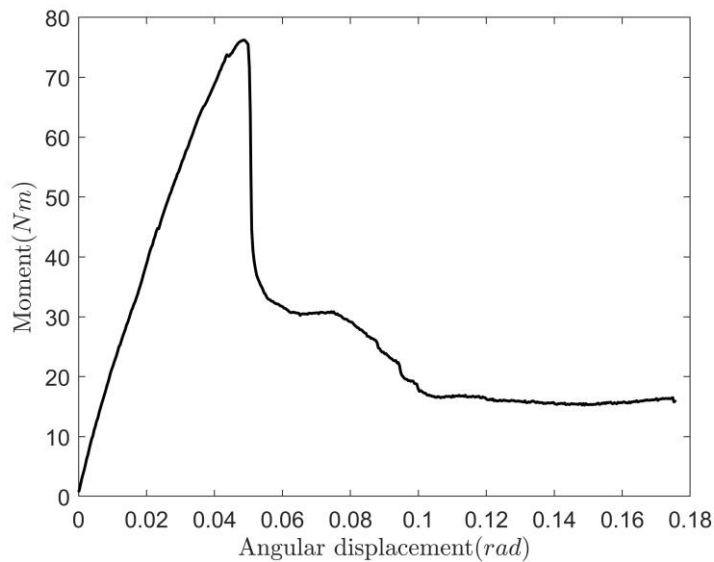**Figure A2.** Quasi-static compression test of an arm of RA3 UAS

Figure A3. Moment M -angular displacement θ curve of arms 1-6 of RA3 UAS

Appendix 5B. Contact Model of RA3 with Human

Properties of human scalp and RA3 UAS material are in Table B1. Material property of the RA3 UAS carbon fiber is obtained from online source [Matweb, 2022]. The head contact surface is assumed to have the characteristics of human head scalp. The material property of human head scalp is obtained from [Falland-Cheung et al., 2018].

Table B1. Properties of human head scalp and RA3 UAS material

Materials	Young's modulus	Poisson ratio	Radius (m)
Human head scalp	2.23×10^7 Pa	0.29	0.0875
Carbon fiber	5.48×10^{10} Pa	0.34	0.03 (for arm)

The corresponding contact compliance curves for the RA3 main frame and arms are obtained using the Hertz elastic contact model [Brake, 2012] as shown in Figure B1.

106

(a)   (b)
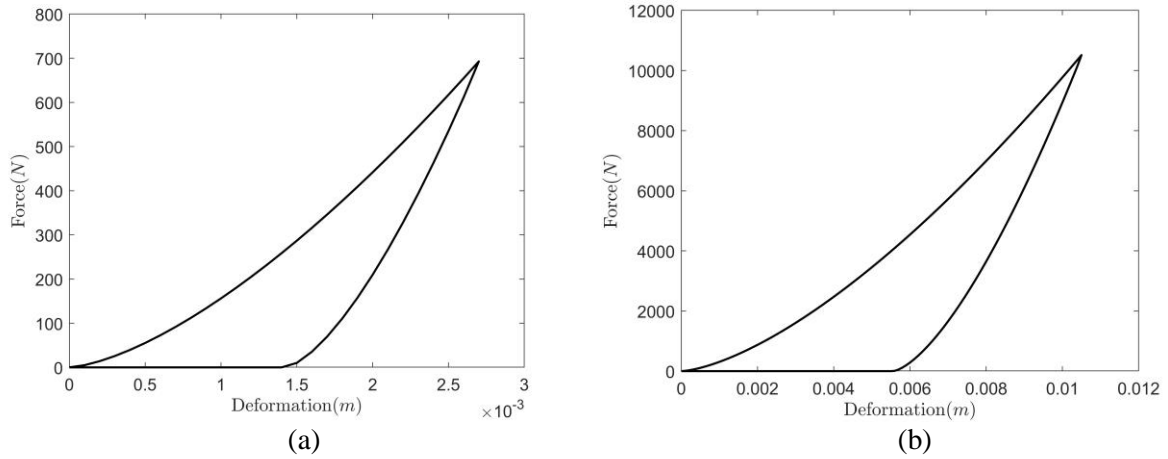
Figure B1. Contact compliance curves for RA3 UAS-human head contact. (a) RA3 arm contact (b) RA3 mainframe contact

The contact compliance curve for cargo box is obtained using ellipsoid-foam contact model [Chou et al., 1994] as shown in Figure B2. This contact compliance curve is obtained as a product of contact area and contact stress. The contact area curve and contact stress curve are shown in Figures B3 and B4. The contact area curve shows the size of cross sectional area as a function of deformation of cargo box impacting human head shape model as a sphere with 0.0875m radius. The contact stress curves for foam loading-unloading are from [Avalle et al., 2018] for EPP foam of density 70kg/m^3.
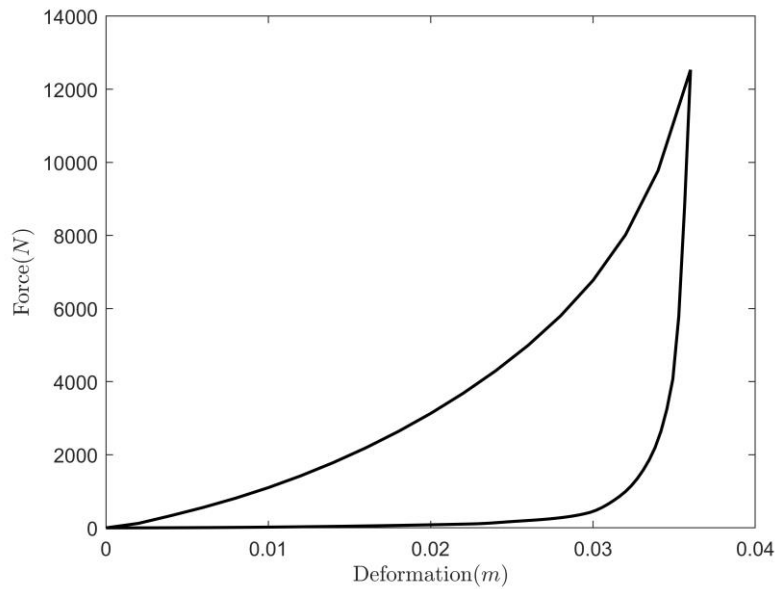
Figure B2. Contact compliance curve for RA3 cargo box-human head contact
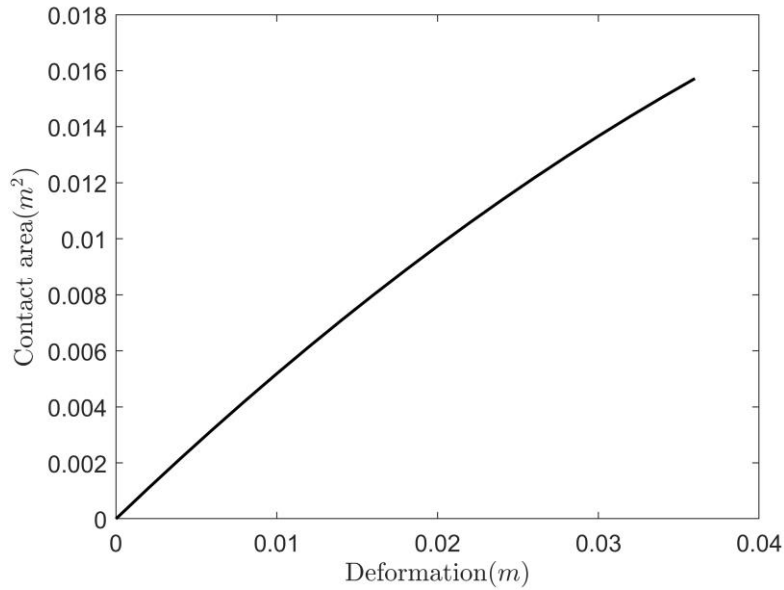
Figure B3. Contact area - deformation curve for RA3 cargo box-human head contact
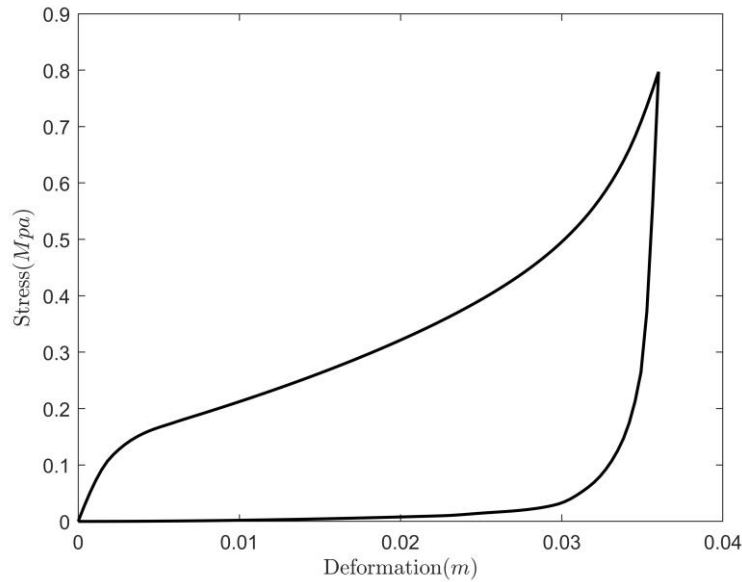
Figure B4. Contact stress - deformation curve for RA3 cargo box-human head contact [Avalle et al., 2018]

Appendix 5C. Conversion of Human Injury Criteria to Probability of Fatality

Head Injury Criterion

The *HIC* equation is defined as follows [Hutchinson et al., 1998] :

$$HIC = \max_{t_1,t_2}\left\{\frac{1}{(t_1-t_2)^{3/2}}\left[\int_{t_1}^{t_2} a(t)dt\right]^{5/2}\right\}$$ (C.1)

where $a(t)$ is the head acceleration observed at center of mass of head as a function of time t, t_1 and t_2 are two time points during the impact. There are two time range limits for $t_1 -$

t_2, which are $15ms$ and $36ms$. Common practice for head injury simulation in a car crash accident is to use a $15ms$ time range limit; this time range is also adopted for UAS impact on human head.

The *HIC* can be converted to percentage of life-threatening injury using the U.S. ISO Delegation recommended curve [Tyrell et al., 1995] in Figure C1. The percentage of life-threatening injury is equivalent to the Probability of Fatality (PoF).
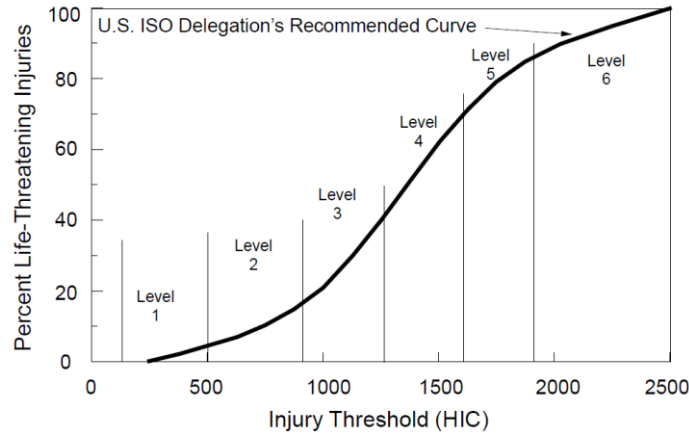
Figure C1. Convention of HIC to percentage of life-threatening injury [Tyrell et al., 1995]

Neck Injury Criterion

For the four types of neck injury N_{ij}, namely N_{TF}, N_{TE}, N_{CF}, N_{CE}, the equation is:

$$N_{ij} = \left| \frac{F_Z}{F_{int}} \left| \frac{M_Y}{M_{int}} \right| \right| \tag{C.2}$$

where F_Z is the upper neck Z-axis loading force, M_Z is the upper neck Y-axis loading moment, F_{int} and M_{int} are the corresponding critical intercept value of load for normalization. For neck injury, the highest of the four assessed N_{ij} values is converted to Probability of Fatality (PoF). In doing so we use the transformation curve in Figure C2, which curve provides an upper bound in PoF as a function of assessed N_{ij} value.
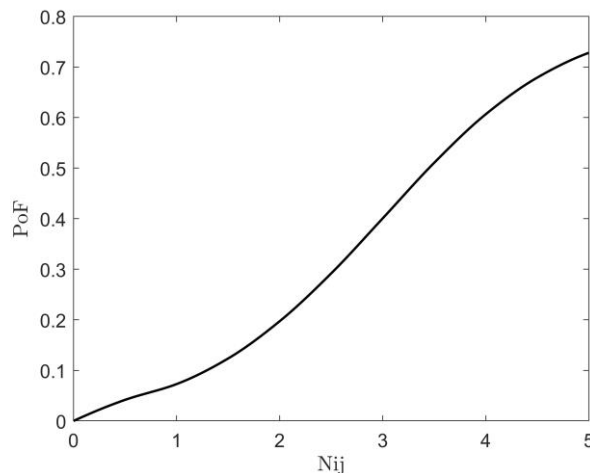

Figure C2. Probability of Fatality $P\{F|N_{ij}\}$ as a function of N_{ij}

Figure C2 is obtained below, following a sequence of four steps. The first step is to adopt the AIS probability curve fittings as function of N_{ij} levels by [Eppinger et al., 1999] on realistic injury data; these are given in Figure C3.a. As can be seen in Figure C3a, the left and right parts of these curve fittings sometimes show unrealistic patterns. The second step is to resolve these unrealistic patterns by applying the following two logical to the curves in Figure C3.a: i) $P\{AIS|N_{ij} = 0\} = 0$; and ii) $P\{AIS \geq k|N_{ij}\} \geq P\{AIS \geq k + 1|N_{ij}\}$ for $k = 4,3,2$ and all N_{ij}. Application of these conditions to the curves in Figure C3.a yields the curves in Figure C3.b.

(a) Original curve fittings [Eppinger et al., 1999]   (b) Applying logical conditions to (a)
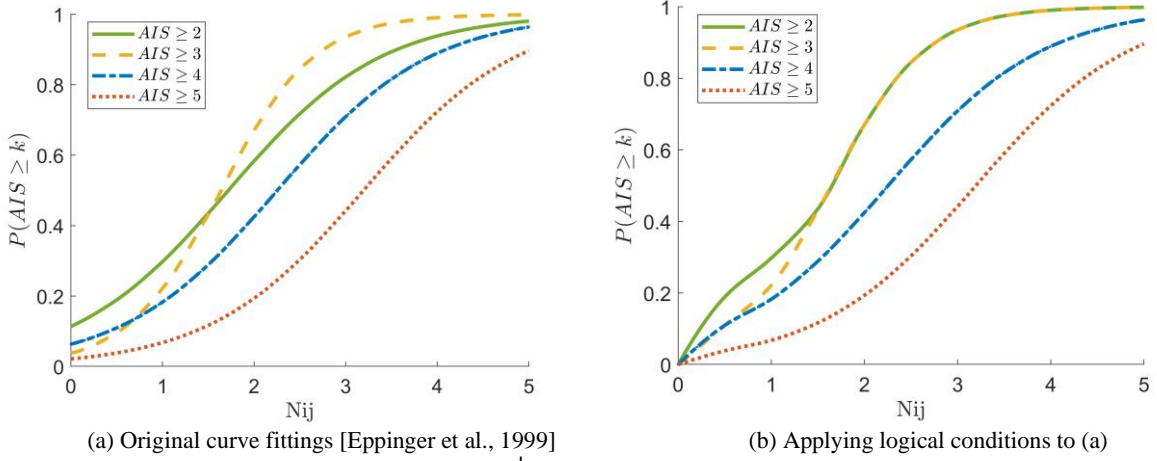
Figure C3. $P\{AIS \geq k|N_{ij}\}$ as a function of N_{ij} for $k = 2,..,5$

The third step is to transform each of the four AIS curves in Figure C3.b, to PoF curves. For this transformation we adopt the conversion by [Gennarelli and Wodzin, 2006], to transform AIS levels to probability of fatality; this curve is shown in Figure C4.
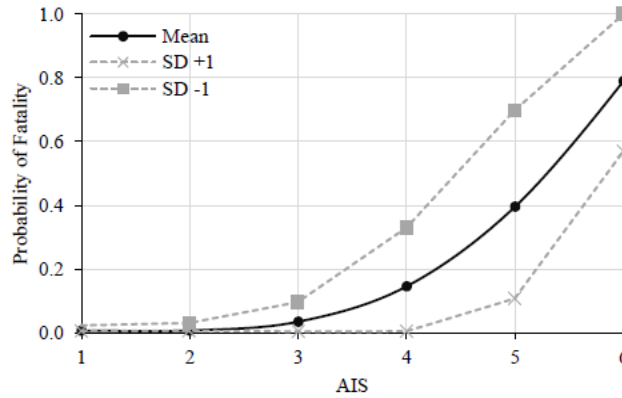

Figure C4. Conversion of AIS to probability of fatality [Gennarelli and Wodzin, 2006]

The fourth step is to combine the four $P\{AIS \geq k|N_{ij}\}, k = 1,2,3,4$, curves in Figure 3C.b with the conversion curve $P\{F|AIS = k\}$ in Figure C4, to a single PoF curve as function of N_{ij} . For this fourth step we develop the following probabilistic analysis:

$$P\{F|N_{ij}\} = \sum_{k=2}^{4}\left[P\{F|AIS = k\}P\{AIS = k|N_{ij}\}\right] + P\{F|AIS \geq 5\}P\{AIS \geq 5|N_{ij}\}$$

$$\leq \sum_{k=2}^{4}\left[P\{F|AIS = k\}P\{AIS = k|N_{ij}\}\right] + P\{F|AIS = 6\}P\{AIS \geq 5|N_{ij}\} \qquad (C.3)$$

$$= \sum_{k=2}^{4}\left[P\{F|AIS = k\}\left(P\{AIS \geq k|N_{ij}\} - P\{AIS \geq k +1|N_{ij}\}\right)\right] + P\{F|AIS = 6\}P\{AIS \geq 5|N_{ij}\}$$

110

where $P\{AIS \geq k | N_{ij}\}$ is quantified in Figure C3.b, and $P\{F|AIS = k\}$ is quantified in Figure C4. Subsequent evaluation of the latter inequality, by using the curves in Figures C3.b and C4, yields the curve in Figure C2.

Viscous Criterion (VC)

The VC injury level VC for a specific body part is generated as follows:

$$VC = \max_{t,r}[V(t,r) \times C(t,r)] \tag{C.4}$$

where $V(t,r)$ is the deformation speed of the body part at moment t and location r. $C_B(t,r)$ is the compression in the percentage of the thickness of the body part at moment t and location r.

The VC injury level VC is converted to PoF $P\{F|VC\}$ using the following equation:

$$P\{F|VC\} = P(F|AIS)P(AIS|VC) \tag{C.5}$$

The curve for $P(AIS|VC)$ is shown in Figure C5 [Sturdivan et al., 2004] which is based on blunt impact experiment on cadavers [Canavaugh et al., 1990; Viano et al., 1989]. For $P(F|AIS)$ use is made of the curve in Figure C4. Combining the curves in figures C4 and C5, by using eq. (C5), yields the curve in Figure C6 for conversion of VC injury level to PoF value.
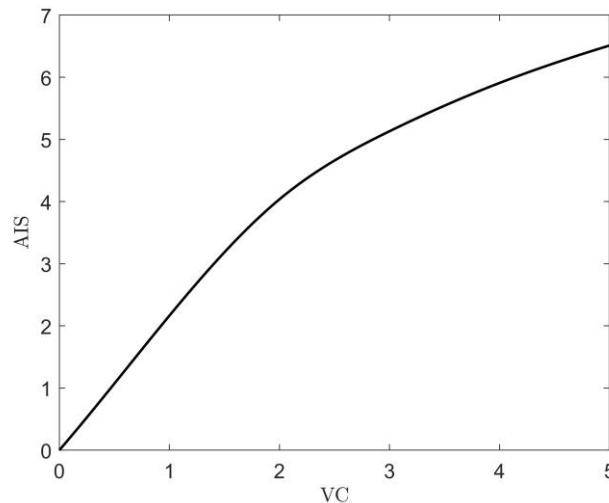

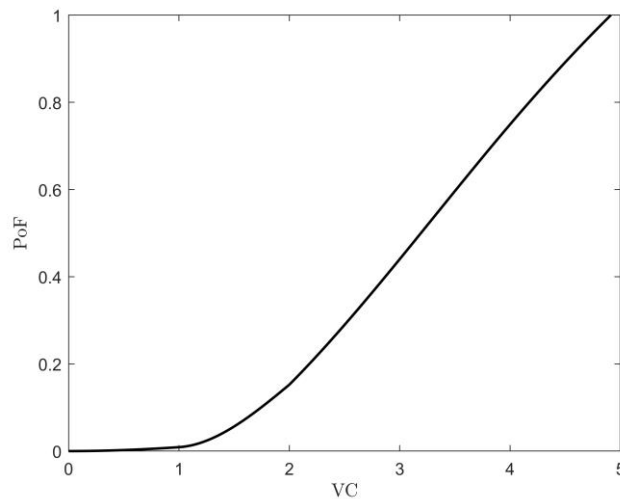**Figure C5.** Conversion of VC injury level to AIS level [Sturdivan et al., 2004]

Figure C6. Conversion of VC injury level to PoF

References

Ale, B., Piers, M. (2000). The assessment and management of third party risk around a major airport. Journal of Hazardous Materials, 71(1-3), 1-16.

Ancel, E., Capristan, F.M., Foster, J.V., Condotta, R.C. (2017). Real-time Risk Assessment Framework for Unmanned Aircraft System (UAS) Traffic Management (UTM). Proceedings of 17th AIAA Aviation Technology, Integration, and Operations Conference. pages: 1-17. Denver, Colorado. AIAA 2017-3273.

Antwork. (2020), Parachute canopy folding structure, parachute, landing system, unmanned aerial vehicle, Chinese patent: CN111216900A

Antwork, 2023, Antwork Introduction, URL: https://www.antwork.link/introduction.html [retrieved 24th, July, 2023]

Arterburn, D., M. Ewing, R. Prabhu, F. Zhu, D. Francis (2017). UAS Ground Collision Severity Evaluation, ASSURE Task A4 Final Report. FAA UAS Center of Excellence. , URL: https://www.assureuas.org/projects/completed/a4/ASSURE_A4

Arterburn, D., G. Olivares, J. Bolte, R. Prabhu and S. Duma (2019). UAS Ground Collision Severity Evaluation 2017-2019, ASSURE Task A14 Final Report. FAA, Atlamtic City, NJ, URL: https://www.assureuas.org/projects/completed/a14/ASSURE_A14

Avalle, M., Frascio, M., & Monti, M. (2018). An improved model to describe the repeated loading-unloading in compression of cellular materials. Procedia Structural Integrity, 12, 19-31.

Bertrand, S., Raballand, N., Viguier, F., & Muller, F. (2017). Ground Risk Assessment for Long-Range Inspection Missions of Railways by UAVs. Proceedings of 2017 International Conference on Unmanned Aircraft Systems. pages: 1343-1351. Miami, FL.

Blom H. A. P., Jiang C., Grimme W. B. A., et al (2021). Third party risk modelling of Unmanned Aircraft ystem operations, with application to parcel delivery service[J]. Reliability Engineering & System Safety, 2021: 107788.

Brake, M. R. (2012). An analytical elastic-perfectly plastic contact model. International Journal of Solids and Structures, 49(22), 3129-3141.

Cavanaugh, J. M., Walilko, T. J., Malhotra, A., Zhu, Y., and King, A. I., "Biomechanical response and injury tolerance of the pelvis in twelve sled side impacts," SAE Technical Papers, vol. 99, 1990, pp. 1678–1693, doi: 10.4271/902305.

Cawthorne D. Development of a Multirotor Drone Airbag. Master thesis, 2016.

Chou, C. C., et al. "Experimental validation of ellipsoid-to-foam contact model." SAE transactions (1994): 667-678.

Clothier, R. A., Williams, B. P., & Hayhurst, K. J., 2018. Modelling the risks remotely piloted aircraft pose to people on the ground. Safety science, 101, 33-47.

Disney, 2016, Impact absorption apparatus for unmanned aerial vehicle, United States Patent: US2016/0332739

DJI, 2019, Impact protector equipment, Chinese patent: CN106029499B

DJI, 2022, Dropsafe, URL: https://www-v1.dji.com/nl/dropsafe.html [retrieved 24th, July, 2023]

EASA, 2021, Study on the societal acceptance of Urban Air Mobility in Europe, European Union Aviation Safety Agency, 19th, May, 2021

EC, 2021, Commision implementing regulation on a regulatory framework for the U-Space, 22nd April 2021.

Ehang, 2023, Passenger transportation an logistics, URL: https://www.ehang.com/uam/ [retrieved 20th, July, 2023]

Eppinger, R., Sun, E., Bandak, F., Haffner, M., Khaewpong, N., Kuppa, S., Maltese, M., ... & Zhang, A. (1999). Development of improved injury criteria for the assessment of advanced automotive restraint systems: II. National Highway Traffic Safety Administration.

FAA, 2016, "Operation and Certification of Small Unmanned Aircraft Systems," Department of Transportation, Washington, USA.

Falland-Cheung, L., Scholze, M., Lozano, P. F., Ondruschka, B., Tong, D. C., Brunton, P. A., ... & Hammer, N. (2018). Mechanical properties of the human scalp in tension. Journal of the mechanical behavior of biomedical materials, 84, 188-197.

Flyfire, 2022, drone safety parachute, https://www.flyfiretech.com/ [retrieved 24th, July, 2023]

Foster, J.V., & Hartman, D. (2017). High-Fidelity Multi-Rotor Unmanned Aircraft System (UAS) Simulation Development for Trajectory Prediction Under Off-Nominal Flight Dynamics. Proceedings of 17th AIAA ATIO Conference. pages: 1-17. Denver, Colorada.

Gennarelli, T. A., & Wodzin, E. (2006). AIS 2005: a contemporary injury scale. Injury, 37(12), 1083-1091.

Happee, R., Hoofman, M., Van den Kroonenberg, A. J., Morsink, P., & Wismans, J. S. H. M. (1998). A mathematical human body model for frontal and rearward seated automotive impact loading. SAE transactions, 2720-2734.

Happee, R., Ridella, S., Nayef, A., Morsink, P., de Lange, R., Bours, R., & Van Hoof, J. (2000, September). Mathematical human body models representing a mid size male and a small female for frontal, lateral and rearward impact loading. In IRCOBI Conference (pp. 67-84).

He, X., Jiang, C., Li, L., & Blom, H. A. P., 2022. A Simulation Study of Risk-Aware Path Planning in Mitigating the Third-Party Risk of a Commercial UAS Operation in an Urban Area. Aerospace, 9(11), 682.

Hutchinson, J., M.J. Kaiser, and M. Lankarani (1998), The Head Injury Criterion (HIC) functional, J. of Applied Mathematics and Computation, Vol. 96, pp. 1-16.

Lau, I.V., & Viano, D.C. (1986). The viscous criterion—bases and applications of an injury severity index for soft tissues. SAE transactions, 672-691.

ICAO, 2011, Unmanned Aircraft Systems (UAS), Cir 328, International Civil Aviation Organization.

Ippolito, C. A. (2019). Dynamic ground risk mitigation for autonomous small uas in urban environments. In AIAA Scitech 2019 Forum (p. 0961).

JARUS, 2019, JARUS guidances on Specific Operations Risk Assessment (SORA), Edition: 1.0. Joint Authorities for Rulemaking of Unmanned Systems.

Jiang C, Blom H.A.P., Rattanagraikanakorn, B., 2023. Improved characterization of Third Party Risk posed by UAS flights to ground population, Submitted to Risk Analysis, January 2023.

Klinich, K.D., R.A. Saul, G. Auguste, S. Backaitis and M. Kleinberger (1996), Techniques for developing child dummy protection reference values, measurement, Report 00819638, National Highway Traffic Safety Administration, https://doi.org/10.21949/1403104

Koh, C. H., Low, K. H., Li, L., Zhao, Y., Deng, C., Tan, S. K., Chen, Y., Yeap, B. C., & Li, X. (2018). Weight threshold estimation of falling UAVs (Unmanned Aerial Vehicles) based on impact energy. Transportation Research Part C: Emerging Technologies, 93, 228-255. doi:https://doi.org/10.1016/j.trc.2018.04.021

la Cour-Harbo, A. (2019). Quantifying Risk of Ground Impact Fatalities for Small Unmanned Aircraft. Journal of Intelligent & Robotic Systems, 93(1), 367-384. doi:10.1007/s10846-018-0853-1

la Cour-Harbo, A. (2020). Ground impact probability distribution for small unmanned aircraft in ballistic descent. In 2020 International Conference on Unmanned Aircraft Systems (ICUAS), September 2020, pp. 1442-1451. IEEE.

Lau, I.V., & Viano, D.C. (1986). The viscous criterion—bases and applications of an injury severity index for soft tissues. SAE transactions, 672-691.

MADYMO, (2017a). MADYMO Human body models manual, Release 7.7, TASS International.

MADYMO, (2017b). MADYMO Theory manual Version 7.7, MADYMO utility manual, TASS International.

MADYMO, (2020). MATERIAL.FABRIC_SHEAR, User reference, version 2020.2

MADYMO, (2023). Simcenter Madymo Software, URL: https://plm.sw.siemens.com/en-US/simcenter/mechanical-simulation/madymo/ [retrieved 24th, July, 2023]

Magister, T. (2010). The small unmanned aircraft blunt criterion based injury potential estimation. Safety science, 48(10), 1313-1320.

Manta Air, 2023, UAV recovery systems, URL: https://manta-air.com/ [retrieved 24th, July, 2023]

Melnyk, R., Schrage, D., Volovoi, V., & Jimenez, H. (2014). A third-party casualty risk model for unmanned aircraft system operations. Reliability Engineering & System Safety, 124, 105-116.

Oh, S., J. Cho, N. Kim, Y. Yoon (2020), Preliminary impact assessment of restricting airspace over populated areas for sUAS operations, The Transportation Research Board (TRB) 99th Annual Meeting, 14th January 2020. http://hdl.handle.net/10203/276236

Pang, B., Hu, X., Dai, W., & Low, K. H. (2022). UAV path optimization with an integrated cost assessment model considering third-party risks in metropolitan environments. Reliability Engineering & System Safety, 222, 108399.

Parr, M.J.C., M.E. Miller, N.R. Bridges, J.R. Buhrman, C.E. Perry and N.L. Wright (2012), Evaluation of the Nij neck injury criteria with human response data for use in future research on helmet mounted display mass properties, Proc. Human Factors Ergon. Soc., pp. 2070-2074, doi:10.1177/1071181312561439.

Petritoli E, Leccese F, Ciani L. Reliability and maintenance analysis of unmanned aerial vehicles. Sensors 2018;18. https://doi.org/10.3390/s18093171.

Primatesta, S., Rizzo, A., & la Cour-Harbo, A. (2020). Ground risk map for unmanned aircraft in urban environments. Journal of Intelligent & Robotic Systems, 97(3), 489-509.

Rattanagraikanakorn, B., Schuurman, M., Gransden, D.I., Happee, R., De Wagter, C., Sharpanskykh, A., & Blom, H.A.P. (2019). Modelling Head Injury due to Unmanned Aircraft Systems Collision: Crash Dummy vs Human Body, Proc. 19th AIAA ATIO Conf., June 2019, Dallas, TX, 10.2514/6.2019-2835.

Rattanagraikanakorn, B., Gransden, D. I., Schuurman, M., De Wagter, C., Happee, R., Sharpanskykh, A., & Blom, H.A.P. (2020). Multibody system modelling of unmanned aircraft system collisions with the human head. International Journal of Crashworthiness, 25(6), 689-707.

Rattanagraikanakorn, B., 2021, Modelling Collision Consequences of Unmanned Aircraft Systems on Human, PhD thesis.

RCC (2001). Range Safety criteria for Unmanned Air Vehicles, Rationale and methodology supplement. Supplement to Document 323-99, Range Commanders Coucil, April 2001.

Schmitt, K.-U., P.F. Niederer, D.S. Cronin, B. Morrison III, M.H. Muser and F. Walz (2019), Trauma Biomechanics: An Introduction to Injury Biomechanics, 5th Edition, Springer.

Stark, D.B., A.K. Willis, Z. Eshelman, Y.S. Kang, R. Ramachandra, J.H. Bolte, M. McCrink (2019). Human response and injury resulting from head impacts with unmanned aircraft systems, Stapp Car Crash Journal, Vol. 63, pp. 29-64. doi:10.4271/2019-22-0002.

Sun, S., & de Visser, C. (2019). Aerodynamic model identification of a quadrotor subjected to rotor failures in the high-speed flight regime. IEEE Robotics and Automation Letters, 4(4), 3868-3875.

Sturdivan, L. M., Viano, D. C., & Champion, H. R. (2004). Analysis of injury criteria to assess chest and abdominal injury risks in blunt and ballistic impacts. Journal of Trauma and Acute Care Surgery, 56(3), 651-663.

Touger, M., Gallagher, E. J., & Tyrell, J. (1995). Relationship between venous and arterial carboxyhemoglobin levels in patients with suspected carbon monoxide poisoning. Annals of emergency medicine, 25(4), 481-483.

THUMS (2015), Documentation Total Human Model for Safety (THUMS), AM50 occupant model academic version 5.0_20150527, Toyota Motor Corporation.

THUMS (2018), Documentation Total Human Model for Safety (THUMS), AM50 pedestrian/occupant model academic version 4.02_20181226, Toyota Motor Corporation.

Tyrell, D. C., Severson, K. J., & Marquis, B. P. (1995). Analysis of occupant protection strategies in train collisions. Crashworthiness and Occupant Protection in Transportation System, ASME AMD Vol 210/BED Vol 30,1995

Viano, D.C., I.V. Lau, C. Ashbury, A.I. King, P. Begeman (1989), Biomechnaics of the human chest, abdomen and pelvis in lateral impact, Accident analysis and prevention, Vol. 21, pp. 553-574.

Weibel, R., & Hansman, R. J. (2004). Safety considerations for operation of different classes of UAVs in the NAS. Unmanned Unlimited, Technical Conf., Workshop and Exhibit, 20-23 Sept. 2004, Chicago, IL, AIAA-2004-6421, pp. 1-11.

Weng, Y. B. Bian, K. Gunasekaran, J. Gholipour, C. Vidal and H. Mao (2021). Modelling Small Remotely Piloted Aircraft System to Head Impact for Investigating Craniocerebral Response, J. of Biomechanics, doi:https://doi.org/10.1016/j.jbiomech.2021.110748

Wing, 2023, Drone delivery, URL: https://wing.com/ [retrieved 20th, July, 2023]

Zipline, 2023, Instant delivery & logistics, URL: https://www.flyzipline.com/ [retrieved 20th, July, 2023]

6

Conclusion

The advancements in UAS technology offers great potential for Urban Air Mobility (UAM) applications. Innovation in urban mobility needs to be accompanied and supported by an appropriate safety risk assessment framework. Gaining public acceptance is crucial for facilitating further development of UAS operation in urban environment. The public concerns are majorly related to safety of UAS operations. Therefore for regulators it is important to gain a better understanding of safety risk assessment of UAS operations. This forms the overall aim of the thesis:

To improve the understanding and analysis of safety risk posed by
UAS operations for UAM

To achieve this overall aim, a series of interconnected studies have been conducted in this thesis. This concluding chapter discusses the various findings and synthesizes the results. The chapter is structured as follows: First, for the four objectives outlined in the introduction key findings and insights gained from the research are summarized. Subsequently, the novel contributions are summarized. Finally, potential future research is discussed.

6.1 Results Obtained for Research Objectives

Four objectives in support of the overall research aim have been studied in-depth. The main conclusions drawn for each objective are presented below.

Objective 1: To identify TPR indicators for UAS operations

In Chapter 2, TPR indicators for UAS operations are identified based on that of conventional manned aviation. The key difference between TPR of commercial aviation and UAS operation is that for UAS operation, third party includes not only the uninvolved ground persons, but also the potential crew members and passenger on board other aircrafts. Therefore the proposed TPR indicator consider different types of TPR associated with UAS operations, taking into account both the risks on the ground and in the air. The air TPR indicators involve fatal injuries on board other aircrafts caused by mid air collision of UAS with other aircrafts. The ground TPR indicators involves risk caused by ground impact of UAS itself and ground impact of other aircrafts as a consequence of mid-air collision. By doing so, the research provides a more comprehensive understanding of the overall third party risk posed by UAS operations.

The safety regulations from EASA/JARUS and FAA are summarised for low, medium, and high risk UAS operations, which are then evaluated against the identified TPR indicators for UAS operations. The findings revealed that current safety regulations for medium risk UAS operations do not address any of the identified TPR indicators, while for high risk UAS operations, only certain indicators are addressed. Moreover, none of these safety methods capture the accumulation of contributions by multiple UAS flights per annum to TPR indicators, emphasizing the need for a quantitative safety management framework that accounts for the accumulation of individual UAS flight contributions to collective ground risk and individual risk.

Objective 2: To develop a safety risk assessment approach for the novel ground TPR indicators identified in chapter 2.

In Chapter 3, ground TPR indicators are focused for the development of a safety risk assessment approach. The study addresses the need for TPR models that capture the risk posed to the population by a large number of UA flights per annum. By extending existing TPR models for commercial aviation, Individual Risk and Collective ground risk model for UAS operations have been developed. A Monte Carlo (MC) simulation method for assessment of the TPR models is developed. The MC simulation method takes into account UA operational characteristics and environmental factors to simulate nominal flight paths and failure descent trajectories of UA flights. The outcome of the simulation is combined with the TPR model to generate the individual risk and collective ground risk of the UAS operation for the given area over an annum.

The extended TPR models and MC simulation method are applied to a hypothetical UAS-based parcel delivery service in the city of Delft, The results demonstrate the importance of considering the risks from a population perspective. Different sub models are adopted for the simulation and assessment of TPR, e.g. failure rate model, ballistic descent model, impact risk model, etc. There is a non-negligible level of uncertainty in the models adopted. This highlights the need for further development of more accurate sub models for UAS ground TPR assessment.

Objective 3: To enhance the commonly adopted ground TPR model and its assessment through dynamical simulation of a Multi Body System (MBS) model.

In Chapter 4, the focus is on the development and application of a method to enhance the ground TPR model and its assessment through the dynamical simulation of a Multi-Body System (MBS) model. This novel approach aims to address the limitations and uncertainties associated with the existing models for the product of impact area and Probability of Fatality (PoF) for a ground person impacted by a crashing UAS. The enhanced ground TPR model replaces the product with an integration over simulated risk values for different offsets between the UAS crash center and the location of the impacted human, also taking into account the effects of impact geometries between UAS and human.

The enhanced TPR model is realized by integrating an MBS model of UAS collision with a human body. The application of this approach to a DJI Phantom III UAS crash demonstrates the effectiveness of the proposed method, revealing critical insights into the influence of impact geometries such as UAS attitude, impact velocity and human face direction. Furthermore, it is shown that the true risk value for a DJI Phantom III falls outside the range of risk values from nine existing model combinations.

Objective 4: To evaluate the effect of risk mitigation measures implementing the enhanced TPR model with dynamical simulation approach

In Chapter 5, the enhanced model is applied to the risk analysis of a delivery UAS with airbag and parachute system. Dynamical simulation models for failure descent and impact collision are developed for the UAS. For failure descent, the effect of parachute is taken into consideration. For impact simulation of UAS on human body, MBS and FE models are developed for the UAS and airbag system.

Impact simulations are conducted for various cases, considering different wind condition and comparing cases with and without airbag and parachute. The results demonstrate that the ground TPR posed by the 15kg UAS can be reduced by an order in magnitude by proper equipment of parachute and airbag. Moreover, the effect in mitigating risk is shown to be effective when horizontal wind is limited up to 4 m/s.

The findings of the analysis show the effectiveness of the proposed enhanced model, which integrates the dynamical simulation approach to explore the effect of airbag and parachute systems. In the comparison to existing classical models, the enhanced model shows the advantage in assessing UAS impact in a more comprehensive and accurate way.

6.2 Novel Contributions of the thesis

The thesis made novel contributions to the following five domains:
1. Novel UAS Third Party Risk indicators,
2. UAS Third Party Risk modelling and Assessment for the novel indicators,
3. Enhanced UAS ground TPR model,
4. Dynamical simulation based quantification of UAS impact on a human,
5. Evaluate the effect of airbag and parachute in UAS ground TPR.

1. Novel UAS ground Third Party Risk Indicators

In Chapter 2, novel ground Third Party Risk indicators for UAS operations are proposed based on existing ground TPR indicators for annual commercial flights around large airports and other safety-critical industries. These novel ground TPR indicators are: i) "Collective ground risk", i.e. the expected number of fatalities on the ground posed by annual UAS operations over a given area; and ii) "Individual risk", i.e. the probability that an unprotected person at a given ground location will be killed due to annual UAS operations.

In contrast to the commonly used ground TPR indicator, the novel indicators consider the accumulation of risk posed by annual UAS flight over an area.

2. UAS ground Third Party Risk Modelling and Assessment

In Chapter 3, existing UAS ground TPR risk assessment approach is extended for the novel ground TPR indicators from Chapter 2: Individual risk and Collective ground risk.

For the quantitative analysis, a Monte Carlo simulation based approach is developed. The simulation approach is able to take into account different sub models for risk analysis, and consider environmental factors and UAS operational characteristics, which can be applied to different UAM scenarios. The novel approach is illustrated for a UAS based parcel delivery service in the city of Delft.

3. Enhanced UAS ground TPR Model

For the assessment of the existing UAS ground TPR model it is assumed that crash impact area and impact Probability of Fatality (PoF) are independent. An extra complication is that the existing models for each of these two terms lead to a significant range of possible assessment outcomes. To improve this situation, in Chapter 4, an enhanced ground TPR model has been developed, in which the product of crash impact area and impact Probability of Fatality (PoF) is mathematically transformed to an integration of location dependent PoF values over all possible offset values between crash location and human location. This transformation resolves the need for separate models for the crash impact area and impact PoF; instead it requires assessment of impact PoF as a function of the offset between crash location and human location, followed by a numerical integration over all possible offsets.

4. Dynamical simulation based quantification of UAS impact on a human

The enhanced TPR model can be quantified through conducting dynamical simulation of a Multi Body System (MBS) model of a UAS hitting a human on the ground, as a function of offset between crash location and human location. It is shown that this novel approach provides ground TPR risk estimates that are much more accurate than the results obtained by the common approach. The novel method can also take into account parameter values for UAS attitude and impact velocity, as well as human face direction.

5. Assess the effect of airbag and parachute for UAS ground TPR

In Chapter 5, the effect of airbag and parachute systems are evaluated using the enhanced TPR model and dynamical simulation. To achieve this, an MBS model of the urban delivery UAS and an FE model of the airbag system are developed. The parachute system

influences the impact velocity of UAS at moment of human impact. Subsequently, the airbag influences the impact PoF. It is also demonstrated that in case of parachute only, the novel approach yields much improved ground TPR estimation over using the existing methods from literature.

6.3 Future Research

List of relevant follow-on ground TPR research directions:

1. Combining the Monte Carlo simulation based risk assessment in Chapter 2 with the enhanced TPR model and dynamical simulation approach of Chapter 4;

2. Using the novel risk assessment approach of Chapter 3 for risk aware path planning;

3. To apply the novel TPR indicators of Chapter 2, and the MC simulation approach of Chapter 3, for allocation of ground infrastructure for UAS operation;

4. Using six DoF descent models in UAS ground TPR assessment of Chapter 4;

5. To apply the dynamical simulation of MBS and FE model of airbag and parachute for ground TPR risk assessment of chapter 5, to other types of UA;

6. Regulators can improve their current safety risk assessment frameworks.

1. Combination of Monte Carlo simulation risk assessment with the dynamical simulation and enhanced TPR model

In Chapter 4 and 5, dynamical simulation of Multi Body System (MBS) and Finite Element (FE) models has been integrated in the UAS ground TPR model, contributes to providing risk evaluation of UAS impacting on human body. On the other hand, in Chapter 3 the MC simulation risk assessment method has been proposed to address UAS operations involving large numbers of flights, which considers the UAS operation before impacting on human body, including flight path, failure probability and descent trajectory after failure. A logical follow-on work is to combine the dynamical simulation of MBS and FE model with MC simulation approach to conduct a comprehensive ground TPR risk assessment of a UAS operation that involves multiple flights. This will provide more accurate and precise risk evaluation of UAS operation in a given operating environment.

2. Using the novel risk assessment approach for risk aware path planning

The ground TPR assessment methodology has the potential for application in UAS risk aware path planning [Primatesta et al.,2019; Levasseur et al., 2020; Lin and Shao, 2020; Pang et al., 2022], in which the existing TPR model is adopted. For improvement the novel TPR indicator and risk assessment approach can be applied. Use of the novel TPR indicator can enable the risk based path planning for multiple flights, e.g. [He et al., 2022]. The use of dynamical simulation with enhanced TPR model provide more realistic risk assessment, and provide the potential to consider mitigation measures such as parachute and airbag.

3. To apply the novel TPR indicator and MC simulation approach for allocation of ground infrastructure for UAS operation

For UAS operations, the ground infrastructures such as vertiport and ground shelters have to be established before the operation of UAS. The related TPR has to be assessed for

UAS operations involving multiple flights during a certain time period. This can be achieved adopting the novel TPR indicator of Chapter 2 and MC simulation approach proposed of Chapter 3 in this thesis.

4. Using six DoF descent models in ground TPR assessment of UAS operations

The results of Chapter 4 and 5 show that the evaluated risk is highly dependent of the initial impact conditions of the UAS and human body, which is largely determined by the failure descent of the UAS. Currently for failure descent model use is made of ballistic descent model of three Degrees of Freedom (DoF), i.e. the 3D location of the descent trajectory. Further improvements can be applied to the failure descent model of six DoF [Foster & Hartman, 2017; Sun and Visser, 2019] that furtherly takes into consideration the 3D attitude of the UAS. This will provide more accurate impact location and initial impact condition of the UAS.

5. To apply the dynamical simulation of MBS and FE model of airbag and parachute for other types of UAS

In Chapter 5 the risk mitigating effect of parachute and airbag are investigated, using dynamical simulation of MBS and FE model with the enhanced ground TPR model. This method can be further extended to other types of UAS, such as fixed wing UAS, e.g. [Zipline, 2023] and VTOL systems, e.g. [Ehang, 2023; Wing, 2023]. The effectiveness of parachute and airbag may be different on different types of UAS, given the different UAS operating characteristics and environment.

6. Improving current UAS regulatory safety risk assessment frameworks

In the current regulatory risk assessment frameworks for UAS [EASA, 2023; FAA, 2023], risk is considered for single flight. This may not be suitable for the potential future UAS operation in UAM environment involving multiple UAS flights. The novel TPR indicator proposed in this thesis can be integrated in the risk assessment framework. Moreover, in the risk assessment for UAS operations, e.g. [JARUS, 2017] a qualitative approach is adopted for ground TPR assessment, because at the time of developing the method, literature had significant gaps. This situation has now significantly been improved. The quantitative risk assessment approach can be adopted in the risk assessment framework.

References

EASA, 2023, Civil drones (Unmanned aircraft), URL: https://www.easa.europa.eu/en/domains/civil-drones [retrieved 20th, July, 2023]

Ehang, 2023, Passenger transportation an logistics, URL: https://www.ehang.com/uam/ [retrieved 20th, July, 2023]

FAA, 2023, "Drones". Federal Aviation Administration, URL: https://www.faa.gov/uas [retrieved 20th, July, 2023]

Foster, J. V., & Hartman, D., 2017. High-fidelity multi-rotor unmanned aircraft system (UAS) simulation development for trajectory prediction under off-nominal flight dynamics. In 17th AIAA Aviation Technology, Integration, and Operations Conference (p. 3271).

He, X., Jiang, C., Li, L., & Blom, H. A. P., 2022. A Simulation Study of Risk-Aware Path Planning in Mitigating the Third-Party Risk of a Commercial UAS Operation in an Urban Area. Aerospace, 9(11), 682.

JARUS, 2019, JARUS guidances on Specific Operations Risk Assessment (SORA), Edition: 2.0.

la Cour-Harbo, A. (2019). Quantifying Risk of Ground Impact Fatalities for Small Unmanned Aircraft. Journal of Intelligent & Robotic Systems, 93(1), 367-384. doi:10.1007/s10846-018-0853-1

Levasseur, B., Bertrand, S., & Raballand, N., 2020. Efficient generation of ground impact probability maps by neural networks for risk analysis of UAV missions. In 2020 International Conference on Unmanned Aircraft Systems (ICUAS) (pp. 1398-1406). IEEE.

Lin, C. E., & Shao, P. C., 2020. Failure analysis for an unmanned aerial vehicle using safe path planning. Journal of Aerospace Information Systems, 17(7), 358-369.

Pang, B., Hu, X., Dai, W., & Low, K. H., 2022. UAV path optimization with an integrated cost assessment model considering third-party risks in metropolitan environments. Reliability Engineering & System Safety, 222, 108399.

Primatesta, S., Rizzo, A., & la Cour-Harbo, A., 2020. Ground risk map for unmanned aircraft in urban environments. Journal of Intelligent & Robotic Systems, 97(3), 489-509.

Sun, S., & de Visser, C., 2019. Aerodynamic model identification of a quadrotor subjected to rotor failures in the high-speed flight regime. IEEE Robotics and Automation Letters, 4(4), 3868-3875.

Wing, 2023, Drone delivery, URL: https://wing.com/ [retrieved 20th, July, 2023]

Zipline, 2023, Instant delivery & logistics, URL: https://www.flyzipline.com/ [retrieved 20th, July, 2023]

Curriculum Vitae

Chengpeng Jiang

Chengpeng Jiang was born on 20th October 1992 in Sichuan, China. From 2011 to 2015, he attended Nanjing University of Aeronautics and Astronautics in Nanjing where he received his BEng degree in Transportation, major in air traffic control and flight dispatch. In 2015, he continued his study in Nanjing University of Aeronautics and Astronautics to pursue an MSc degree, joining the National Key Laboratory of Air Traffic Flow Management. There, he leveraged machine learning algorithms to research in the identification and forecasting of air traffic congestion states within terminal maneuvering areas. He also undertook a project in low-altitude flight simulation and analysis. He developed a C# based simulation platform, in which he developed and implemented a multi-flight conflict detection and resolution algorithm.

In 2018, after receiving his MSc degree in Transportation Planning and Management, Chengpeng began his position as a PhD candidate at the faculty of Aerospace Engineering, Delft University of Technology (TU Delft). He undertook research on Third Party Risk (TPR) assessment of Unmanned Aircraft System (UAS) for Urban Air Mobility (UAM). His PhD research focuses on the TPR assessment of Unmanned Aircraft Systems (UAS) for Urban Air Mobility (UAM). He developed TPR indicators and analysis methods for UAS operations involving multiple flights. He focused on the drone-human impact simulation and fatality risk analysis, adopting Multi Body System (MBS) and Finite Element (FE) modelling methods. In the collaboration with the drone delivery company Antwork, he emphasizes the risk analysis of a medical delivery drone with parachute and airbag systems. He also enrolled at doctoral training programme at TU Delft.

List of Publications

- Blom, H. A.P., **Jiang, C.**, Grimme, W. B. A., Mitici, M., & Cheung, Y. S., "Third party risk modelling of Unmanned Aircraft System operations, with application to parcel delivery service", Reliability Engineering & System Safety, 2021, 214, 107788.

- **Jiang, C.**, Blom, H. A. P., & Sharpanskykh, A., "Third party risk indicators and their use in safety regulations for UAS operations", In AIAA aviation forum, 2020.

- Blom, H. A. P., **Jiang, C.**, "Safety risk posed to persons on the ground by commercial UAS-based services", 14th USA/Europe Air Traffic Management Seminar, 2021.

- He, X., **Jiang, C.**, Li, L., & Blom, H. A. P., "A Simulation Study of Risk-Aware Path Planning in Mitigating the Third-Party Risk of a Commercial UAS Operation in an Urban Area". Aerospace 2022, 9, 682.

- Rattanagraikanakorn, B., Blom, H. A.P., Sharpanskykh, A., De Wagter, C., **Jiang, C.**, Schuurman, M., Gransden, D.I., & Happee, R. (2020). Modeling and Simulating Human Fatality due to Quadrotor UAS Impact. In Proc. AIAA AVIATION 2020 FORUM, 15-19 June, Virtual Event, (p. 2902).

Under Review:

- **Jiang, C.**, Blom, H. A. P., Rattanagraikanakorn, B., "Effect of Parachute and Airbag in Reducing Safety Risk Posed by Small UAS to People on the Ground", Manuscript submitted to Transportation Research Interdisciplinary Perspectives, August 2023.

- **Jiang, C.**, Blom, H. A. P., Rattanagraikanakorn, B., "Joint Assessment of Impact Area and Human Fatality of Ground Crash by an Unmanned Aircraft System", Manuscript submitted to Risk Analysis, January 2023.